INSTITUTE OF
PAPER CHEMISTRY
Appleton · Wisconsin

A STUDY OF BONDING MECHANISMS OF
CORRUGATING MEDIUM

Project 2696-17

Report One
A Progress Report
to THE
FOURDRINIER KRAFT BOARD GROUP
of THE
AMERICAN PAPER INSTITUTE

July 15, 1977

THE INSTITUTE OF PAPER CHEMISTRY

Appleton, Wisconsin

A STUDY OF BONDING MECHANISMS OF CORRUGATING MEDIUM

Project 2696-17

Report One

A Progress Report

to THE

FOURDRINIER KRAFT BOARD GROUP

of THE

AMERICAN PAPER INSTITUTE

July 15, 1977

TABLE OF CONTENTS

ABSTRACT

An experimental and analytical investigation was made of a reverse-roll, corrugating glue machine. Film thickness measurements were made on a laboratory adhesive applicator and the effects of various system parameters were tested for several Newtonian and non-Newtonian fluids. An analytical model was formulated to simulate the metering flow in the nip and to predict the film thicknesses on the applicator roll.

Experimentally, several results of industrial significance were discovered:

    a) For typical starch adhesives, there is an optimum metering to applicator roll speed ratio which yields a constant film thickness regardless of operating speed.

    b) The optimum speed ratio is inversely related to the fluid viscosity measured at the shear rates experienced in the nip.

    c) Viscosity measurements made with a Stein-Hall cup viscometer do not provide adequate information to determine the optimum speed ratio and an alternative technique for in-plant viscosity measurements is proposed.

    d) The non-Newtonian characteristics of the adhesive are not significant to the metering process because at high shear rates experienced in the nip, the adhesives exhibit a nearly Newtonian behavior.

Additionally, important system parameters were investigated. These include: the gap between rolls, temperature effects, and the depth of roll submersion into the fluid.

The analytical model was based on the hydrodynamic theory of lubrication and was modified to include developing flow effects. The model qualitatively

predicts the trends seen in the experimental data. However, no attempt was made

to duplicate experimental results because two essential parameters could not be

obtained with the existing experimental equipment. The undetermined parameters

were the point of fluid separation from the metering roll and the location of the

maximum pressure below the nip.

LIST OF TABLES

LIST OF ILLUSTRATIONS

NOMENCLATURE

Symbol	Meaning
h	Gap between rolls
m, n	Summation indices
P	Pressure
Q	Flow rate
r	Radius
t	Time
t_1	Time constant for developing flow
u	Velocity
x	Vertical coordinate
y	Horizontal coordinate
δ	Film thickness
μ	Viscosity
$\nu(\mu/\rho)$	Kinematic viscosity
ρ	Density

Subscripts

a	Applicator roll
m	Metering roll; maximum pressure
s	Separation point of fluid from the metering roll

THE INSTITUTE OF PAPER CHEMISTRY

Appleton, Wisconsin

A STUDY OF BONDING MECHANISMS OF CORRUGATING MEDIUM

1.0 INTRODUCTION

1.1 HISTORICAL BACKGROUND

Project 2696-17 was initiated to study the adhesive bonding mechanisms
of corrugated medium. In particular, the objective was to understand the process
by which adhesive is transferred from the applicator roll to the flute nips of the
corrugated medium. The initial work involving surface receptivity and surface
roughness of the medium proved unsuccessful and it was concluded that in order
to properly examine the adhesive bonding mechanisms, the dynamics of the applica-
tor system must be described. The project was then divided into two phases. The
first phase would be a study of the dynamics of the system and would include
the metering of the adhesive film and the translation of the film on the surface
of the applicator roll. The second phase would examine the transfer of the
adhesive from the applicator roll to the flute tips of the medium. This report
concludes the work on the first portion of Phase 1.

Before undertaking this project, the Institute was aware of the research
being done at the Forest Products Laboratory for CID (1). The CID effort dealt
with modifying the adhesive formulation to provide a uniform film thickness
regardless of the applicator roll speed. The results showed that for a typical
Stein-Hall adhesive there is a metering-to-applicator roll speed ratio for which
the film thickness is independent of speed. The CID effort has since moved to
in-plant trials where the metering ratio and other system variables are being
studied to determine their effect on consumption and board quality.

The emphasis of the work at The Institute of Paper Chemistry was directed at understanding the fundamental mechanics of the applicator system through experimental tests on a laboratory glue machine and the development of an analytical model to predict film thicknesses for various operating conditions. This basic knowledge complements the CID investigations and provides insight for improvements in glue application and equipment design. Throughout the project, there was open communication between the Institute and CID in an effort to avoid possible duplication of effort.

1.2 PROBLEM DESCRIPTION

The common means of applying adhesive to the flute tips of corrugated medium is shown in Fig. 1.1 and is referred to as a reverse-roll applicator system. A layer of glue adheres to the surface of the applicator roll as it rotates in the adhesive tray. The adhesive is then forced into the nip area where most of it is sheared from the applicator roll. Only a thin film passes through the nip and is translated on the surface of the applicator roll to where it contacts the flute tips of the medium. A small amount of adhesive is retained on the flute tip in preparation for bonding with the liner.

One of the problems limiting the development of corrugators is the unpredictable variation in adhesive film thickness that occurs with changing operating conditions. Many of the contributing factors such as nonparallel rolls, poor bearings, out-of-round rolls, differences in surface conditions, and the manner in which the metering roll is wiped can be corrected with proper maintenance. However, the changes in the film thickness caused by system parameters such as the gap between rolls and the metering-to-applicator roll (M/A) speed ratio were unknown. Little previous work has been devoted to the fluid dynamics of

the applicator and its importance in the metering process. This is demonstrated by the frequent association of film thickness variations to the complex rheology of the adhesive without real justification. The objective of this research was to define the fundamental fluid dynamics of the metering process by determining the parameters controlling the film thickness and relating them to the rheological properties of the fluid.

ADHESIVE APPLICATOR SYSTEM
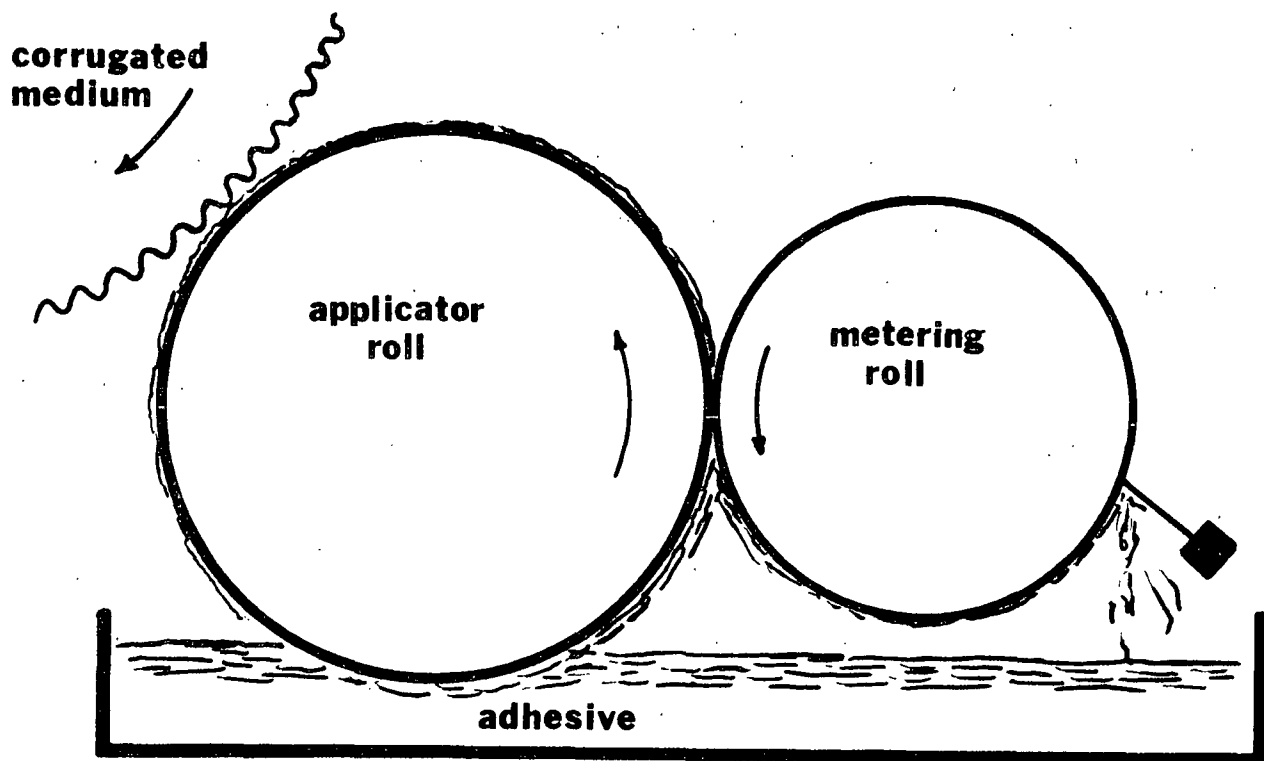
Figure 1.1. Reverse Roll Glue Applicator System

The research program consisted of an analytical model to describe the flow and an experimental applicator system to test various fluids under different operating conditions. The laboratory device was also used to provide data for the verification of the analytical model. The model and the experimental apparatus are described in the following sections.

2.0 ANALYTICAL MODEL

2.1 INTRODUCTION

Initially, a simple Couette flow model was proposed to describe the flow in the nip area. The non-Newtonian characteristics of the fluid and the effects of the pressure distribution under the rolls due to the rapid change of fluid momentum were included in the analysis. These additional factors made it necessary to consider the axial flow direction and involved the use of the hydrodynamic theory of lubrication (2). Most of the analytical work in the modeling of blade and roll coating phenomena also begins with lubication theory (3,4). The modification of the governing equations for non-Newtonian fluids followed the development of Flumerfelt, et al. (5). The detailed description of this preliminary model is contained in an initial progress report for the project (6).

The early experimental data obtained in this study and the data obtained in a similar work by Koning (7), showed that the preliminary analytical model was incapable of describing various flow situations. In particular, it could not account for the observed increase in film thickness with increasing speed ratio. The limitation that caused the discrepancy was the fact that the model considered the flow to be fully developed in the nip. For most operating speeds, the time period for shearing the fluid is smaller than that required for fully developed flow conditions to exist. The model was revised to consider a developing flow regime.

The following two subsections describe the fundamentals of Couette flow and developing flow in more detail. The last subsection describes the analytical model used in the project.

2.2 COUETTE FLOW

Couette flow refers to the motion of a fluid between two parallel boundaries induced by the motion to either or both of the boundaries (see Fig. 2.1). The simplest case is the fluid motion created by the movement of the upper plate while the lower plate remains fixed. The equation of motion for this flow regime is given by Brodkey (8).

$$-\frac{dP}{dx} + \nu \frac{\partial^2 u}{\partial y^2} = 0 \qquad (2.1)$$

For simplicity, the pressure gradient is not considered and with this assumption Equation (2.1) reduces to

$$\frac{d^2 u}{dy^2} = 0 \qquad (2.2)$$

with boundary conditions

$$u = 0 \qquad at \quad y = 0$$
$$u = u_a \qquad at \quad y = h \qquad (2.3)$$

Equation (2.2) is easily integrated and the solution has the form

$$u = C_0 y + C_1 \qquad (2.4)$$

The constants of integration can be solved using the boundary conditions given in Equation (2.3)

$$C_0 = u/h$$
$$C_1 = 0 \qquad (2.5)$$

and the final solution is

$$u = u_a \, y/h \qquad\qquad (2.6)$$

The velocity profile is linear as indicated in the figure.
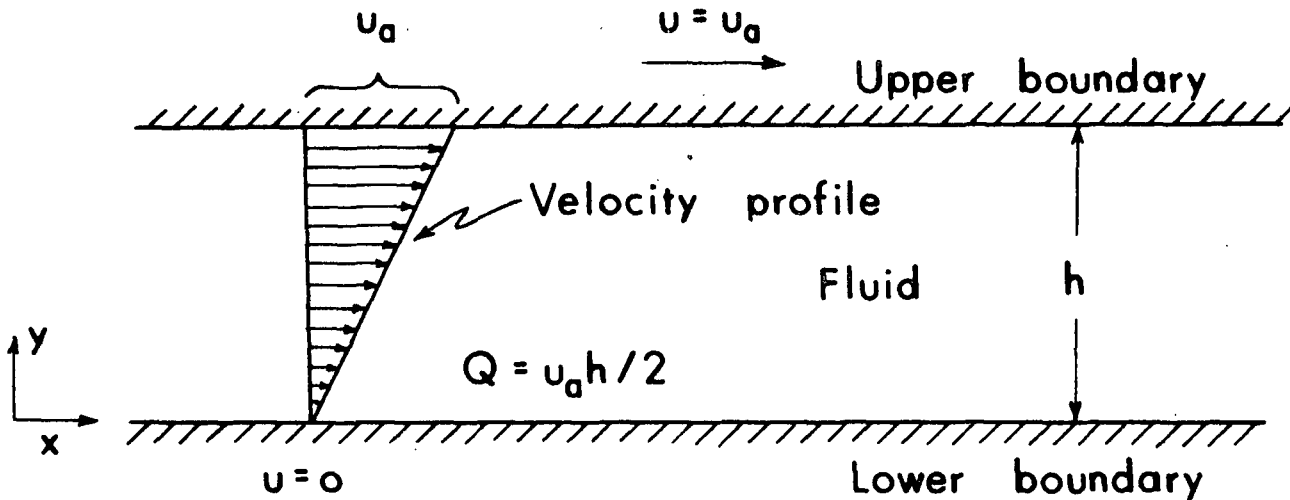
Figure 2.1. Couette Flow: One Wall Stationary

If the same flow regime is considered with the bottom boundary moving
in a direction opposite to the top plate, the equation for velocity is

$$u = (u_a + u_m) \, y/h - u_m \qquad\qquad (2.7)$$

and the velocity profile is shown in Fig. 2.2. Here, the velocity profile is
again linear except that it now possesses a forward and a reverse fluid motion.

The flow rate between the two boundaries can be determined by integrating
the velocity profile across the gap,

$$Q = \int_0^h u \, dy \qquad\qquad (2.8)$$

Using Equation (2.6) for the velocity yields
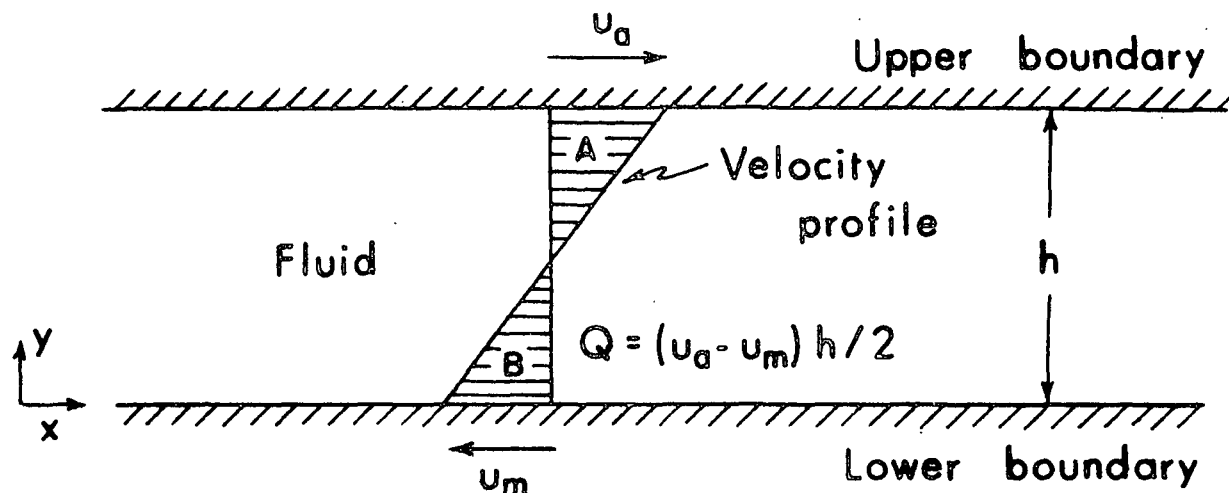
Figure 2.2. Couette Flow: Both Walls Moving

$$Q = u_a y^2/2h \ \bigg|_0^h \tag{2.9}$$

$$Q = u_a h/2 \tag{2.10}$$

If the lower plate is set in motion, as in the second example, the flow rate becomes

$$Q = (u_a - u_m) \, h/2 \tag{2.11}$$

Physically, the flow rate is represented by the area under the profiles in Fig. 2.1

and 2.2. In Fig. 2.2, the area is obtained by subtracting of Area B from Area A.

The model can be used to approximate the flow in the nip by considering the

upper and lower boundaries as the applicator and metering rolls, respectively. This

is demonstrated in Fig. 2.3 where the nip area is magnified 100 times and the flow

geometry is approximately the flow between two parallel plates.

The problem associated with the model occurs when the speed ratio is

greater than one, i.e., the metering roll has a surface speed faster than the

applicator roll. For this condition, the flow rate through the nip becomes negative

and is demonstrated in Equation (2.10) by making u_m larger than u_a.

APPLICATOR ROLL
Radius = 5 inches
Scale 100/1

$r_a \omega_a$

gap = 0.010 in

$r_m \omega_m$
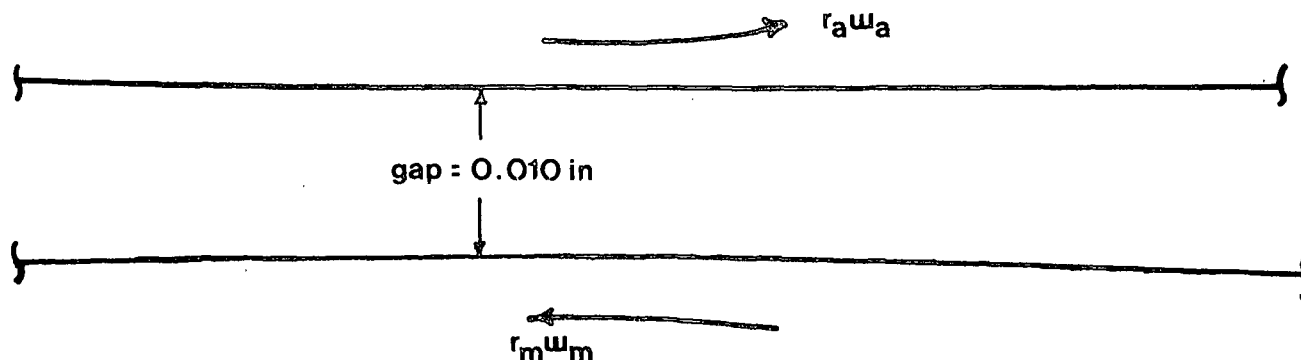
METERING ROLL
Radius = 3 inches

Figure 2.3. Couette Flow in the Nip

$$Q = (u_a - u_m)\, h/2 < 0 \qquad\qquad (2.12)$$

Since in almost all cases films are observed on the applicator roll, the model
appears to fail. However, if the velocity profile is considered to be developing
(time dependent), the difficulty is overcome.

2.3 DEVELOPING FLOW

The equations just developed for Couette flow are based on steady-state
conditions. The same flow situation may be considered with both boundaries
initially at rest. If the top boundary is then set in uniform motion it will
require a specific time interval before all of the intervening fluid is set in
motion. For example, after a time interval t_1, the velocity profile may appear

as shown in Fig. 2.4. Since the fluid must wet the moving boundary, the velocity at the wall must be u_a. However, the effect of this motion is not felt immediately across the entire spacing. After a time interval $5t_1$, the movement of the upper boundary influences more of the profile and after a sufficiently long period of time, the flow eventually approaches a steady-state Couette flow profile.
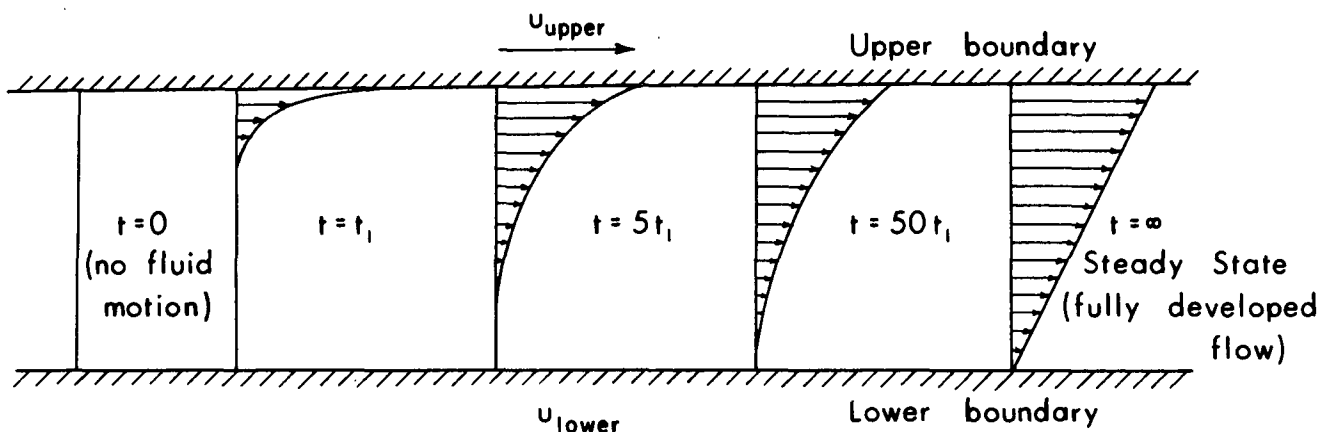
Figure 2.4. Developing Couette Flow

The flow in the nip area of the applicator system can be approximated by assuming a developing flow situation. As the fluid is picked up from the adhesive tray, the entire film rapidly assumes the velocity of the applicator roll (see Fig. 2.5). At some point below the nip, the film being metered back to the adhesive tray joins the film being forced into the nip. From this point to the point where the fluid finally separates from the metering roll, the fluid is being sheared. In this interval the uniform velocity profile is being distorted. The flow regime is very similar to the commencing or developing flow situation described in the previous paragraph. The analysis of developing flow requires that the time derivative remain in the equation of motion and a description of this analysis is presented in the following subsection.
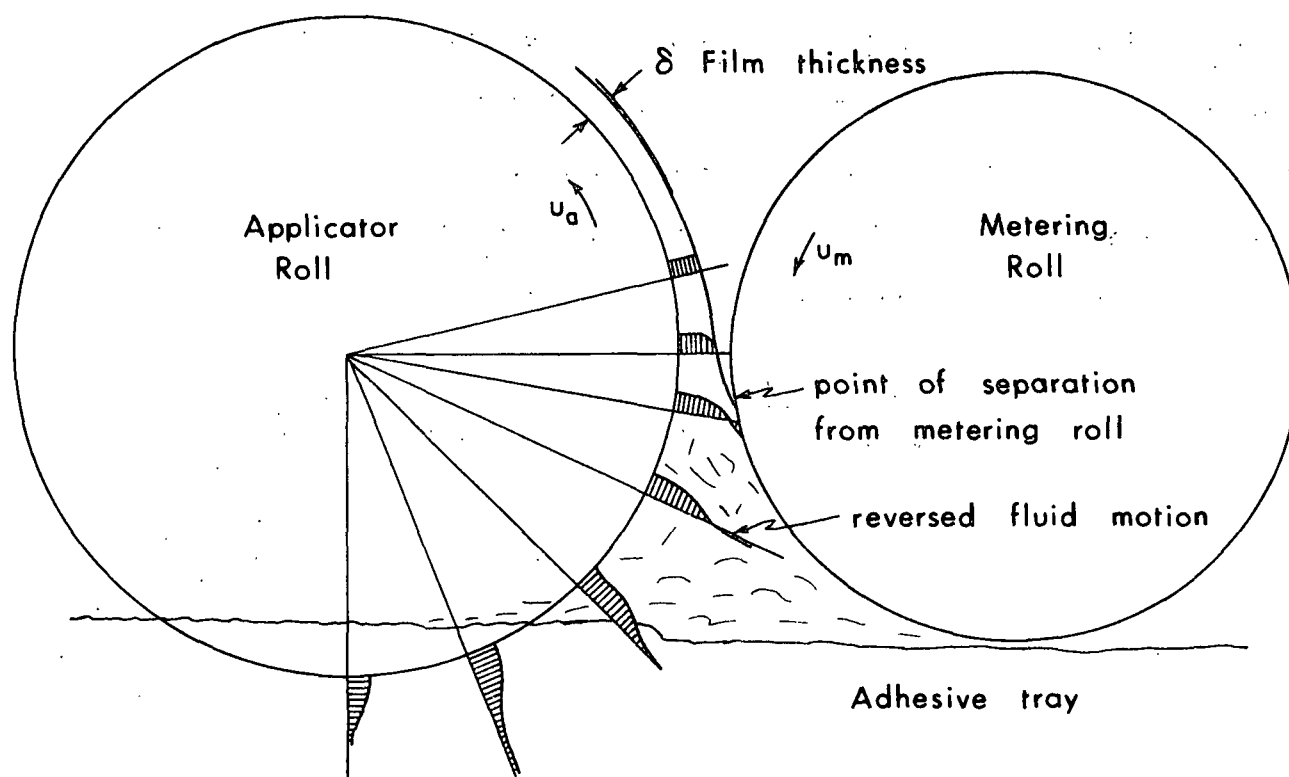
Figure 2.5. Developing Flow in the Nip

2.4 NIP FLOW MODEL

As a prelude to mathematical solution for the film thickness on the applicator roll, Fig. 2.6 illustrates the notation and coordinates considered in the analysis. The axial flow coordinate, $\underline{x}$, is considered to be positive in the direction of the adhesive tray or opposite to the upward motion of the adhesive.

The equation of motion for a fluid flowing in the narrow gap between two rotating cylinders where the hydrodynamic theory of lubrication applies is given by Reference ($\underline{2}$).

$$\rho \frac{\partial u}{\partial t} = - \frac{dP}{dx} + \mu \frac{\partial^2 u}{\partial y^2} \qquad (2.13)$$
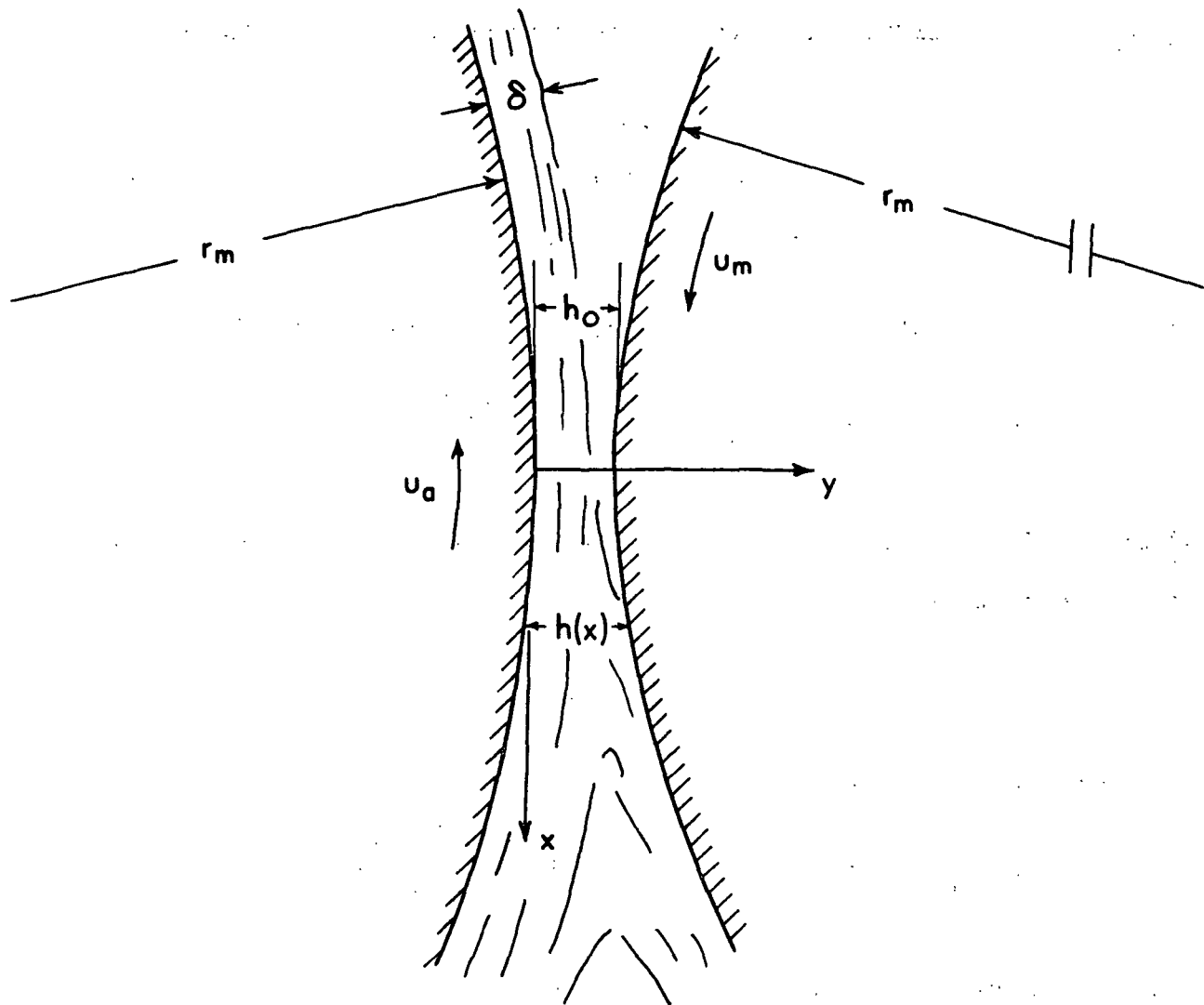
Figure 2.6. Notation for the Analytical Model

Here the time dependency, $\partial u/\partial t$, is retained in the analysis. Since the governing equations are being solved for the velocity at the point of maximum pressure, the first term on the right-hand side of the equation can be dropped.

$$\rho \frac{\partial u}{\partial t} = \mu \frac{\partial^2 u}{\partial y^2} \qquad (2.14)$$

The appropriate boundary conditions are determined by requiring that the fluid wet the surface of the rolls. Therefore, the fluid at the boundary must have the same velocity as the roll. The initial condition is set by assuming that the

incoming profile is uniform and equal to the surface speed of the applicator roll.

$$u = u_a \quad \text{at } y = 0$$

$$u = -u_m \quad \text{at } y = h \tag{2.15}$$

$$u = u_a \quad \text{at } t = 0$$

The solution for the velocity profile is presented in Appendix A and has the form

$$u = u_a - (u_a + u_m)\, y/h - \frac{2}{\pi}(u_a + u_m) \sum_{n=1}^{\infty} (-1)^n \frac{\sin n\pi y/h}{n} e^{-\left[\frac{n\pi}{h}\right]^2 \nu t} \tag{2.16}$$

The adhesive film thickness is obtained by solving for the flow rate using the continuity relationship.

$$Q = \int_0^{h_m} u \, dy \tag{2.17}$$

Substituting Equation (2.16) into (2.17) and integrating yields

$$Q = (u_a - u_m)\, h_m/2 + \frac{4}{\pi^2}(u_a + u_m)\, h_m \sum_{n=1}^{\infty} \frac{e^{-[(2n-1)\pi/h_m)^2]\nu t}}{(2n-1)^2} \tag{2.18}$$

The film thickness on the applicator roll is obtained from

$$\delta_a = Q/u_a \tag{2.19}$$

and substituting Equation (2.18) into (2.19) yields

$$\delta_a = (1 - u_m/u_a)\, h_m/2 + \frac{4}{\pi^2}(1 + u_m/u_a)\, h_m \sum_{n-1}^{\infty} \frac{e^{-[(2n-1)\pi/h_m]^2 \nu t}}{(2n-1)^2} \tag{2.20}$$

Equation (2.20) can be simplified by performing an order of magnitude analysis on each term of the series expansion.

$$\sum_{n=1}^{\infty} \frac{e^{-[(2n-1)\pi/h_m]^2 \nu t}}{(2n-1)^2} = e^{-\pi^2 \nu t/h_m^2} + 1/9\, e^{-9\pi^2 \nu t/h_m^2} + \dots \tag{2.21}$$

Comparing the first and second terms gives

$$\frac{e^{-\pi^2 \nu t/h_m^2}}{1/9 \; e^{-9\pi^2 \nu t/h_m^2}} = 9 \; e^{8 \pi^2 \nu t/h_m^2} \qquad (2.22)$$

Since $\underline{\nu t/h_m^2}$ is of the order of unity for typical values, the ratio of the first

and second term is approximately 10^{15}. Therefore, only the first term of the

series is significant and the solution can be rewritten

$$\delta_a = (1 - u_m/u_a) \; h_m/2 + \frac{4}{\pi^2} (1 + u_m/u_a) \; h_m \; e^{-\pi^2 \nu t/h_m^2} \qquad (2.23)$$

Equation (2.23) is the final form of the film thickness relationship

and consists of two terms; a steady-state or fully developed flow component and a

time dependent or developing flow component. The flow in the nip can be viewed

from either of the two perspectives. The first is to view the flow from the

standpoint of a stationary observer at one location within the nip and evalu-

ate the velocity profiles at that point based on the amount of time available for

shearing the fluid. The second approach is to observe the flow from the view-

point of an observer on the applicator roll watching the profiles develop as the

applicator roll rotates through the nip. Both approaches are identical and are

used interchangeably in subsequent explanations of the flow regime.

The time available for shearing the fluid has already been mentioned

several times and its relationship to the machine speed and the M/A speed ratio

may be confusing. The shearing time refers to the time period in which the fluid

in the nip is exposed to the reverse motion of the rolls. The time period begins

when the fluid picked-up by the applicator roll first contacts the film being

removed from the nip by the metering roll. It ends when the film finally separates

from the metering roll near the nip. Increasing the applicator roll speed at a

constant M/A ratio reduces the shear time provided the point of separation does not change drastically. Increasing the M/A ratio at a constant speed also reduces the shear time since it increases the relative velocity between the rolls.

The first term of Equation (2.23) represents the fully-developed flow or steady-state contribution to the film thickness. The difficulty with using only this portion of the solution is seen in Fig. 2.7. For speed ratios above unity, the film thickness becomes negative and implies that no film remains on the applicator roll or passes through the nip.

FILM THICKNESS

Couette Flow (with developing profile)

Couette Flow (fully developed)

Speed Ratio = 1.0

SPEED RATIO
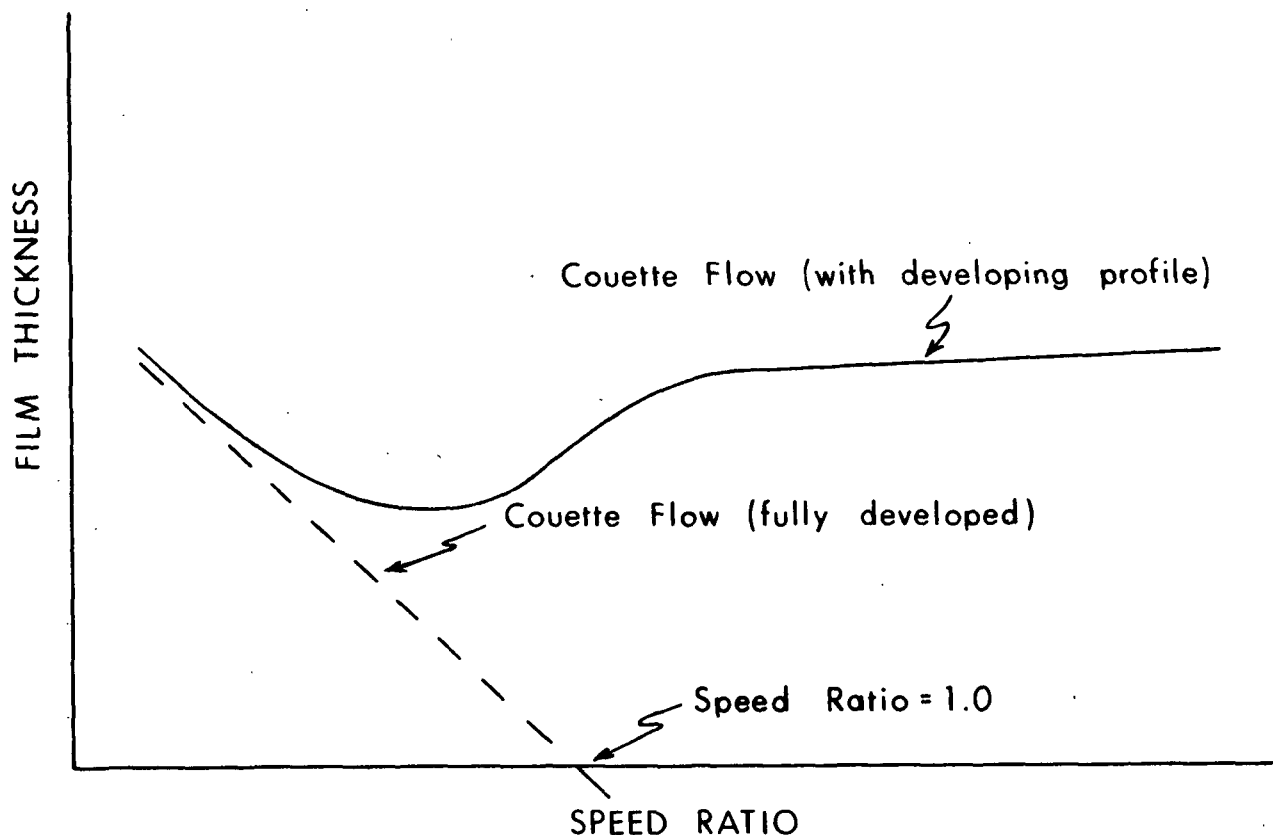
Figure 2.7. Steady-State and Developing Flow Contributions to the Film Thickness

The second term of Equation (2.23) accounts for the developing flow within the nip and is intimately related to the time available for shearing the fluid. If the fluid is sheared for a very short period of time, the second term

becomes the dominant contribution to the film thickness. When the fluid is sheared for a long period of time, the exponential term approaches zero and only the fully developed contribution is significant.

The film thickness in Equation (2.23) is dependent upon the speed ratio, the gap spacing at the point of maximum pressure, the high shear viscosity, and the time the fluid is sheared. The speed ratio and viscosity are considered as input parameters and this leaves the gap spacing and shear time as unknown variables. Two independent relations are required to obtain a closed form solution. The present solution technique is to obtain the two relations from the experimentally determined pressure distribution in the nip. The location of the point of maximum pressure, x_m, is used to calculate the gap spacing, h_m. Also, the point of fluid separation from the metering roll, x_s, can be estimated by assuming that it occurs when the pressure gradient reaches a maximum (see Fig. 2.8). The value of x_s is used to calculate the shearing time.

Only a limited amount of experimental pressure data is available and some results using this data are presented in Section 4.2. The thorough definition of the empirical relationships for x_m and x_s will be part of the second portion of this project.

$$\rho \frac{\partial u}{\partial t} = - \frac{\partial P}{\partial x} + \mu \frac{\partial^2 u}{\partial y^2}$$

$dP/dx = 0$

X_{max} - point of maximum pressure

X_s - point of fluid separation from metering roll

PRESSURE

X_{max}

X_s

DISTANCE FROM THE NIP
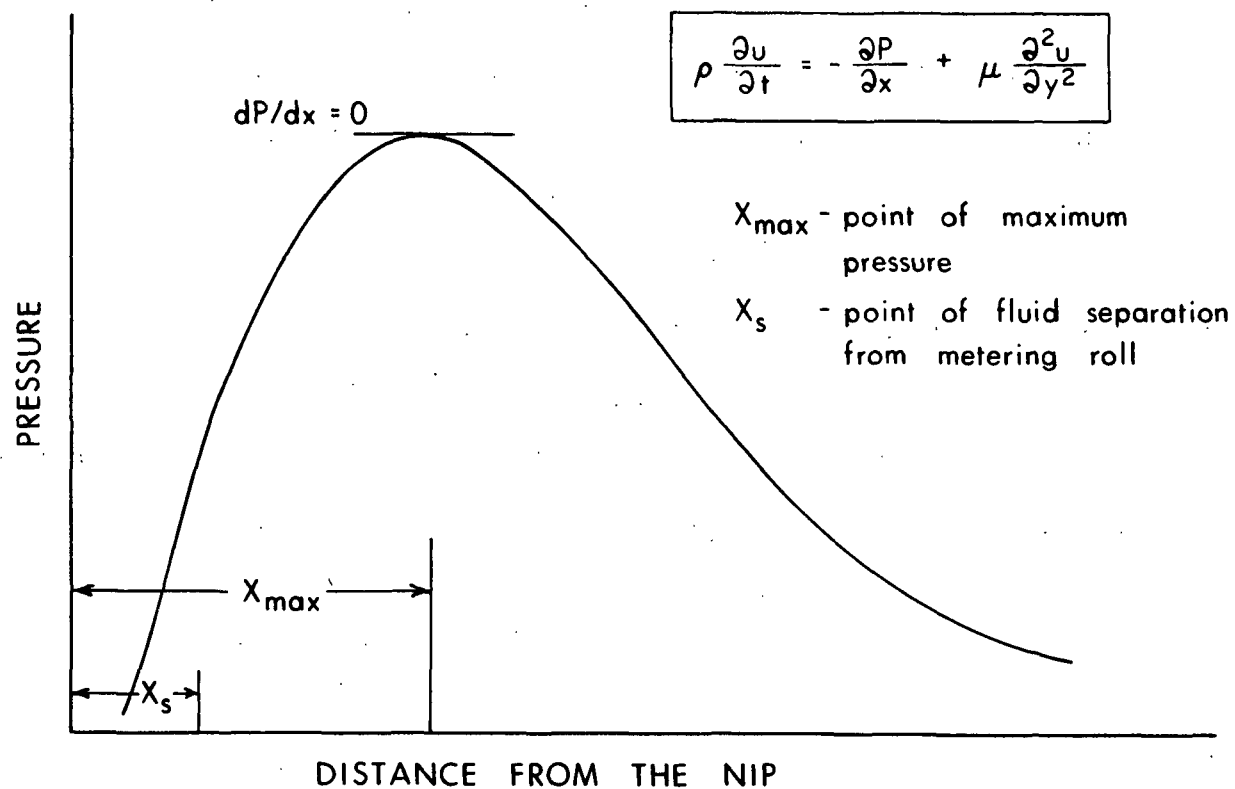
Figure 2.8. Pressure Distribution in the Nip

Fourdrinier Kraft Board Group
of The American Paper Institute
Project 2696-17.

Page 17
Report One

3.0 EXPERIMENTAL

3.1 BASIC APPARATUS

An experimental laboratory applicator similar to industrial reverse-roll systems was built and is shown in Fig. 3.1. A heavy steel frame was constructed to maintain rigidity at high operating speeds, and the frame has interior dimensions of 36 x 26 x 8 inches. The entire device is mounted with the laboratory unit at the top and the drive motors below. Hot and cold water outlets are readily accessible to the unit for temperature control.

The metering and applicator rolls have radial dimensions of 3 and 5 inches, respectively, and are 4-1/2 inches wide. The roll surfaces were ground steel and were not coated, plated, or etched. The rolls and supporting shafts are hollow. This allows them to be heated so the same apparatus can be used in future studies with a set-back adhesive being developed for cold corrugation. Both rolls are independently driven with separate variable speed motors. The roll speeds are monitored electronically. A magnetic sensor counts the number of pulses obtained from teeth of a gear attached to the end of the rolls. The digital output was calibrated to surface speeds obtained from a contact speedometer. The control console is shown in Fig. 3.2. The gap spacing between the rolls is variable from 0.008 to 0.020 inch and is controlled by an eccentric mounting of the metering roll.

The adhesive tray is double-walled and heated with hot water. For most experiments, the tray was heated to 100°F to duplicate industrial conditions. The height of the tray is adjustable and it was positioned at approximately 1/2 inch from the surface of the applicator roll. The fluid in the tray is used continuously and the sample scraped from the roll surface is pumped back into the tray.
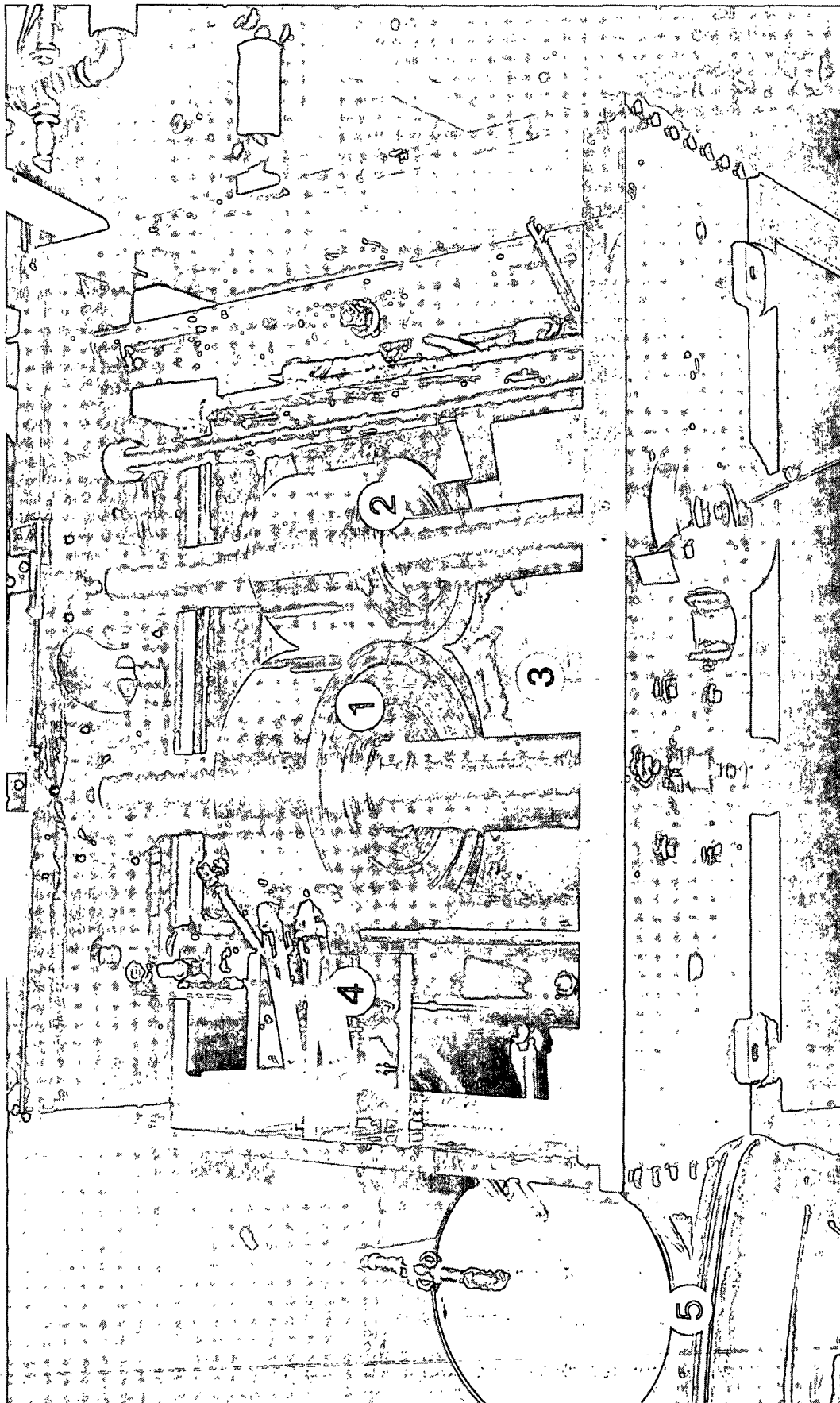
Figure 3.1. Experimental Applicator System.

1. Applicator Roll; 2. Metering Roll; 3. Adhesive Tray;
4. Scraper Blade and Assembly; 5. Scale and Collection Pan

1. Applicator Roll Speed
2. Metering Roll Speed
3. Digital Speed Read-Out
4. Timer
5. Pan Temperature Control
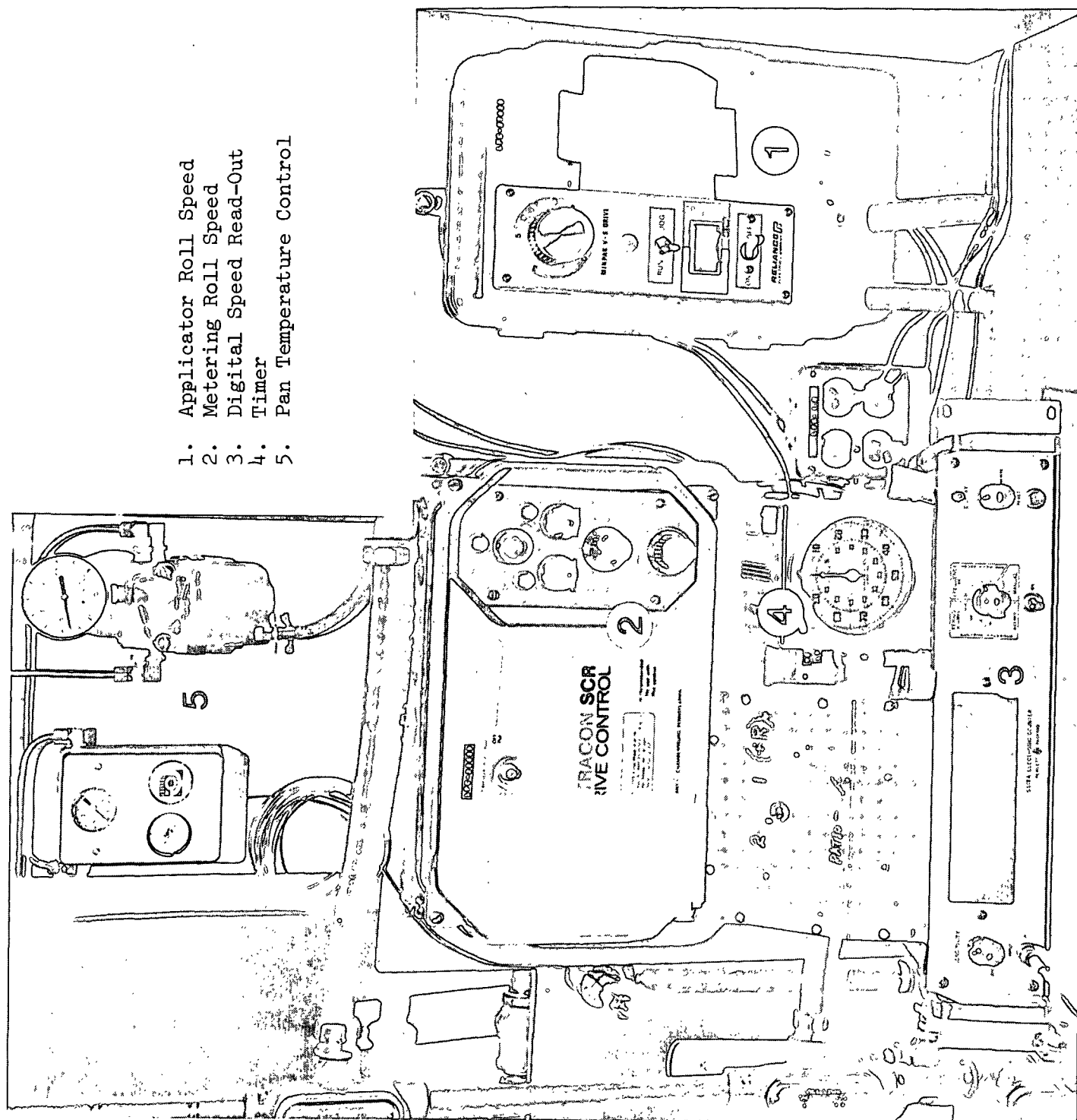
Figure 3.2. Control Console

A schematic of the collection device used in determining the film thickness on the applicator roll is shown in Fig. 3.3. The scraper blade is 2-inches wide and was made of two blue steel sheets. A pivoting rod in the center of the blade holder allows the blade to be pressed to the surface of the roll. The blade pressure is held constant by using a removable pressure rod at lower end of the blade holder. Since the adhesive film thicknesses are in range of a few mils, the constant blade pressure is necessary for repeatable results.

COLLECTION SYSTEM
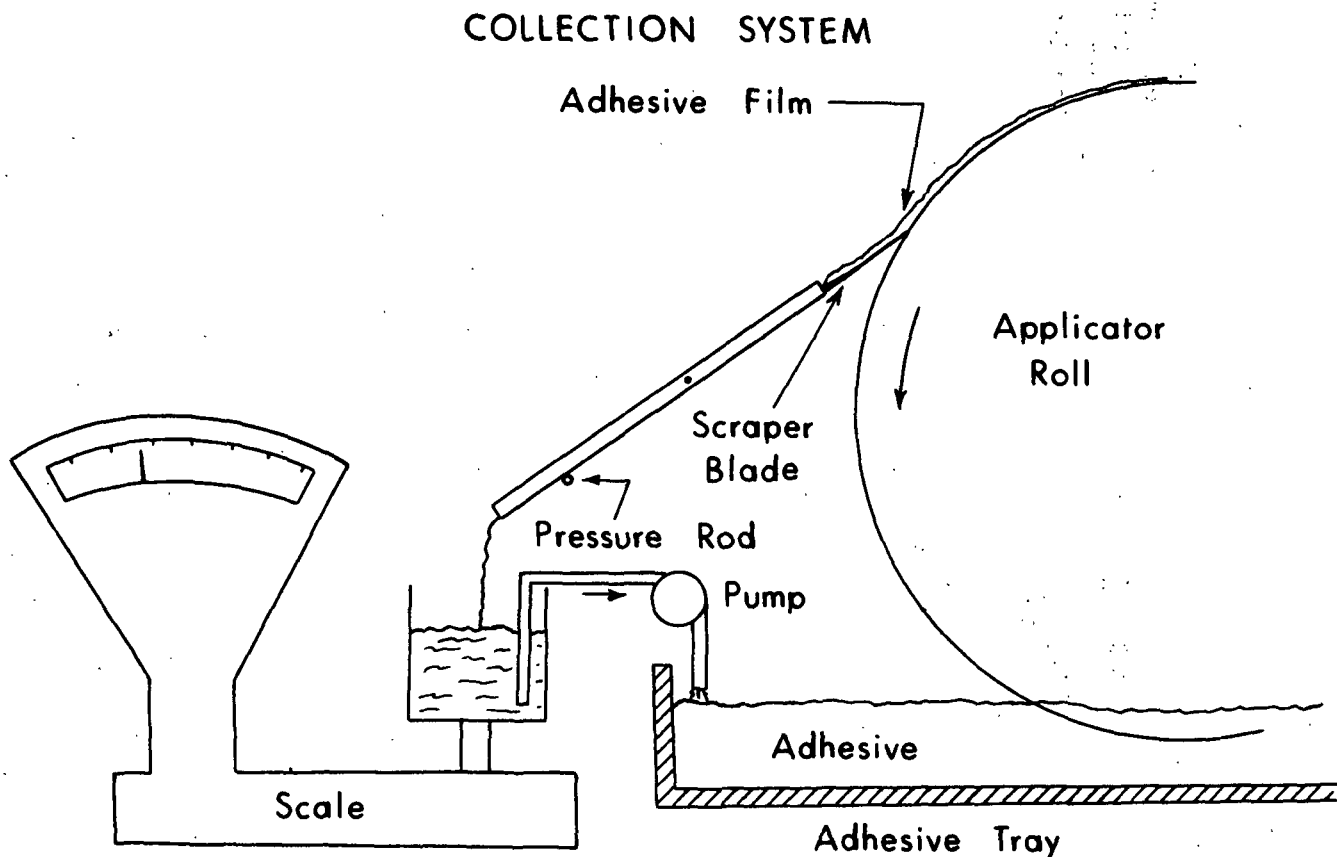
Figure 3.3. Film Thickness Sampling Device

The film scraped from the applicator roll flows down the channel to a collecting pan. A short time interval is required to permit the flow rate down the channel to stabilize. This is approximately 30 seconds. Next, the time required to obtain a 1/2 to 1-pound sample is recorded. The sample weight is

obtained from a visual observation of the dial indicator between the scale grad-
uations. The timer is manually controlled and is accurate to a hundredth of a
second. This process is the major source of experimental error and weighing and
timing mechanisms are currently being modified for future experimentation. Never-
theless, the data is accurate to about ±2.5% and the reproducibility is shown
with several examples in Section 4.1. Approximately one out of every five points
was checked for reproducibility. After a sample is recorded, the collected fluid
is then pumped back into the adhesive tray to maintain a constant fluid level.

3.2 FLUIDS TESTED

It was originally planned to study only 3 fluids. However, the initial
experimental data indicated that a peculiar relationship existed between the film
thickness curves and high shear viscosity of the material. To adequately define
this relationship, some additional fluids were tested. These include:

        Water
        Magie Oil #500
        Polybutene #6
        Polybutene #8
        Stein-Hall (Carrier Adhesive), 17% solids
        Stein-Hall (Carrier Adhesive), 20% solids
        Stein-Hall (Carrier Adhesive), 26% solids
        No Carrier Adhesive, 20% solids

The formulas used in preparing the starch adhesives are contained in Appendix B.

3.3 VISCOSITY MEASUREMENTS

One of the problems faced at the beginning of the project was the method
of obtaining the fluid viscosities. Industrially, low shear viscosity measure-
ments made with a Stein-Hall viscometer are used to compare adhesives (9). The
Stein-Hall cup viscometer is a cylindrical tube with an orifice plate positioned
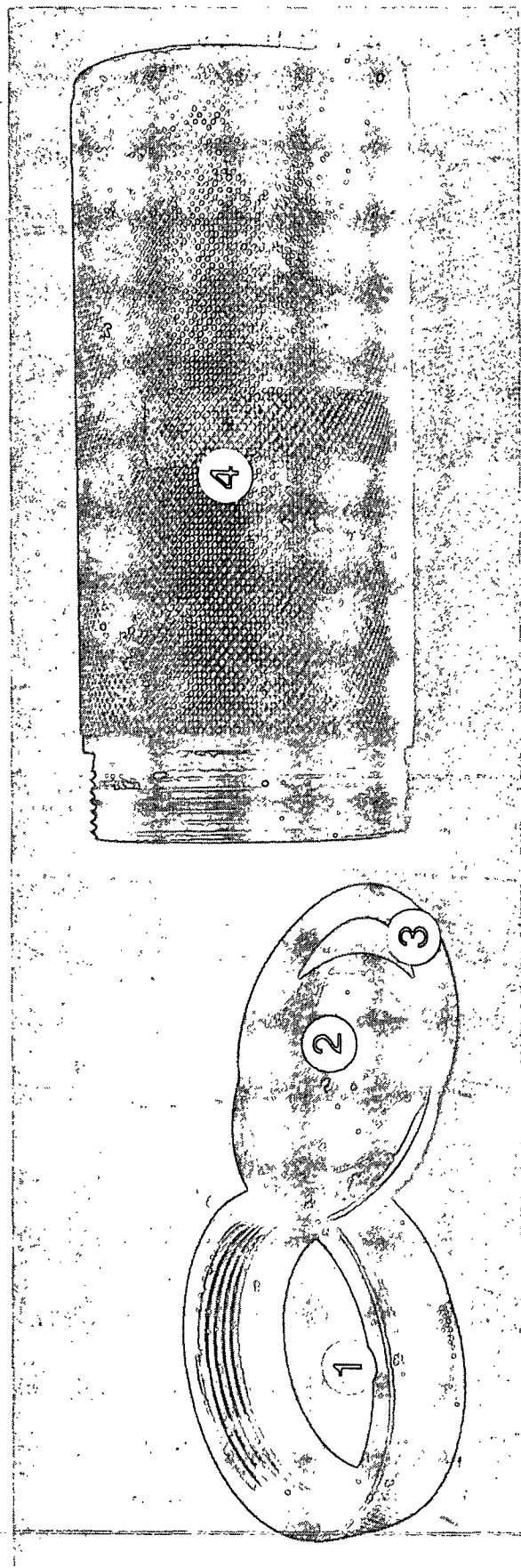at the bottom (see Fig. 3.4). The tube is filled with adhesive and the time

Figure 3.4. Stein-Hall Cup Viscometer

1. End Plate; 2. Orfice Plate;
3. Washer; 4. Holding Cylinder

required for the fluid level to pass between two indicators on the cylinder is used as a measure of viscosity. Since the flow is induced by the gravitational head, which is at most a few inches, the shear rates are generally low (1000 sec^{-1} maximum).

The flow in the nip area is normally under very high shear conditions (5,000 to 20,000 reciprocal seconds based on the gap spacing and relative velocities of the rolls). In order to duplicate this situation, all fluid viscosity measurements were made on a Hercules high shear viscometer shown in Fig. 3.5. The device is based on the principle of Couette flow between two rotating concentric cylinders and typical rheograms are shown in Fig. 3.6. The viscosity of the fluid is related to the inverse of the slope of the curve. Therefore, Curve A represents a low viscosity fluid while Curve D is typical of a much higher viscosity fluid. Also, both curves have a constant slope which implies a constant viscosity, i.e., a Newtonian fluid. Curve C represents a typical rheogram for a starch adhesive. Note that the curve is not a straight line and the adhesive is not a Newtonian fluid. However, at the high shear portion of the curve the relationship is nearly linear. This portion of the curve covers the range of shear rates normally encountered in the nip while the nonlinear portion of the curve exists at the lower shear rates where Stein-Hall cup viscosities are usually made. The rheograms imply that the adhesive behaves like a Newtonian fluid at high shear rates and Stein-Hall cup viscosities may have little bearing on the metering process. Additionally, the up and down portions of the rheogram indicates that the starch adhesive is a slightly thixotropic fluid. When the adhesive was sheared for about a minute, the up and down portions of the curve nearly coincided and this curve was recorded and used in the analysis.

1. Rotating Bob
2. Holding Cup
3. Recording Drum
4. Springs

HERCULES VISCOMETER
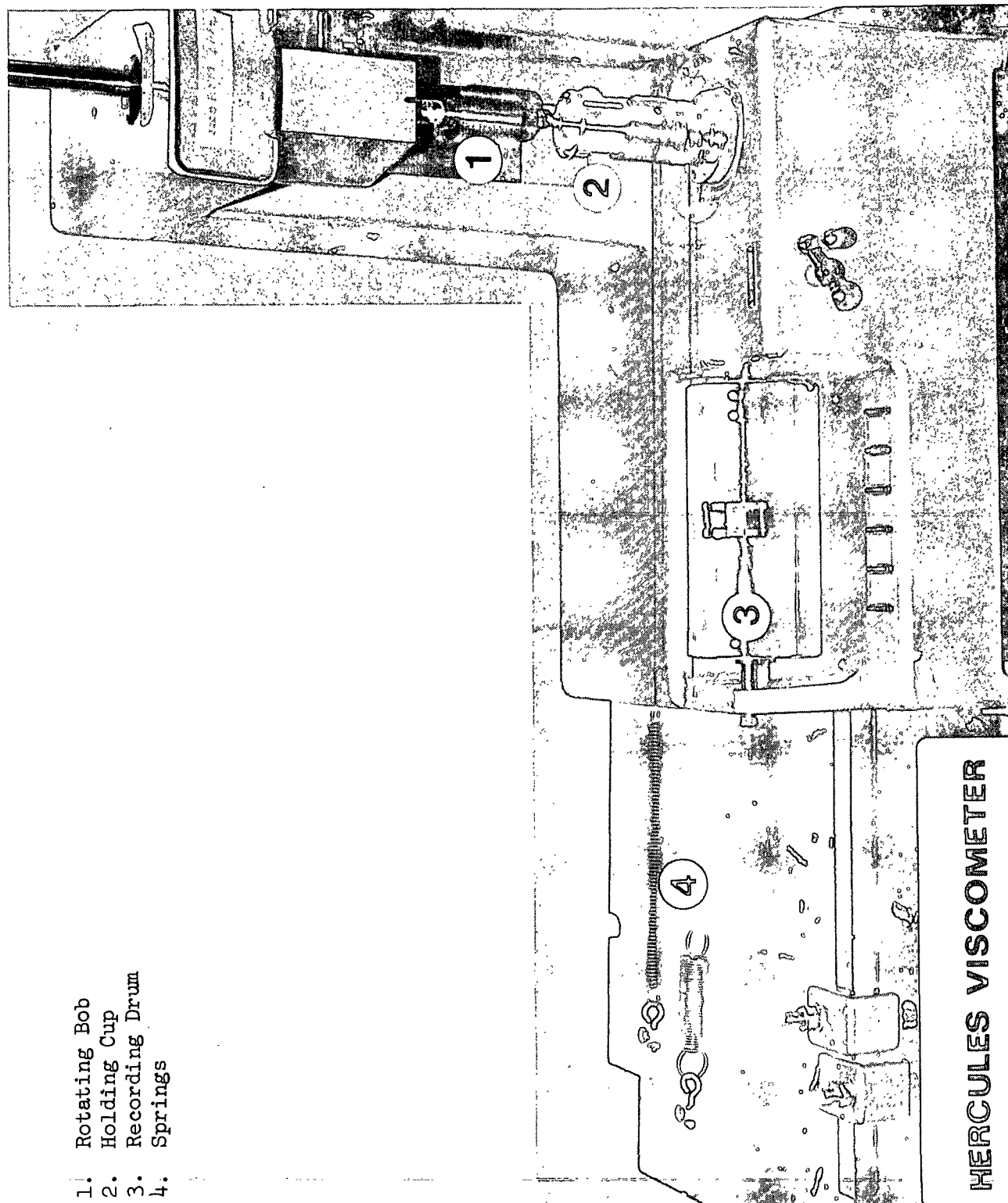
Figure 3.5. Hercules High Shear Viscometer
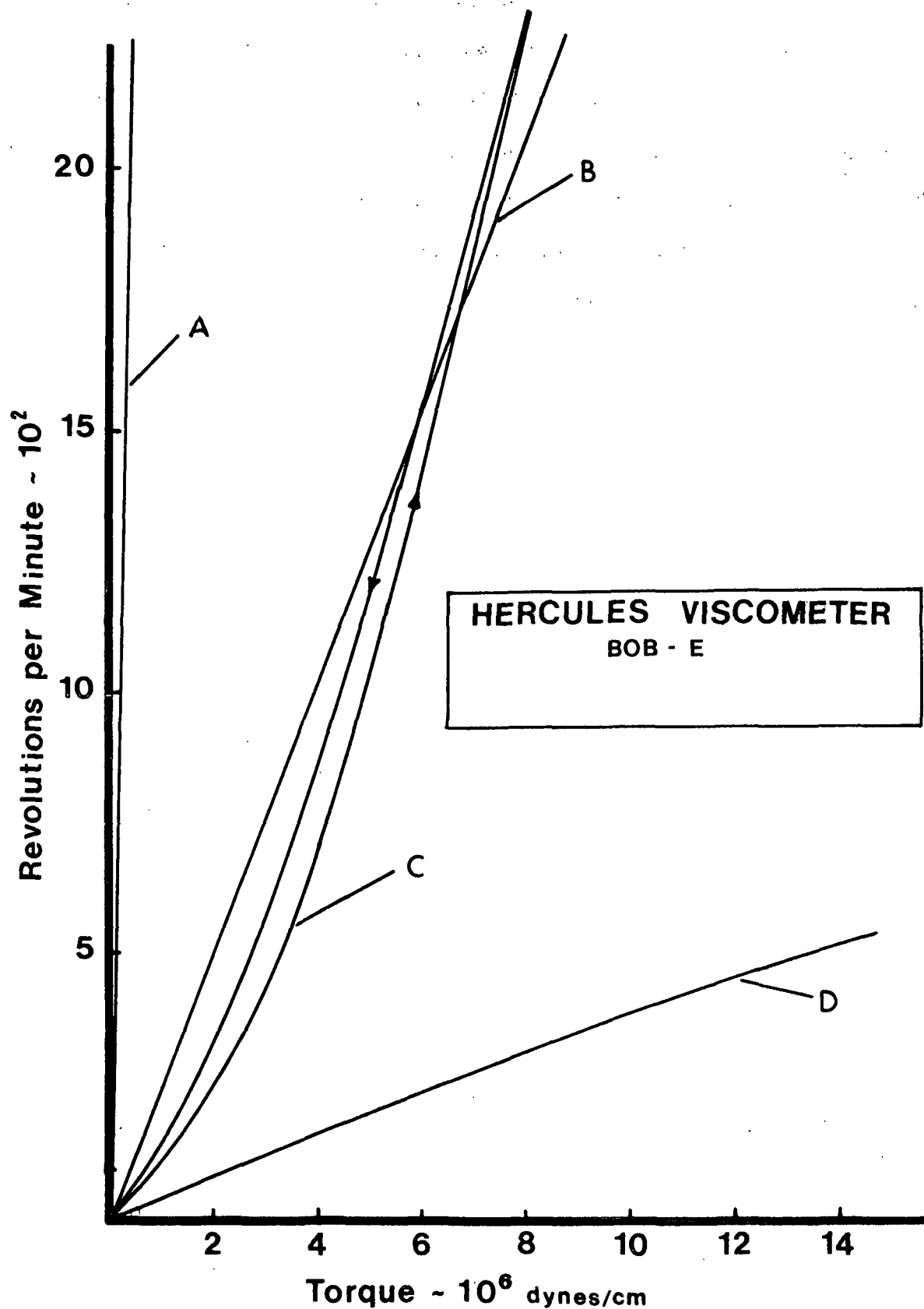
Figure 3.6. Typical Hercules Viscometer Rheogram

The fluids used in the experimental portion of the program are listed in Section 3.2. The results of the Hercules viscometer measurements for these fluids are shown in Fig. 3.7. The oils and water are Newtonian fluids with a viscosity range from 1 to 200 cp. Also, the oils are known to be temperature dependent, but since the tray was temperature controlled, significant variations in rheological properties were avoided. The starch adhesive viscosities at the higher shear rates ranged from about 25 to 45 cp.
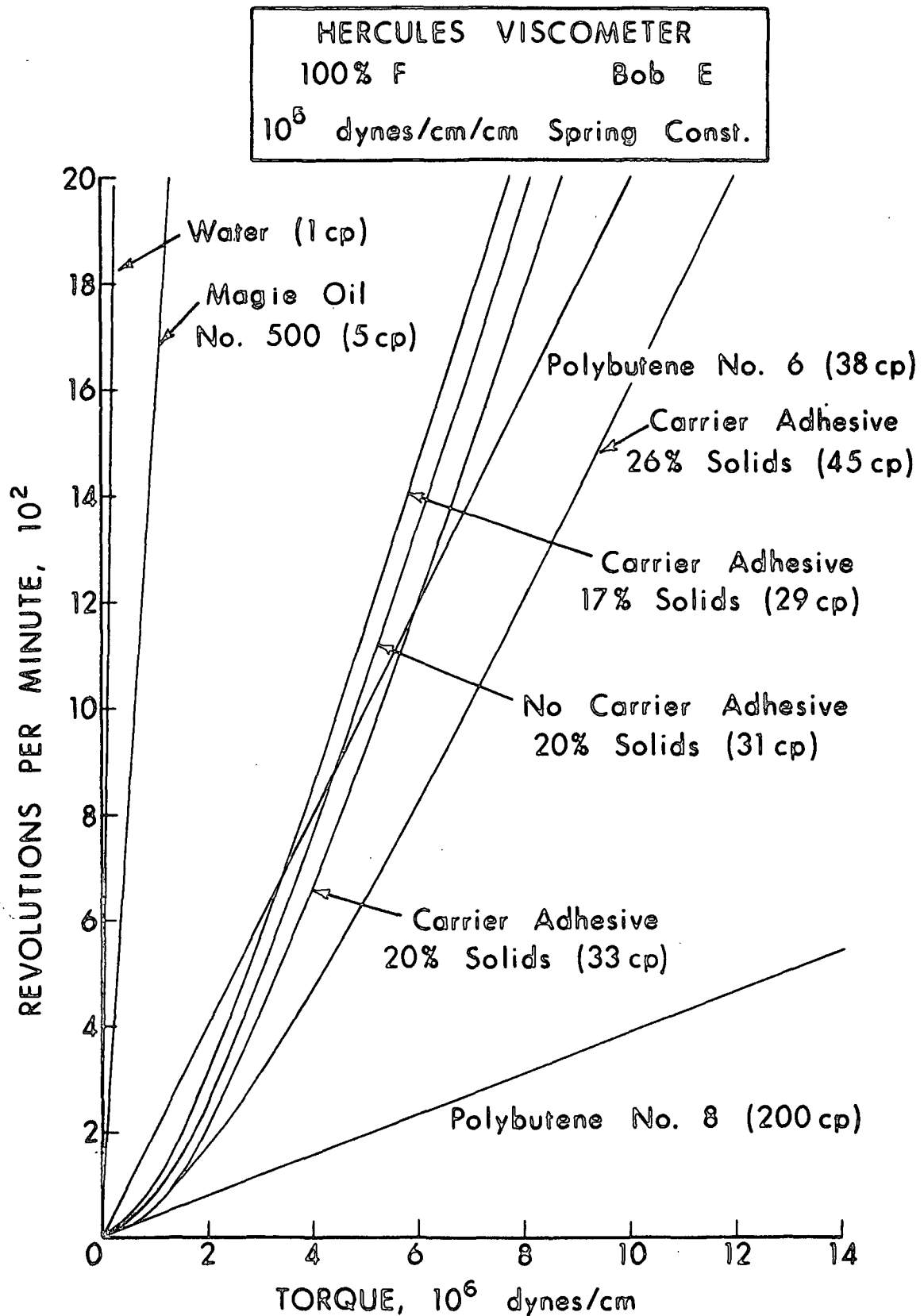
Figure 3.7.   Rheograms of the Tested Fluids

4.0 RESULTS AND DISCUSSION

4.1 EXPERIMENTAL

The behavior of the fluids listed in Section 3.2 was investigated for several applicator system parameters including: machine speed, metering-to-applicator roll speed ratio, gap spacing between rolls, and depth of applicator roll submersion into the adhesive tray. The results are contained in the following subsections.

4.1.1 Applicator Roll Surface Speed

Initially, three fluids were studied: water, an oil (Polybutene #6) and a starch adhesive. The plots of film thickness versus the applicator roll surface speed for these fluids are shown in Fig. 4.1, 4.2, and 4.3.

In Fig. 4.1, the relationship between the film thickness and speed is nearly linear. The slopes of the curves are positive for all speed ratios but the slopes seem to approach a horizontal line as the speed ratio increases.

The results for a Stein-Hall adhesive with a 20% solids content are shown in Fig. 4.2. The slopes of the curves change from positive to negative values as the speed ratios are increased. This implies that at some M/A ratio the curve is a horizontal line, and the adhesive film thickness at this speed ratio is constant for any machine speed. The phenomenon is important industrially since it allows the adhesive applicator to be independent of the operating speed of the corrugator.

In Fig. 4.3, the same phenomenon occurs for Polybutene #6. The lines of constant speed have positive slopes at low speed ratios and they become negative as the speed ratio is increased. Again, this implies that there is a speed

ratio which produces a uniform film thickness at **any operating speed.**

10 MIL GAP BETWEEN ROLLS
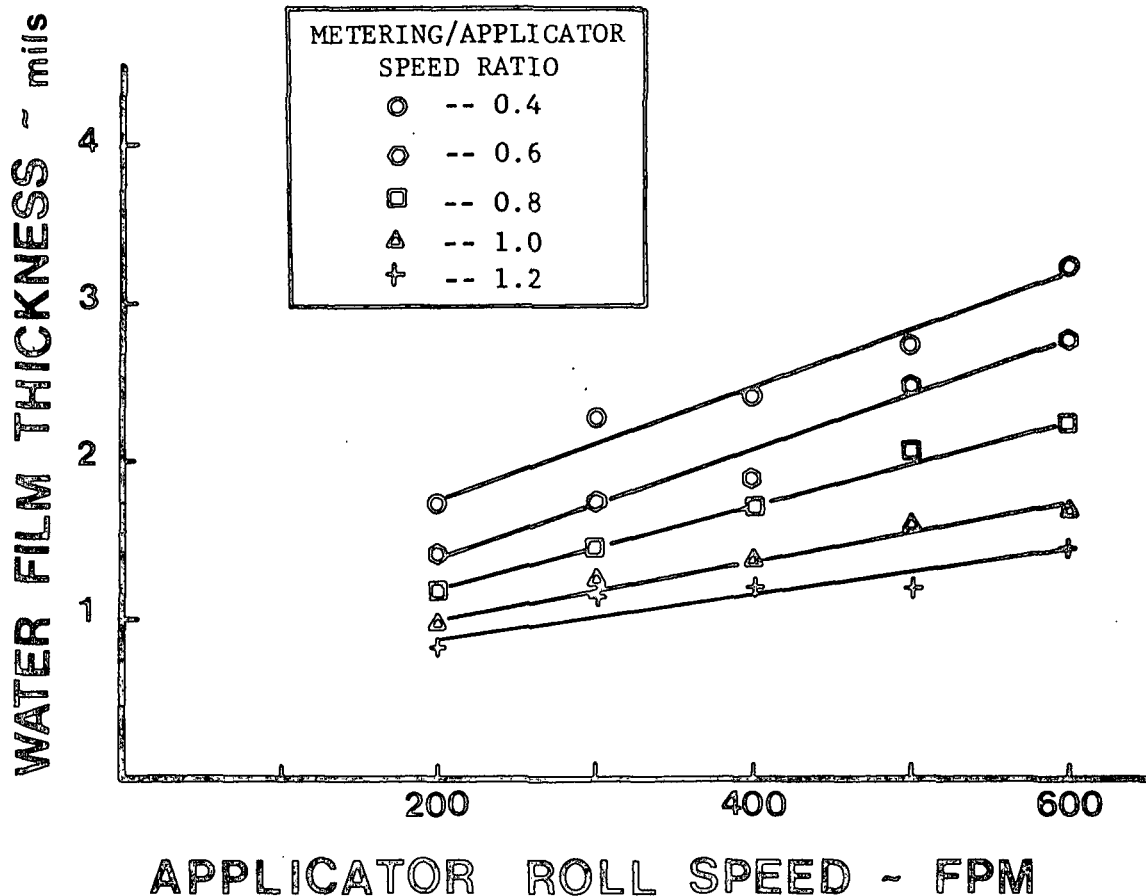
Figure 4.1. Water: Film Thickness Versus Roll Speed

Once this unique phenomenon with speed was discovered, it became obvious that it would be more informative to plot the data with the speed ratio as the abscissa. The experimental results for all the other fluids are presented in this manner.

4.1.2 Metering to Applicator Roll (M/A) Speed Ratio

The result of plotting the data of Fig. 4.1 on a speed ratio basis is shown in Fig. 4.4. The 200, 400, and 600 feet per minute speed lines were extended to higher M/A ratios in an attempt to define a point where the lines of constant speed intersect. The intersection point is indicative of a uniform
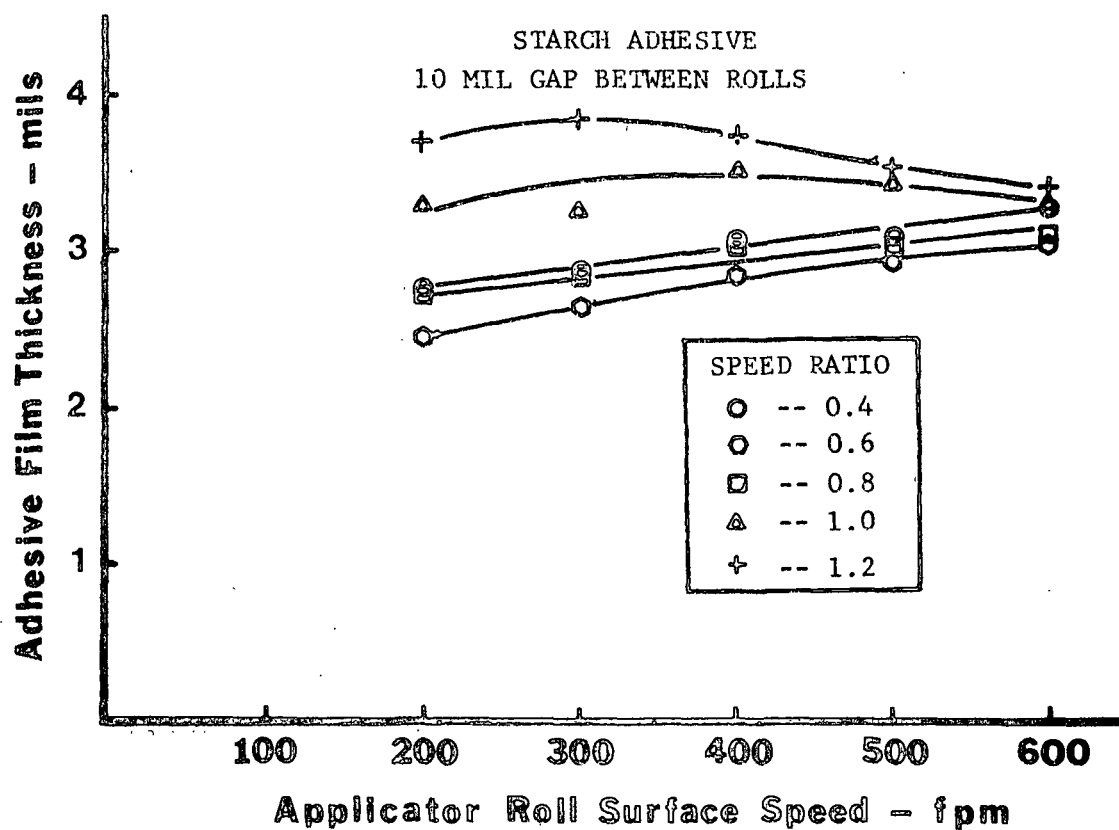
Figure 4.2. Stein-Hall Adhesive (20% Solids): Film Thickness
Versus Roll Speed

POLYBUTENE #6
10 MIL GAP BETWEEN ROLLS
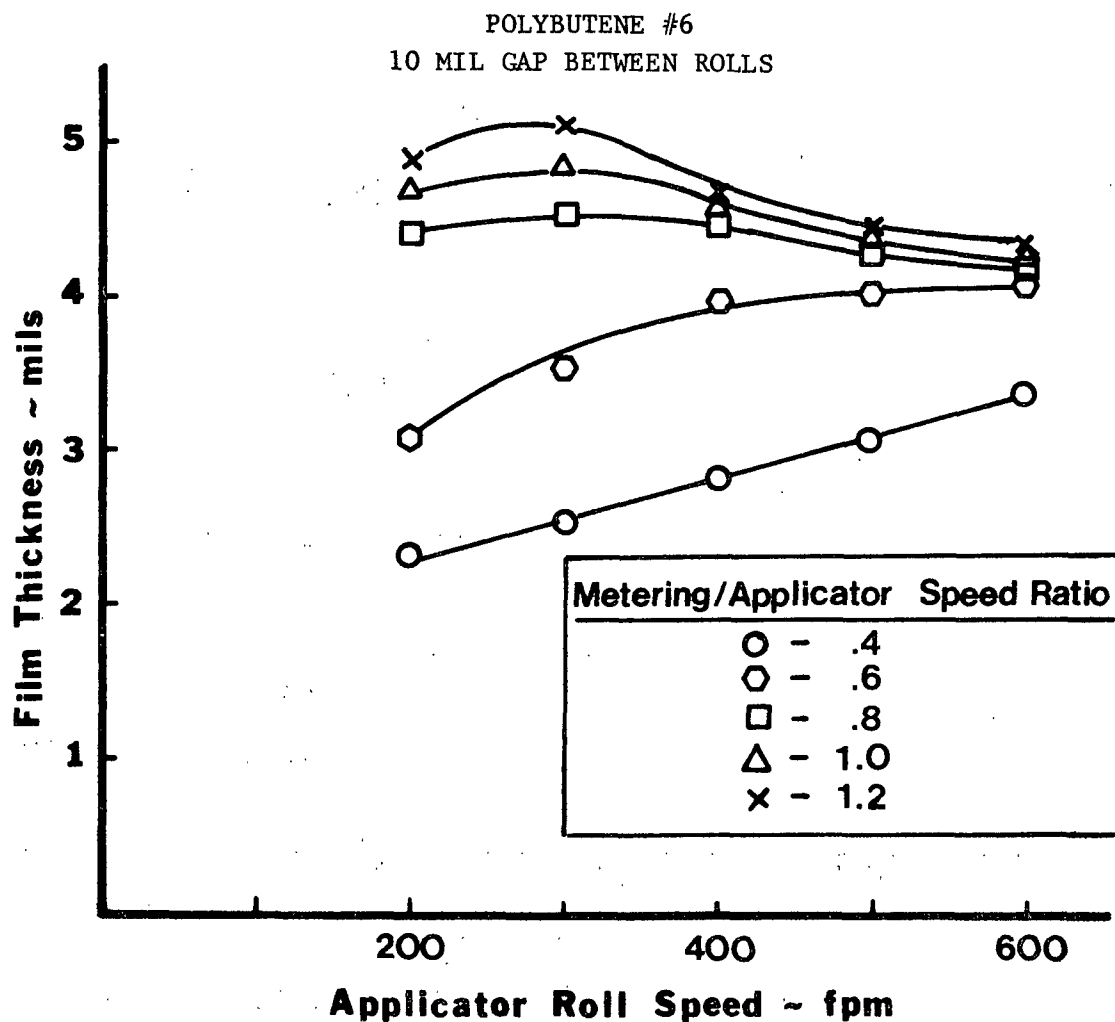
Figure 4.3.   Polybutene #6:   Film Thickness Versus Roll Speed

film thickness for various operating speeds. For water, the speed lines do not

actually intersect for the range of M/A ratios considered but they appear to

reach a common point at a much higher speed ratio.
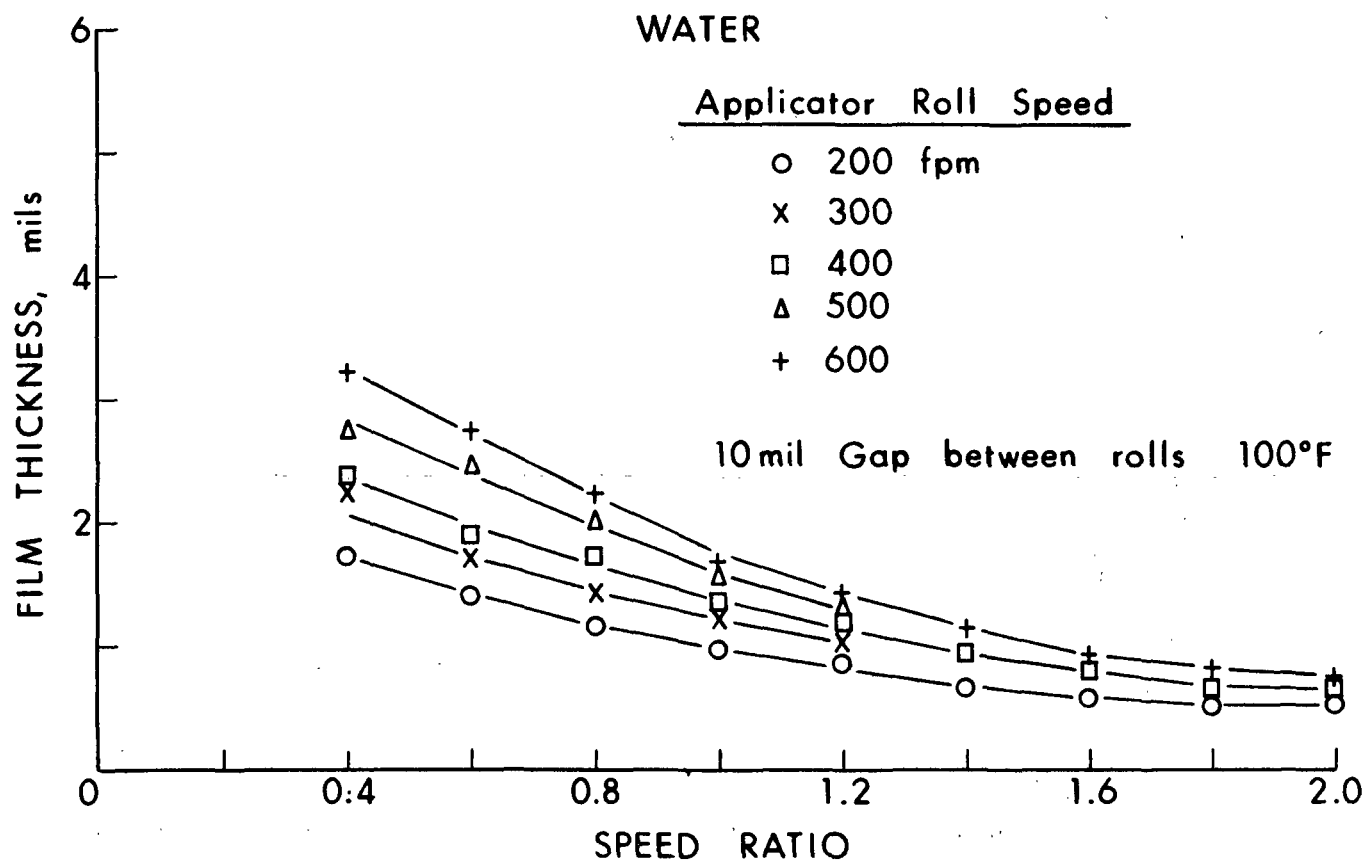
Figure 4.4. Water: Film Thickness Versus Speed Ratio

In Fig. 4.5, the speed lines have an intersection point at a M/A ratio

of approximately 0.6 to 0.8. At speed ratios lower than the intersection point,

higher speeds tend to give larger values for the film thickness. The opposite

tendency is observed for speed ratios greater than the critical value.

Polybutene #6

10 MIL GAP BETWEEN ROLLS
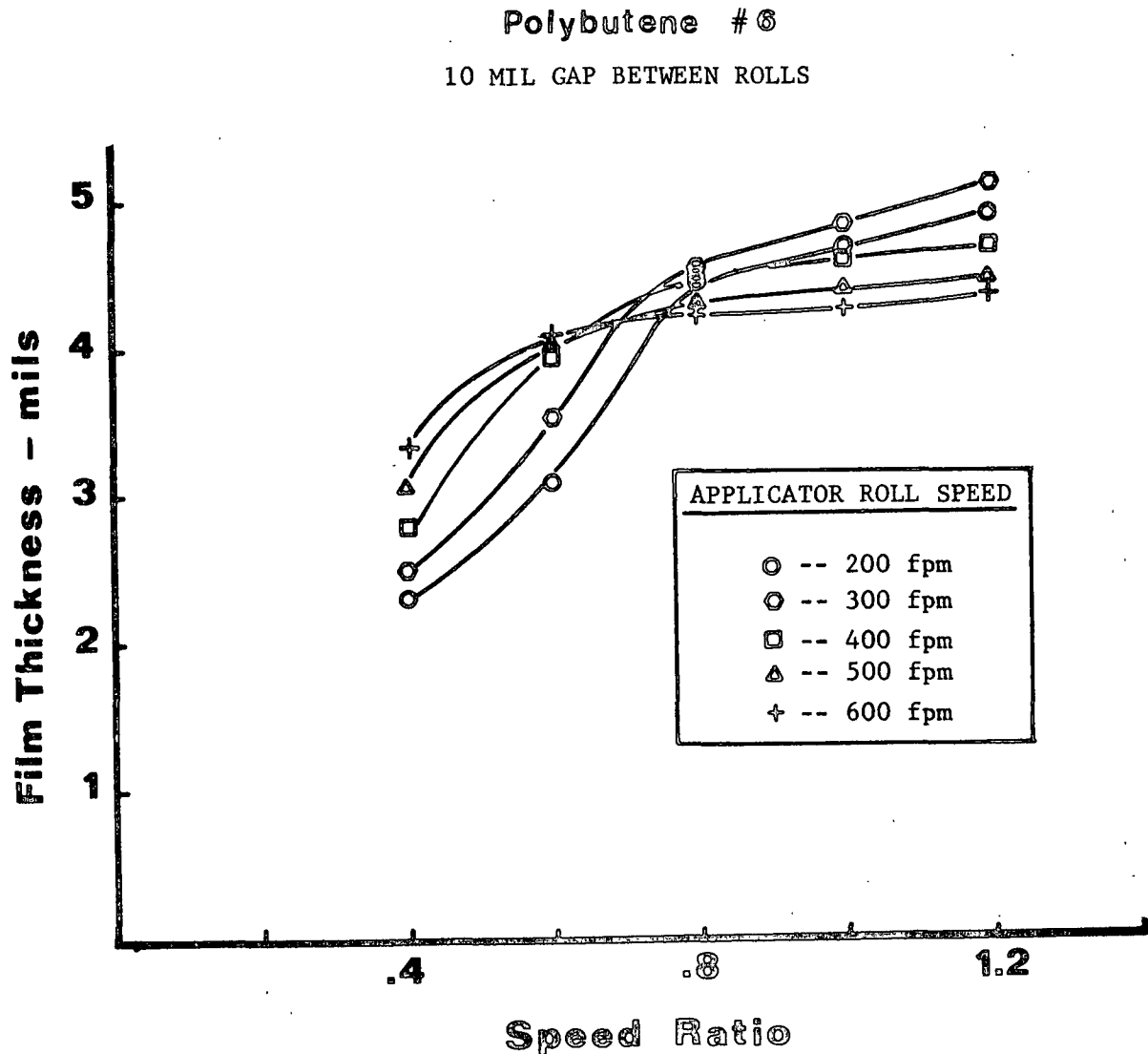
Figure 4.5. Polybutene #6: Film Thickness <u>Versus</u> Speed Ratio

The data for the Stein-Hall adhesive (20% solids) was extended to higher

values of M/A ratio as shown in Fig. 4.6. The intersection point is more clearly

defined at approximately 0.85. Again, there appears to be a great deal of

similarity with the previous curves for oil and water.

When the data for all three fluids are plotted on the same graph (see

Fig. 4.7), the similarity between the fluids is readily seen. All of the fluids

exhibit a preintersection point region where higher speeds yield larger film

thickness. As the M/A ratios increase, the speed lines approach the intersection

point. Both the adhesive and oil have a well defined intersection point. At

M/A ratios greater than the intersection point, the tendency is reversed and the

lower speeds yield the larger films. Additionally, the tendency to reach the

intersection point appears to be correlated with the magnitude of the fluid viscos-

ity. The viscosities of water, adhesive and oil are 1, 33, and 38 cp, respective-

ly, and the intersection point for water occurs at a very large speed ratio while

the critical M/A ratios for the adhesive and the oil decrease according to in-

creasing viscosity (see Table 4.1).

Figure 4.6. Stein-Hall Adhesive (20% Solids): Film Thickness
Versus Speed Ratio

Figure 4.7. The Similarity of Speed Ratio Plots for Water, Adhesive, and Oil

TABLE 4.1

DEPENDENCE OF SPEED RATIO INTERSECTION POINT
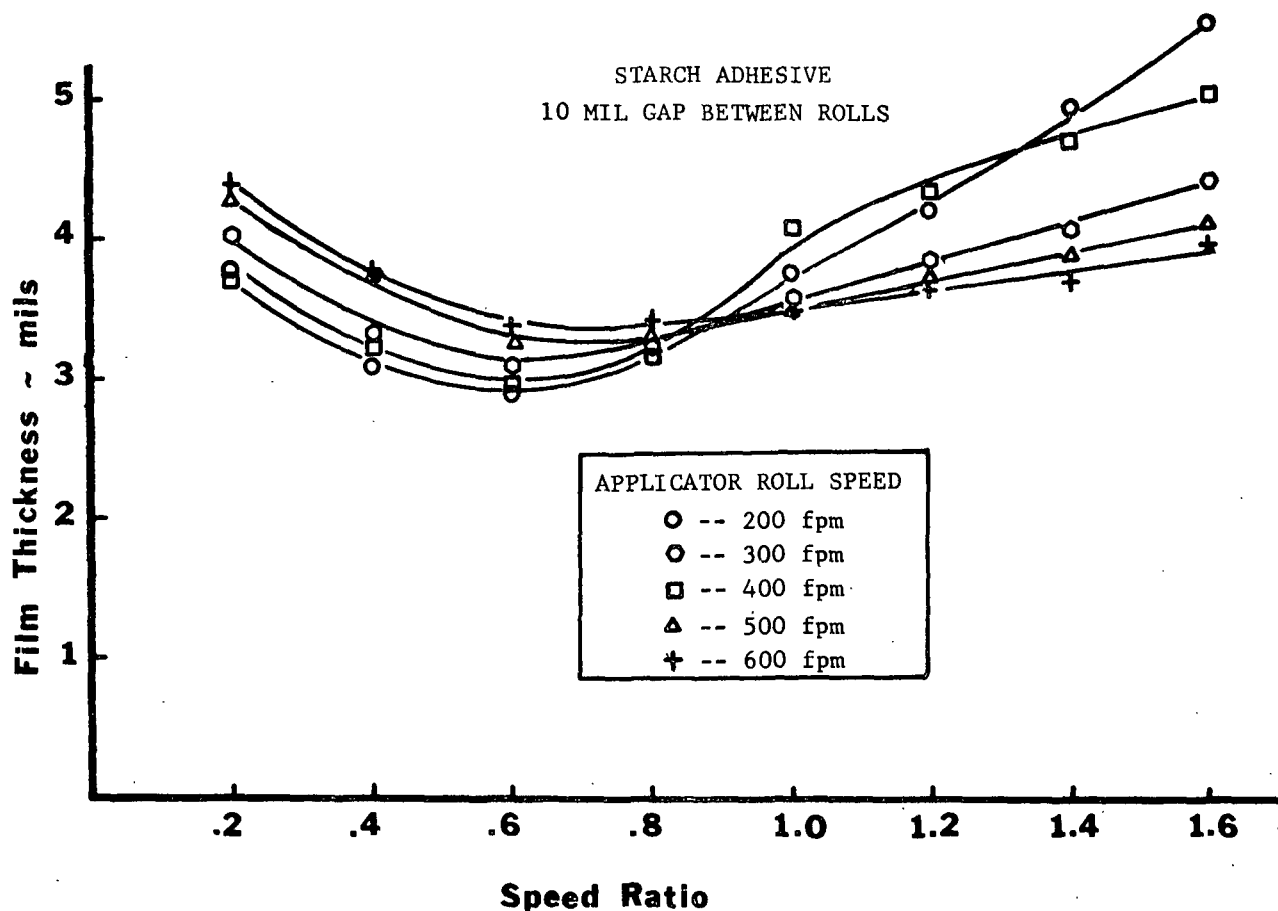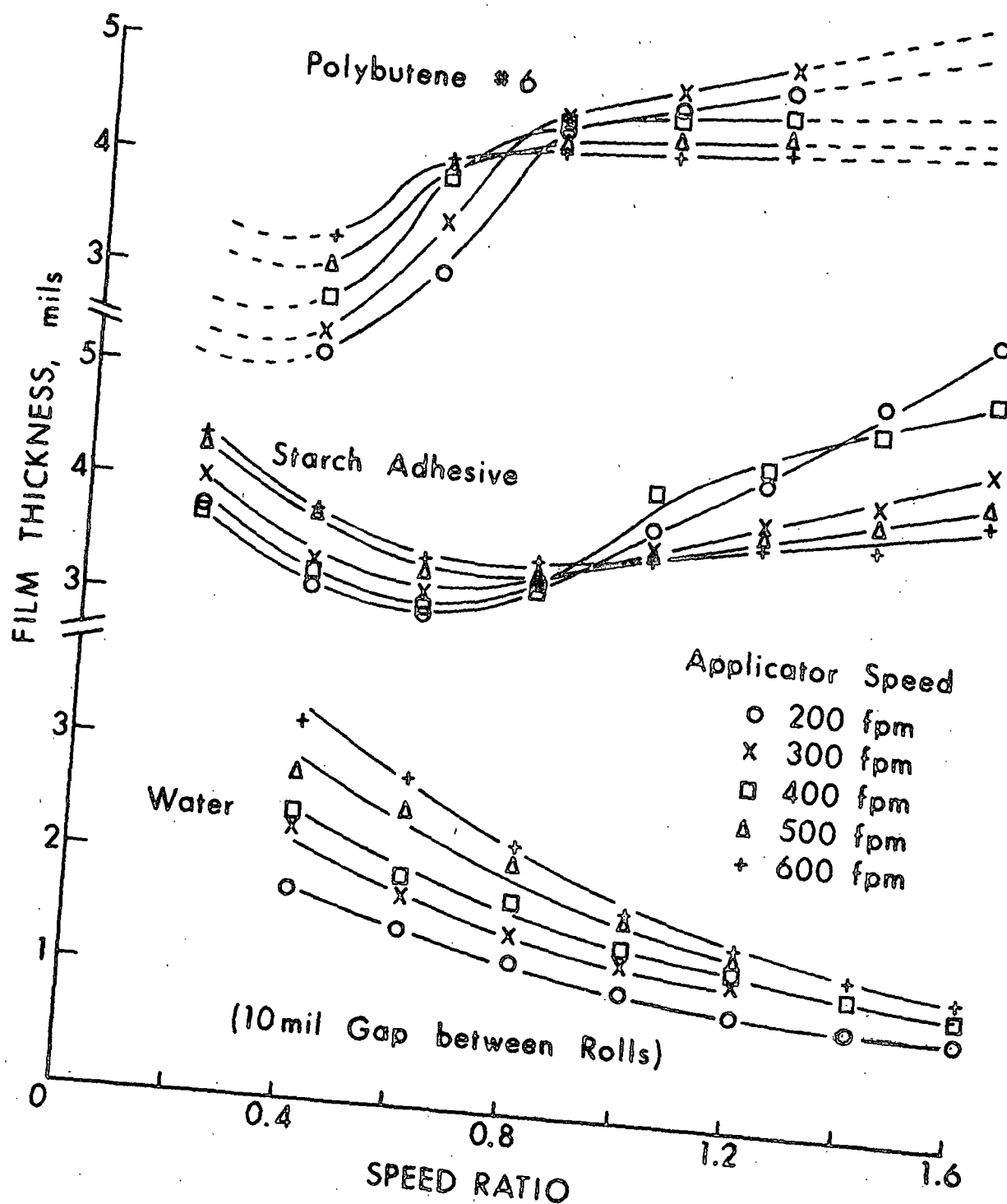ON FLUID VISCOSITY

Fluid	Viscosity, cp	Speed Ratio at Intersection Point
Water	1	Large
Adhesive	33	~0.80
Oil	38	~0.70

The similarity between curves for water, oil, and the starch adhesive is surprising since the water and oil are well-behaved Newtonian fluids and the starch adhesive is slightly thixotropic. In the Introduction, it was stated that the unpredictable variation in the film thickness was often attributed to the complex rheological behavior of the starch adhesive. The similarity shown here indicates that a common mechanism is controlling the behavior of the fluids but it is not related to the thixotropy of the adhesive. The rheogram for a starch adhesive in Fig. 3.6 supports this premise. At the high shear rates experienced in the nip, i.e., above 5000 sec^{-1}, the relationship is nearly linear for both the up and down portions of the curve. This implies that in this range the adhesive behaves like a Newtonian fluid. Additionally, there is only a small spacing between the lines and this is equivalent to at most a few centipoise in viscosity. The similarity of the fluids discussed in the preceeding paragraph implies that the mechanisms controlling the film thickness are related to the fluid dynamics of the system and the magnitude of the high shear viscosity. This dependence on the system dynamics and fluid viscosity rather than the complex rheology of the adhesive is demonstrated by the bulk of material remaining in this section.

To clarify the relationship between the intersection point and viscosity, several other fluids with a variety of viscosities were tested. In Fig. 4.8, the speed ratio plot for a no-carrier adhesive with a 20% solids content is shown. The curve is very similar to Fig. 4.6 for the Stein-Hall adhesive at 20% solids. The high shear viscosity of the no-carrier adhesive is approximately 31 cp and is slightly lower than the value of the Stein-Hall adhesive. Assuming that an increase in viscosity drives the intersection point closer to the origin, the intersection point for this fluid should have a slightly larger value than that of the Stein-Hall adhesive. A comparison of Fig. 4.8 and 4.6 shows that the correct tendency is predicted.
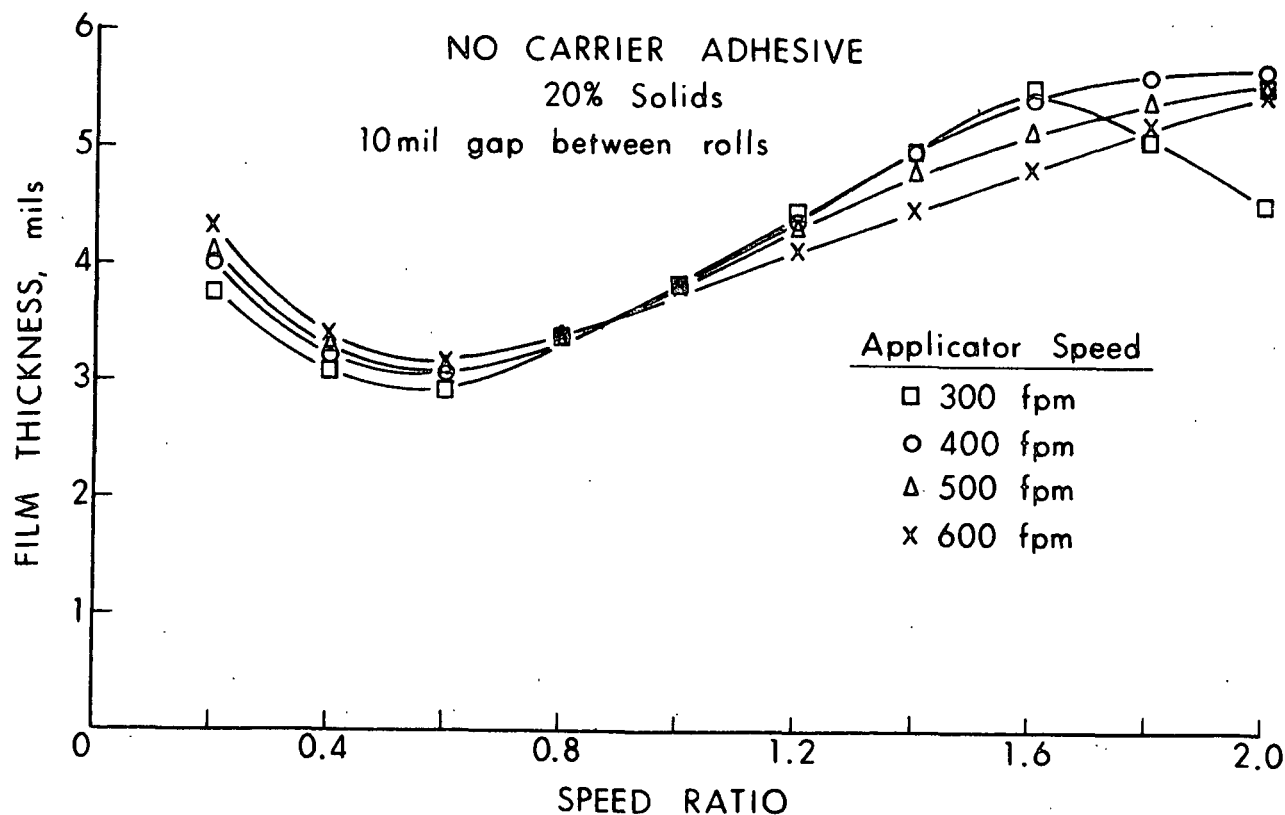
Figure 4.8. No-Carrier Adhesive (20% Solids): Film Thickness Versus Speed Ratio

Thus far, all the fluids considered except water have had approximately the same high shear viscosity and appear to have similar mechanisms controlling the shape of the speed ratio curves. Several other fluids were tested to verify the relationship between viscosity and intersection point and to possibly define the behavior of fluids with viscosities between water and those of approximately 30 cp.

The results for Magie oil #500, an oil with a viscosity of about 5 cp, are shown in Fig. 4.9. Although the constant speed lines do not reach an intersection point, they do resemble the speed ratio curves for water (Fig. 4.4). The film thickness decreases and the speed curves level out as the M/A ratios are increased above 1.0. The similarity with water is expected since the fluids have nearly the same viscosity.

MAGIE OIL No. 500

Applicator Roll Speed

o 200 fpm
x 300
Δ 500
+ 600

10 mil Gap between rolls
100°F 1.5" Pan depth
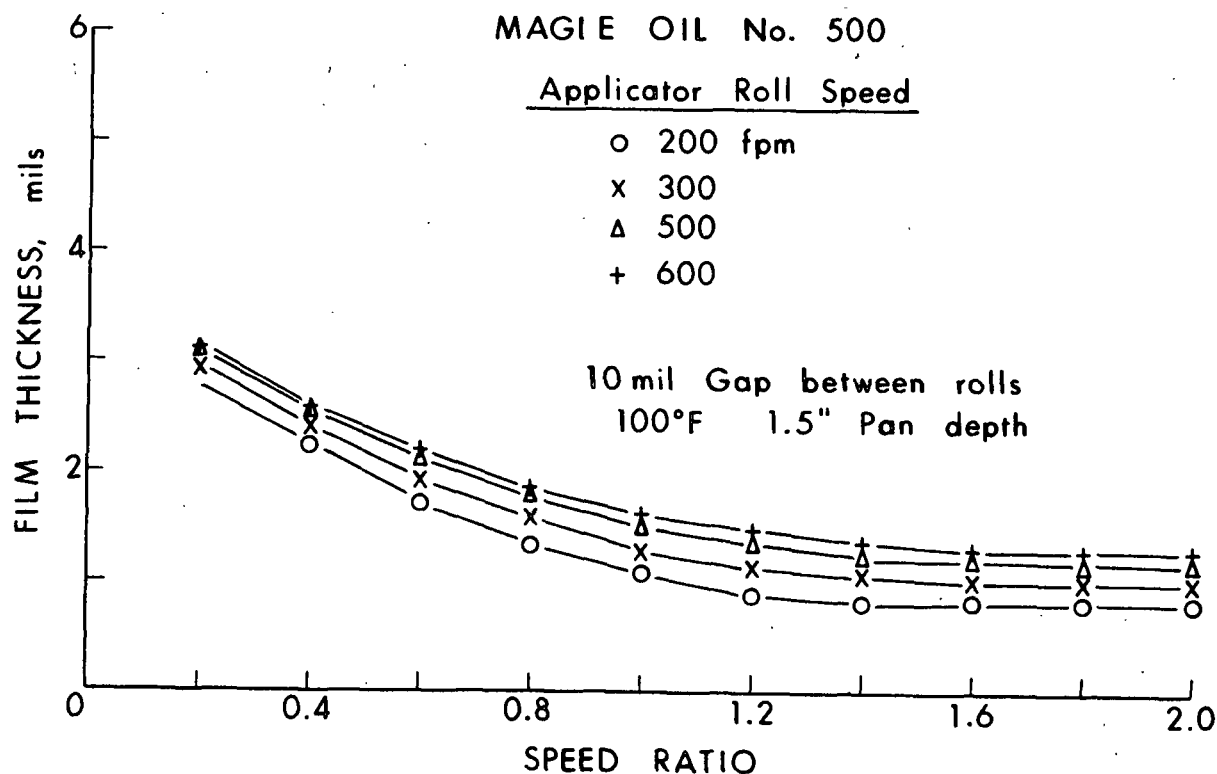
Figure 4.9. Magie Oil #500: Film Thickness Versus Speed Ratio

Two more Stein-Hall adhesive formulations are compared in Fig. 4.10 and 4.11. The first adhesive is a 17% solids mix and has a viscosity of approximately 29 cp. The shape of the curve is similar to the other adhesives and, as expected, the intersection point moves to a slightly higher M/A ratio (just over unity). The other adhesive formulation has a 26% solids content and a high shear viscosity of approximately 45 cp. With the higher viscosity, it is expected that the intersection point would move closer to the origin (speed ratio = 0). Unfortunately some problems were encountered with maintaining the starch consistency and a well-defined intersection point was not obtained. However, by comparing the general shape of this curve with previous results, a rough estimate of the location of the intersection point or the area in which a change in controlling mechanisms takes place can be made. The estimated location is at a speed ratio between 0.4 and 0.6. Again the hypothesis is reinforced.
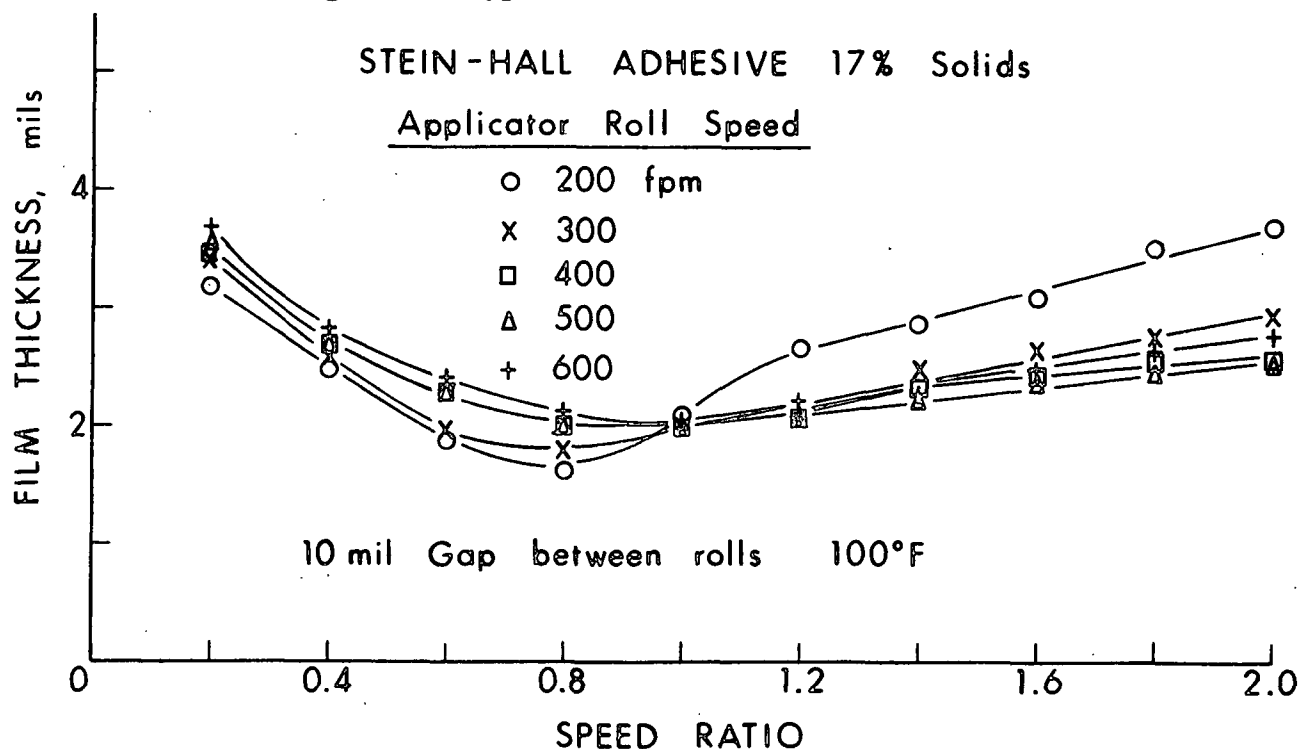
Figure 4.10. Stein-Hall Adhesive (17% Solids): Film Thickness Versus Speed Ratio at 100°F
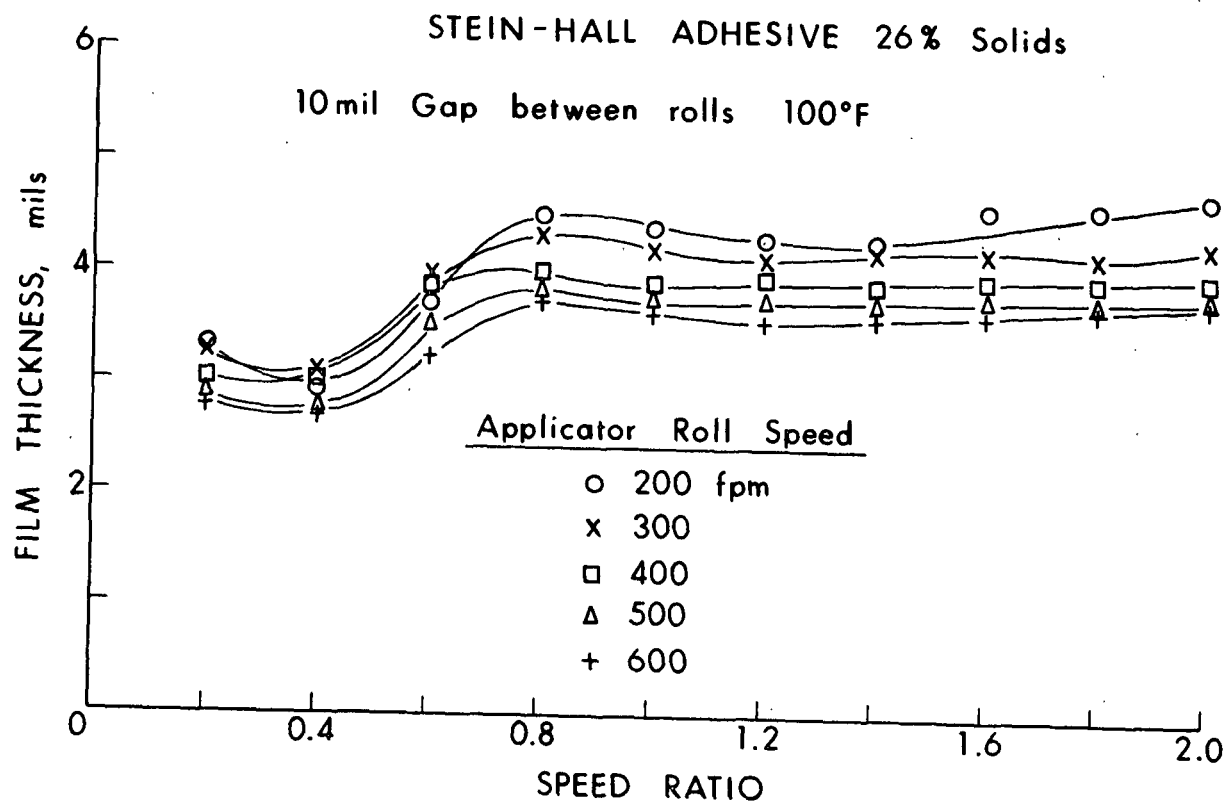
Figure 4.11. Stein-Hall Adhesive (26% Solids): Film Thickness Versus
Speed Ratio at 100°F

To complete the investigation of the intersection point-viscosity

relationship, a high viscosity fluid (Polybutene #8) was tested. The viscosity

of the oil is about 200 cp and is an order of magnitude larger than the other

fluids. In Fig. 4.12, the speed lines are similar to those observed at M/A

ratios beyond intersection point, i.e., lower speeds have the larger films

thicknesses. This implies that the change in mechanisms which causes the

point of intersection occurs at a very low speed ratio and only the postinter-

section point region is observed. Again, the relationship between intersection

point and high shear viscosity is supported.

As a brief summary for this section, Fig. 4.13 shows a plot of inter-

section points versus the high shear viscosities for all of the tested fluids.

Very high and very low viscosity fluids appear to represent extremes where

different mechanisms are dominating the behavior of the fluids in the applicator system. Starch adhesives and the Polybutene #6 oil have intermediate viscosities for which the shift from one mechanism to the other causes an intersection of the speed lines.
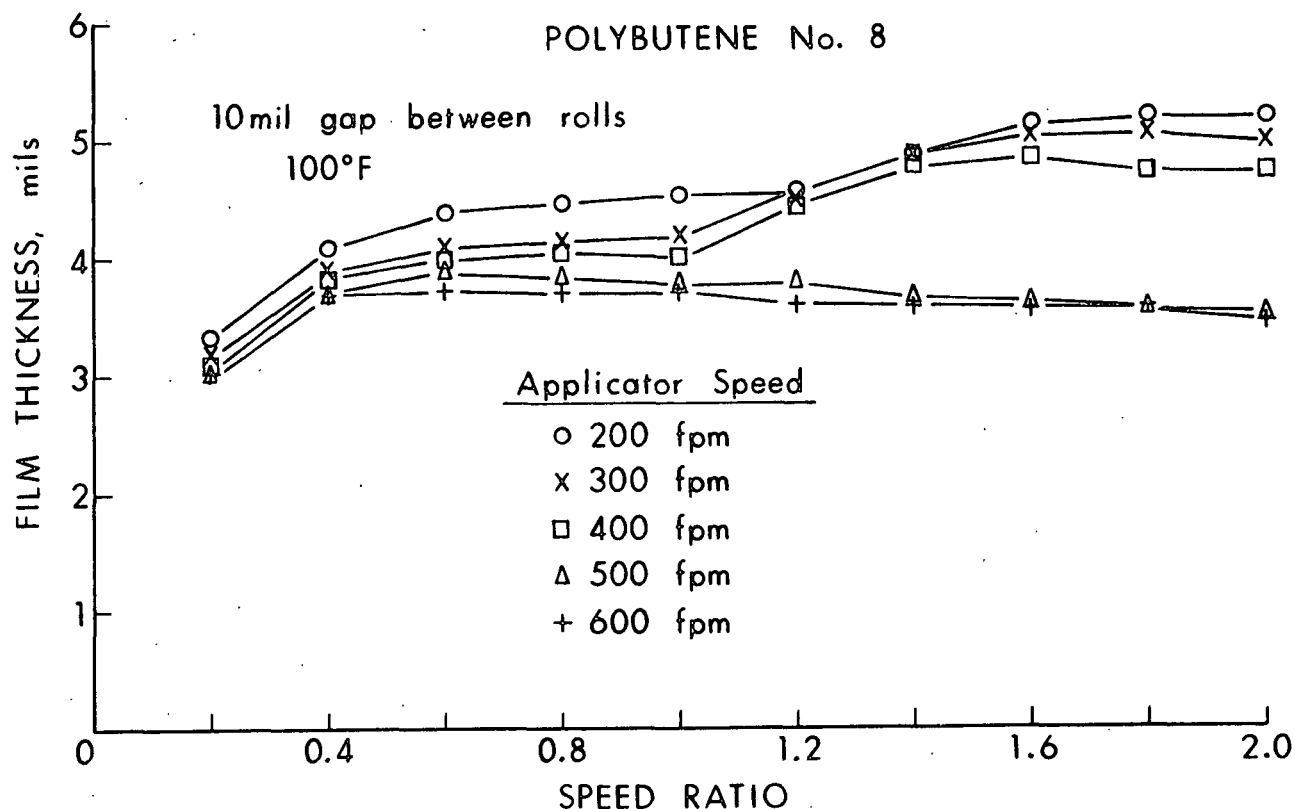
Figure 4.12. Polybutene #8: Film Thickness _Versus_ Speed Ratio

4.1.3 Temperature Effects

The effect of increasing the temperature of the Magie oil is shown in Fig. 4.14. Raising the temperatures corresponds to a drop in the fluid viscosity and the film thickness becomes slightly larger at the low M/A speed ratios.

The Fig. 4.15 and 4.16 illustrate the movement of the intersection point as the viscosity is changed for a starch adhesive. The temperature effect on viscosity is exactly opposite of the trend seen with the oil. Recall that increasing the temperature of the adhesive drives it closer to its gel point and
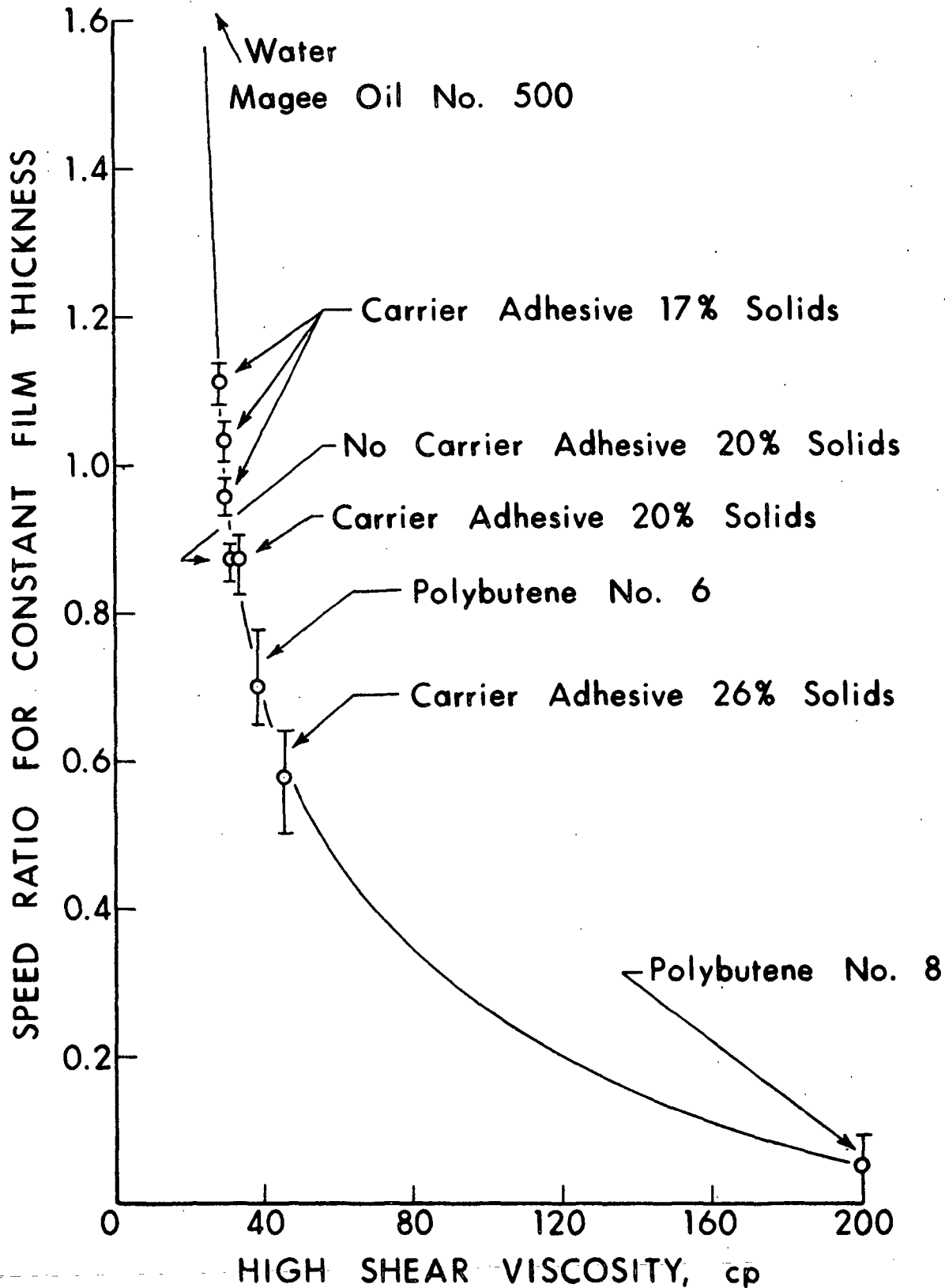
Figure 4.13.   Speed Ratio Intersection Points Versus High Shear Viscosity
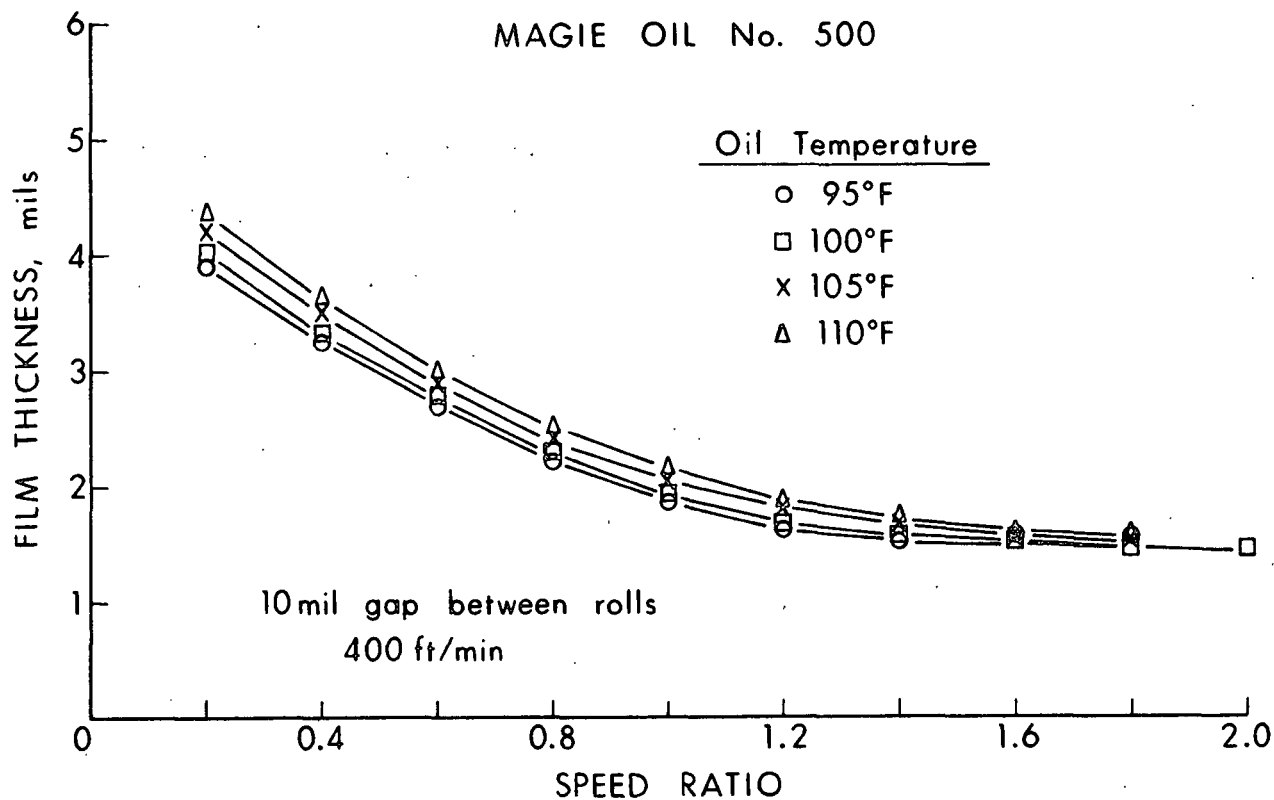
Figure 4.14. Temperature Effect on Film Thickness, Magie Oil #500

therefore increases its viscosity. As the temperature is increased from 95°F to

105°F, the intersection point moves from about 1.1 to 0.95. In fact if the data

from Fig. 4.10, 4.15, and 4.16 are plotted together as shown in Fig. 4.17, the

motion of the point of intersection with viscosity is clearly illustrated. The

film thickness is uplifted with increasing temperature and the intersection point

is moved toward lower values of speed ratio. The increased viscosity is respon-

sible for a larger film thickness at the higher M/A ratios but it has little

effect at the lower values.
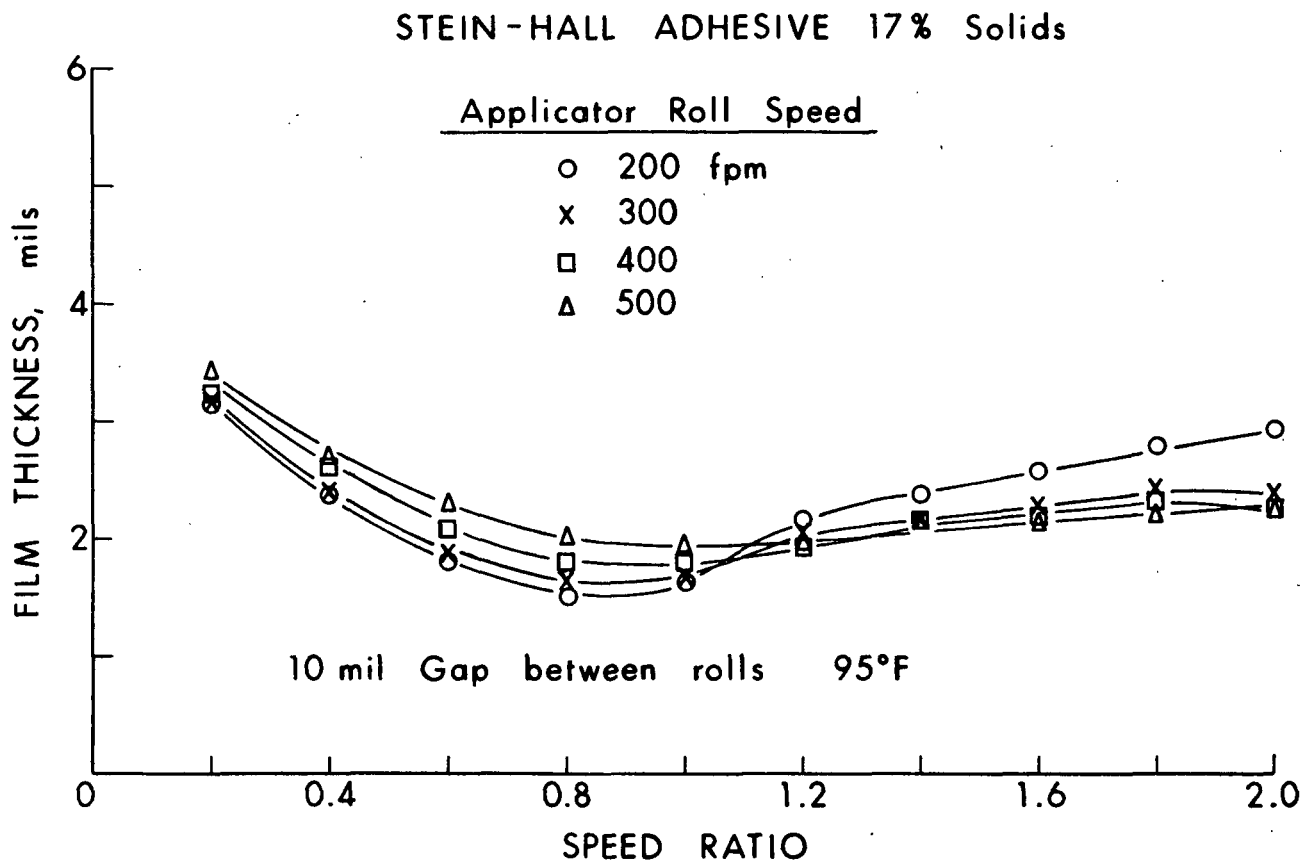
Figure 4.15. Stein-Hall Adhesive (17% Solids): Film Thickness Versus
Speed Ratio at 95°F
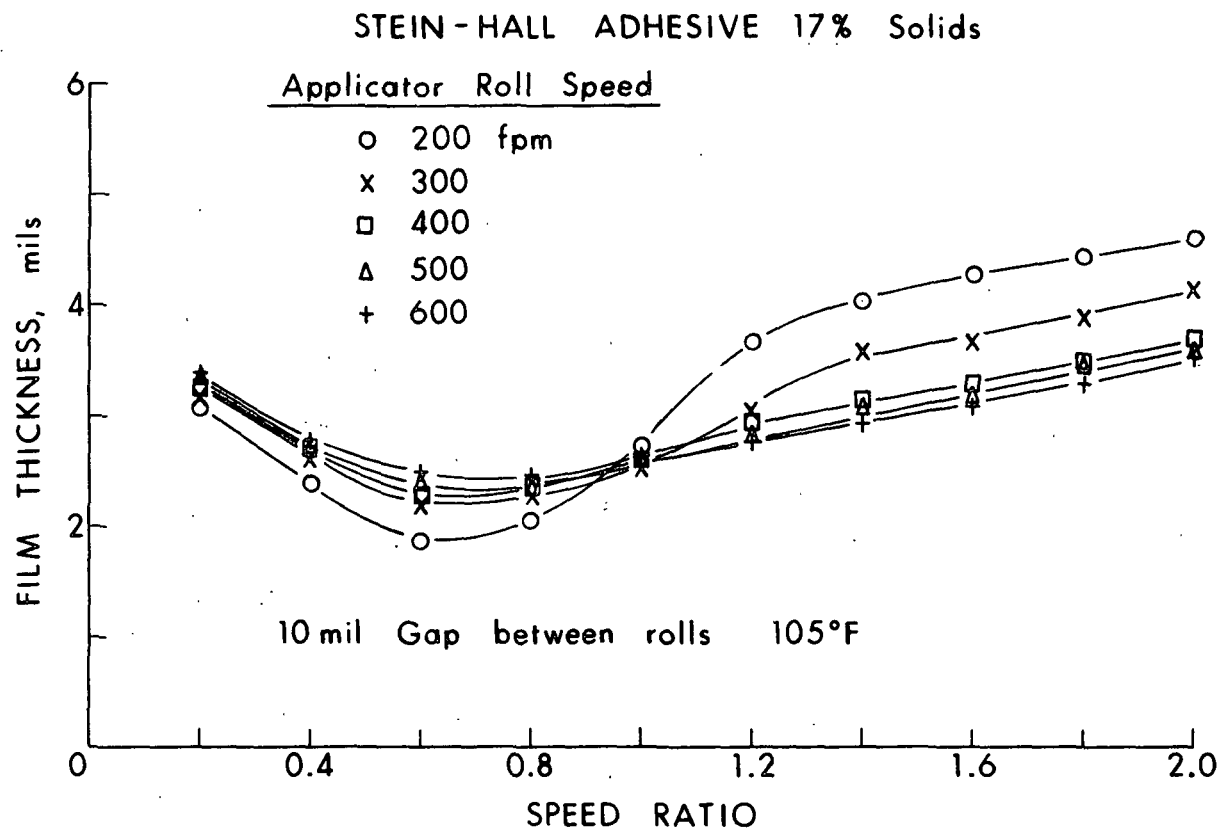
Figure 4.16. Stein-Hall Adhesive (17% Solids): Film Thickness Versus
Speed Ratio at 105°F

STEIN-HALL CARRIER ADHESIVE 17% Solids

Adhesive Temperature

o 95°F
□ 100°F
Δ 105°F

🖎 Intersection Points

FILM THICKNESS, mils

10 mil gap between rolls
200 ft/min

SPEED RATIO
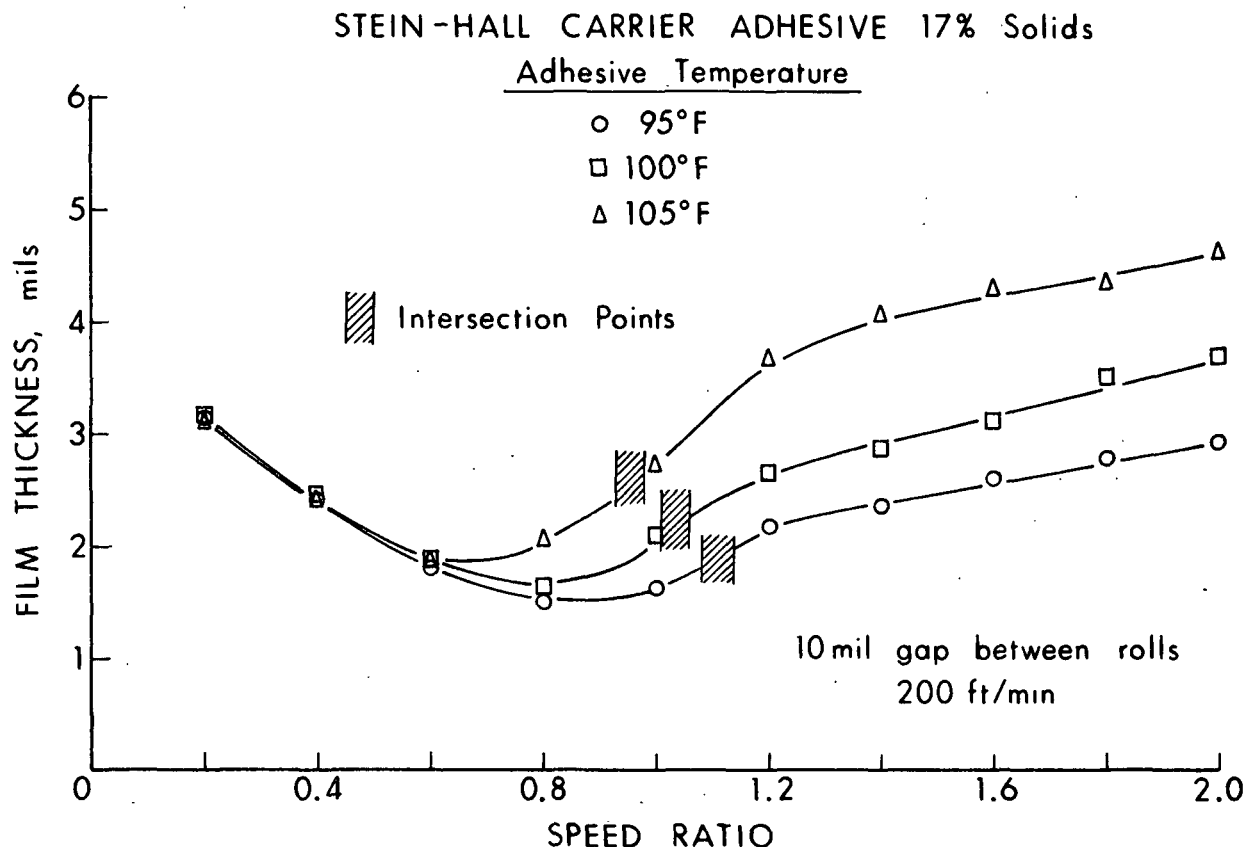
Figure 4.17. Temperature Effect: Stein-Hall Adhesive (17% Solids)

Finally, a similar phenomena is observed in Fig. 4.18 which shows the effect of temperature on the 26% solids Stein-Hall adhesive. With increasing temperature and therefore viscosities, the uplifted portion of the curve moves toward the origin. The uplifting of the speed lines cause the intersection point and is highly correlated with the fluid viscosity.

4.1.4 Gap Spacing

Logically, the gap spacing between the rolls is expected to exert a large influence on the film thickness. The following results demonstrate that although the variations in film thickness with gap spacing are sizable, they are quite predictable and well behaved.

STEIN - HALL ADHESIVE 26% Solids
10 mil Gap between rolls
400 fpm (Applicator roll speed)
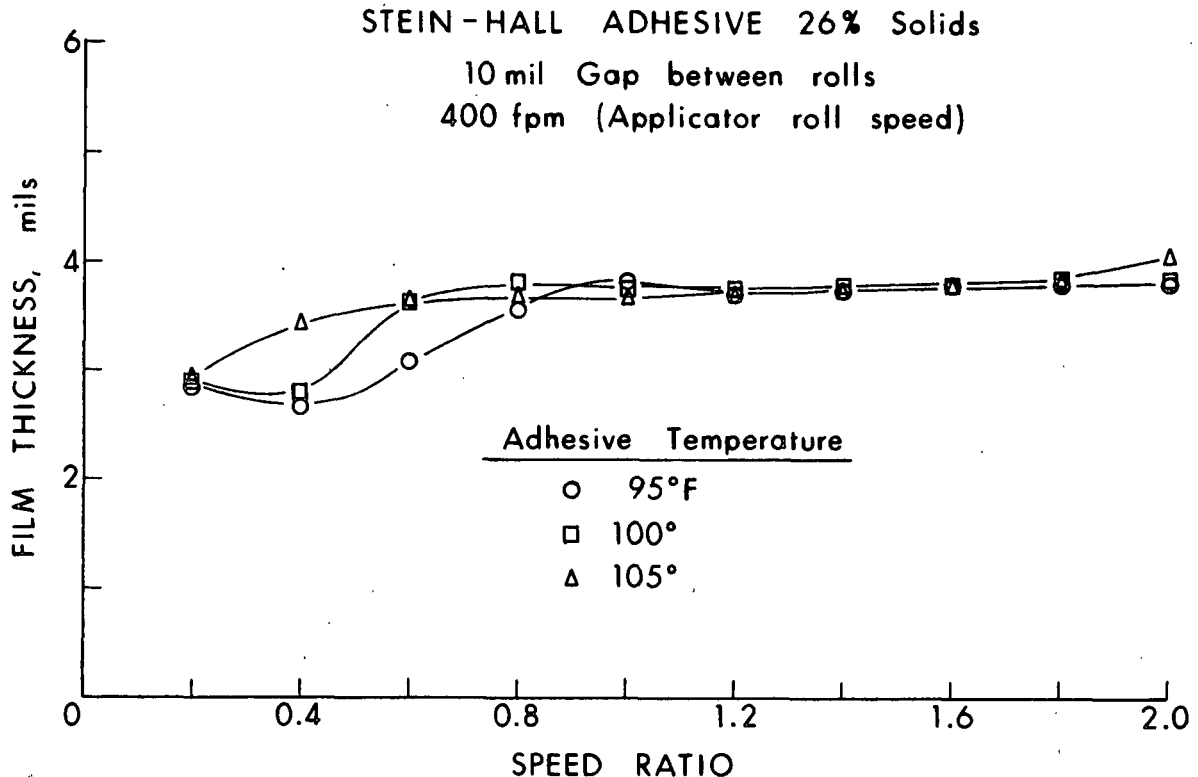
Figure 4.18. Temperature Effect: Stein-Hall Adhesive (26% Solids)

In Fig. 4.19, 4.20, 4.21, and 4.22, the increases in film thickness

with gap spacing are uniform whether the data is plotted on a speed or speed ratio

basis. Also, the percentage increase in the film thickness for a specific gap

increment is not strongly dependent upon the fluid. In general, the higher vis-

cosity fluids tend to yield a slightly larger percentage increase in film thick-

ness. The relationship between the gap spacing and film thickness is almost con-

stant and linear as shown in Fig. 4.23. This result suggests that the gap spacing

is a suitable control variable for making modifications in the film thickness.

Also, the repeatibility of the data is demonstrated in Fig. 4.23.

4.1.5 Depth of Roll Submersion

Another parameter that was believed to exert some influence on the

film thickness is the depth of roll submersion into the fluid. The results
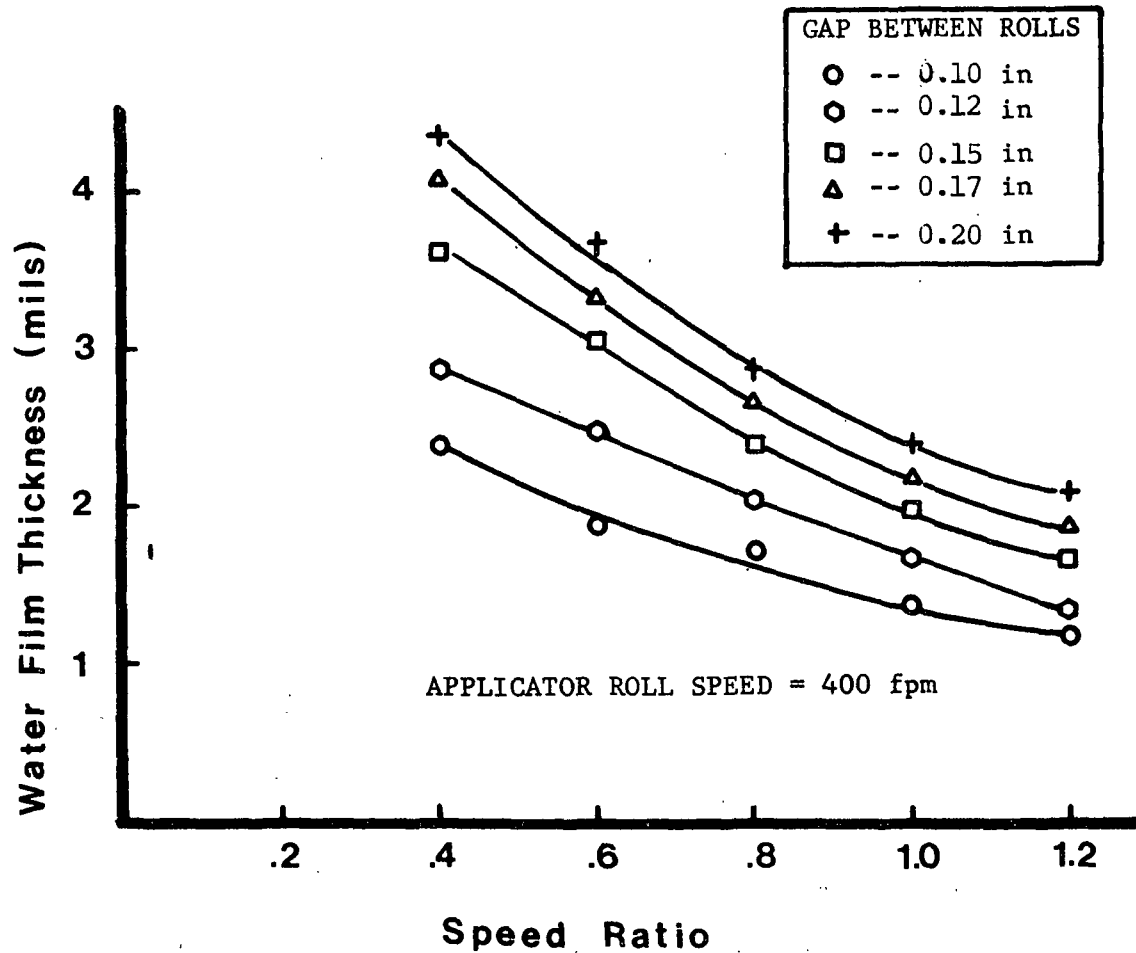
Figure 4.19. Gap Between Rolls: Water
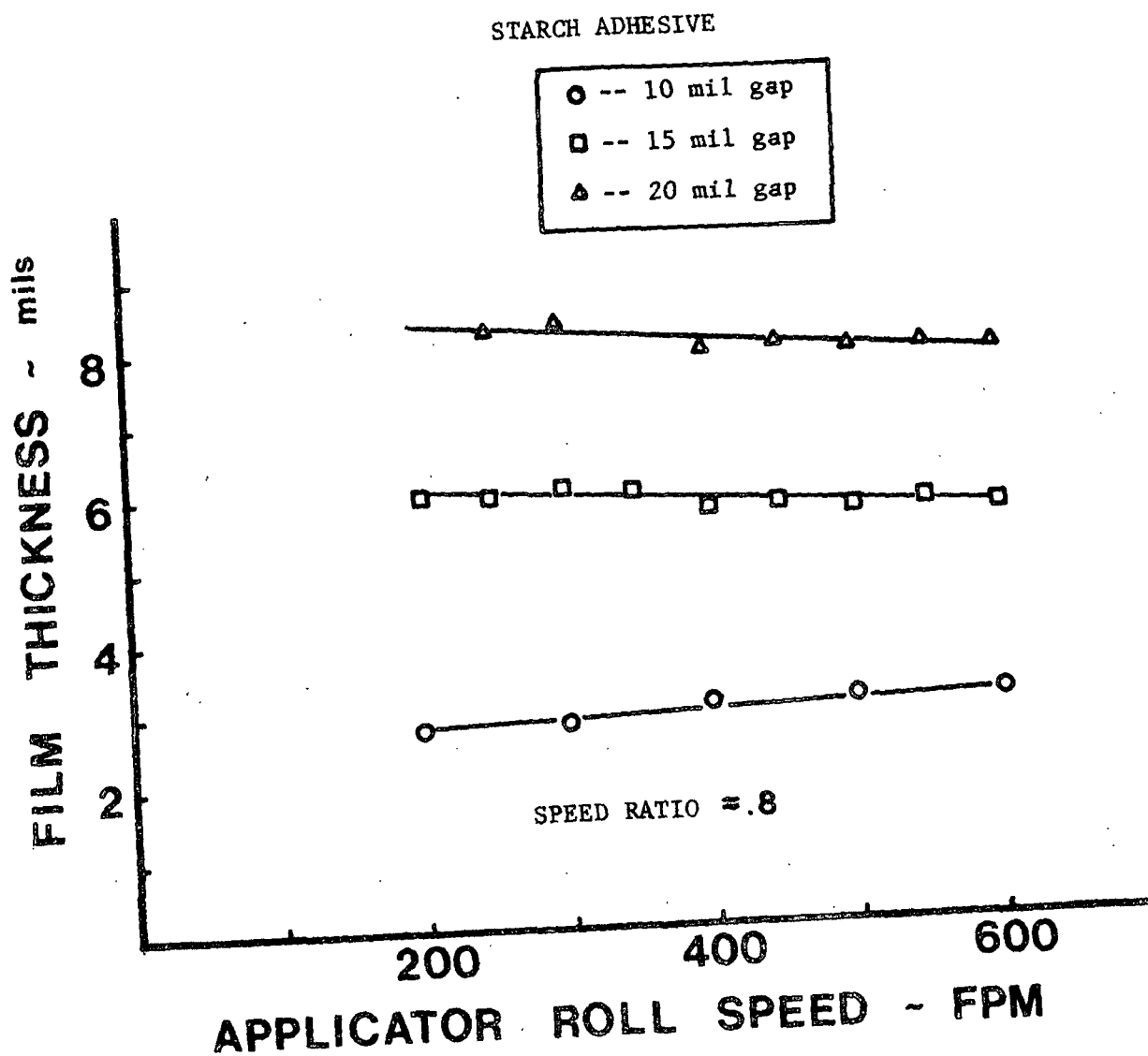
Figure 4.20. Gap Between Rolls: Stein-Hall Adhesive (20% Solids)
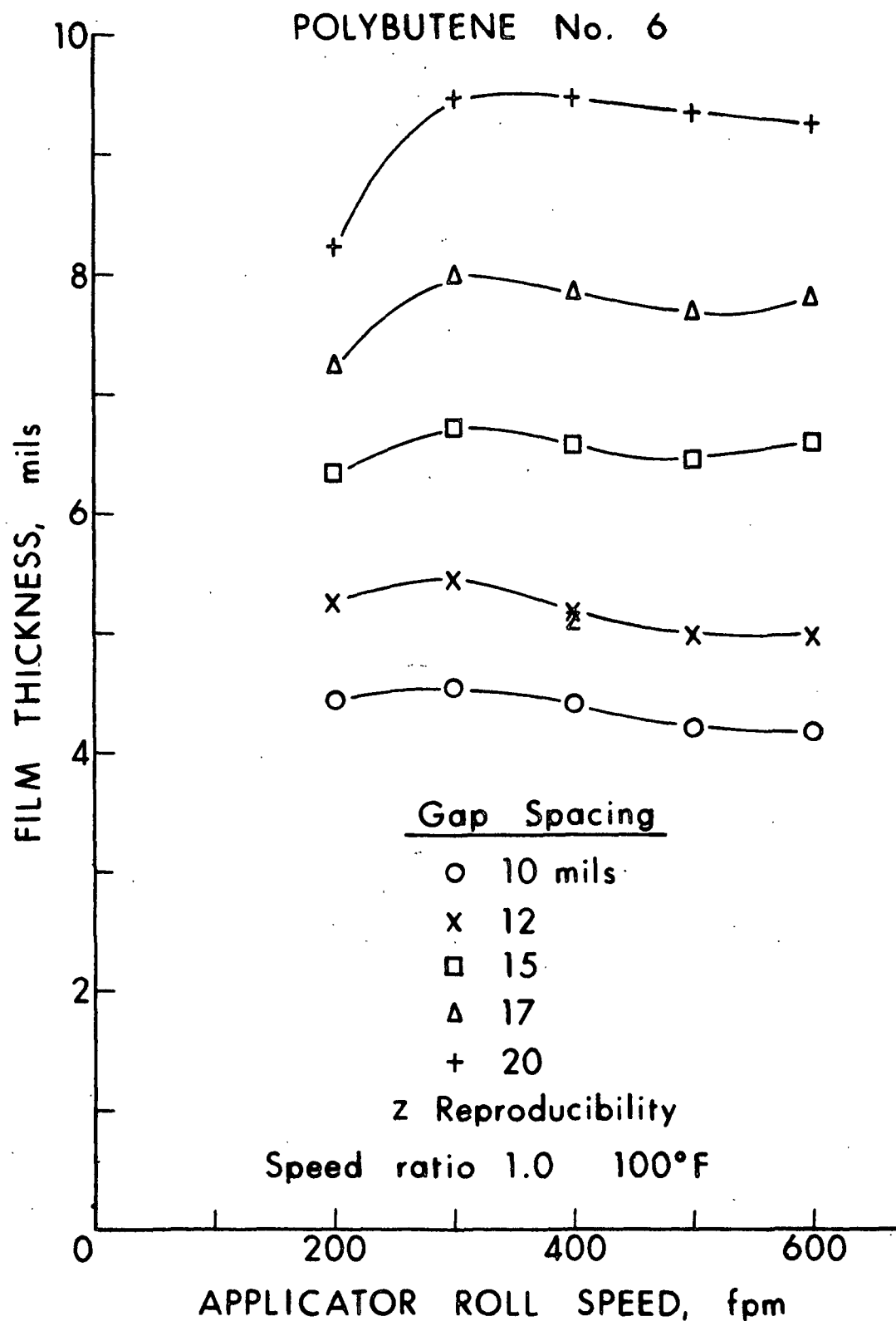
POLYBUTENE No. 6

Figure 4.21.   Gap Between Rolls: Polybutene #6
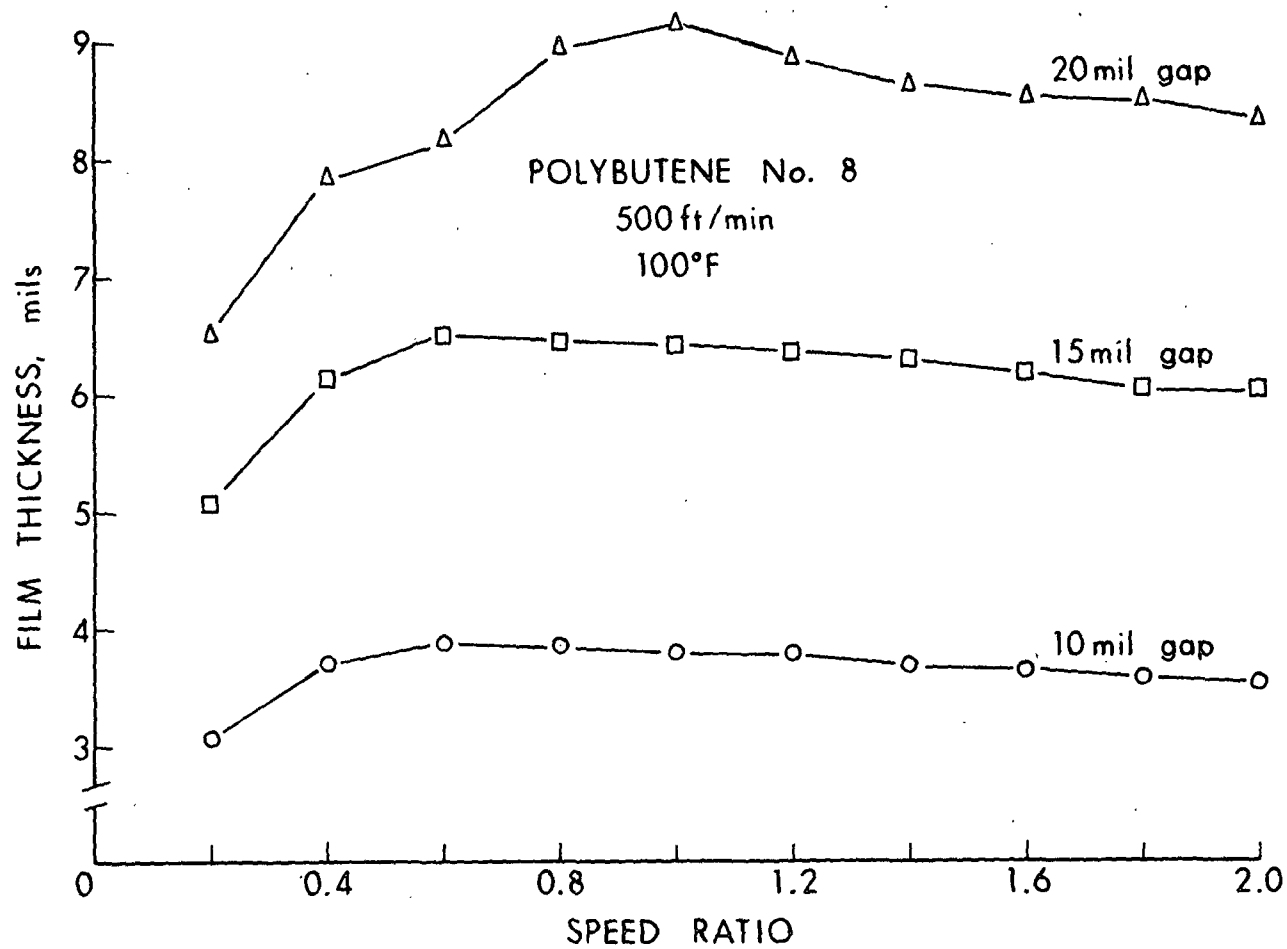
Figure 4.22.   Gap Between Rolls: Polybutene #8
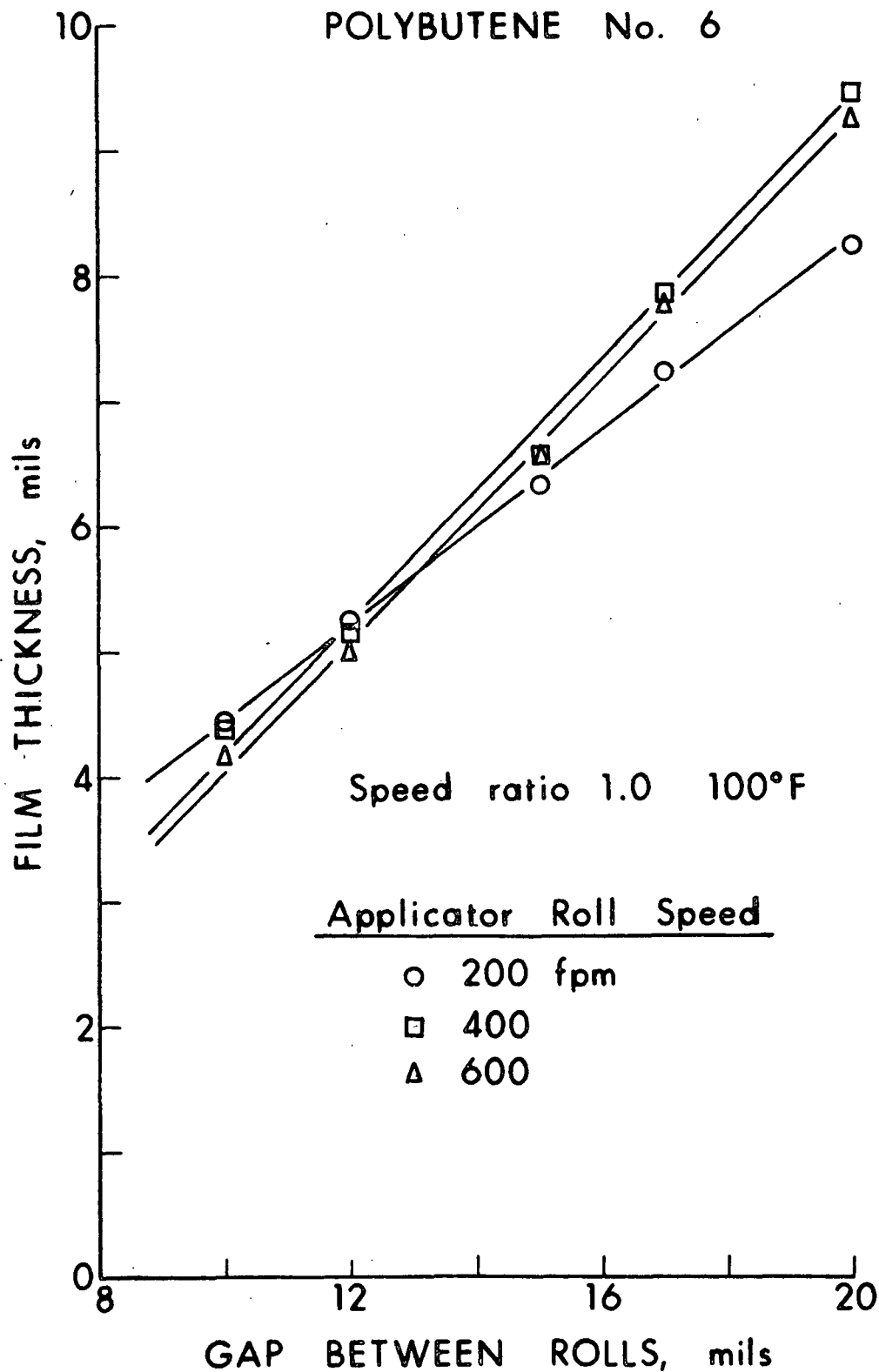
Figure 4.23. Effect of Gap Between Rolls on Speed

are shown in Fig. 4.24, 4.25, and 4.26 for water, Magie oil, and Polybutene #6.

For water (Fig. 4.24), the film thicknesses for the 1.0 and 1.5 inch depths

are almost identical. However, when the depth is lowered to 0.5 inch, there

is a small increase in film thickness. This last result is somewhat surprising

since the opposite trend would be expected. The film thicknesses for Magie oil

in Fig. 4.25 appear to be only slightly affected by depth changes and it is dif-

ficult to analyze the differences since the error bands are of the same order of

magnitude as the differences. In Fig. 4.26 for Polybutene #6, there is a dramatic

change in film thickness. At high speeds, the film thickness drops substantially

for the 1.0-inch depth implying that the roll contact time with the fluid in the

tray is reduced to a point where a smaller amount of fluid is picked up. Since

less fluid is forced into the nip, the film thickness decreases.

4.2 ANALYTICAL RESULTS

The basic equation for the film thickness on the applicator roll is

derived in Section 2 and Equation (2.23) is restated here for convenience.

$$\delta_a = (1 - u_m/u_a)\, h_m/2 + \frac{4}{\pi^2}\,(1 + u_m/u_a)\, h_m\, e^{-t/t_1} \qquad (4.1)$$

The equation consists of steady state and developing flow contributions, and the

exponent of the time dependent contribution is expressed in terms of the shearing

time, t, and the time constant, t_1. No attempt was made to use this equation for

modeling the experimental data because the gap spacing, h_m, and the shearing

time, t, are unknown functions of the system parameters and fluid properties.

However, the model qualitatively predicts the tendencies seen in experimental

data.

SUBMERSION DEPTH
O -- 0.5 inches
▢ -- 1.0 inches
▲ -- 1.5 inches

10 MIL GAP BETWEEN ROLLS

APPLICATOR ROLL SPEED = 400 fpm

SPEED RATIO = 0.8

Water Film Thickness ~ mils

Applicator Roll Speed ~ fpm
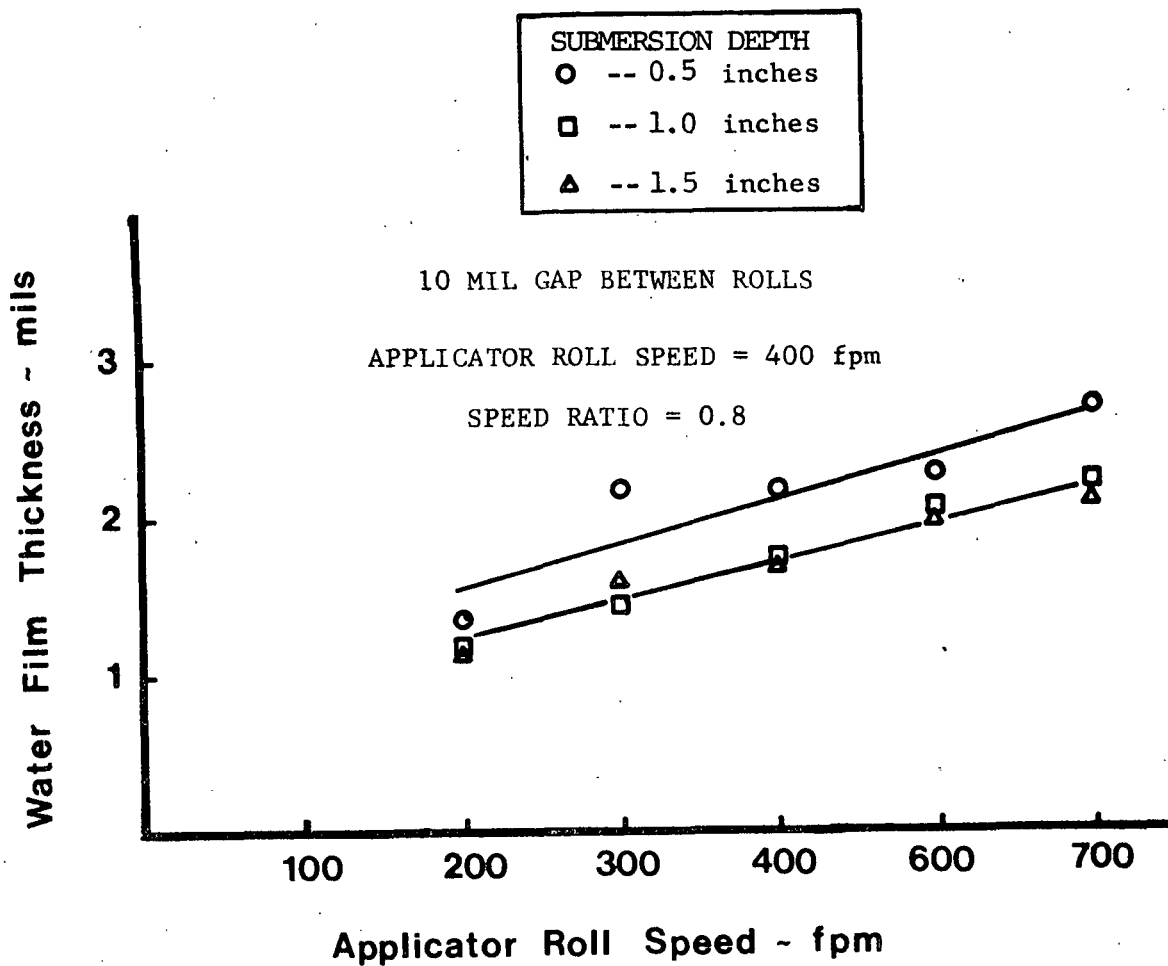
Figure 4.24. Depth of Submersion: Water

MAGIE OIL No. 500

Depth of Roll Submersion

o	0.50
□	0.75
x	1.00
△	1.50

FILM THICKNESS, mils

10 mil Gap between rolls   100°F

SPEED RATIO
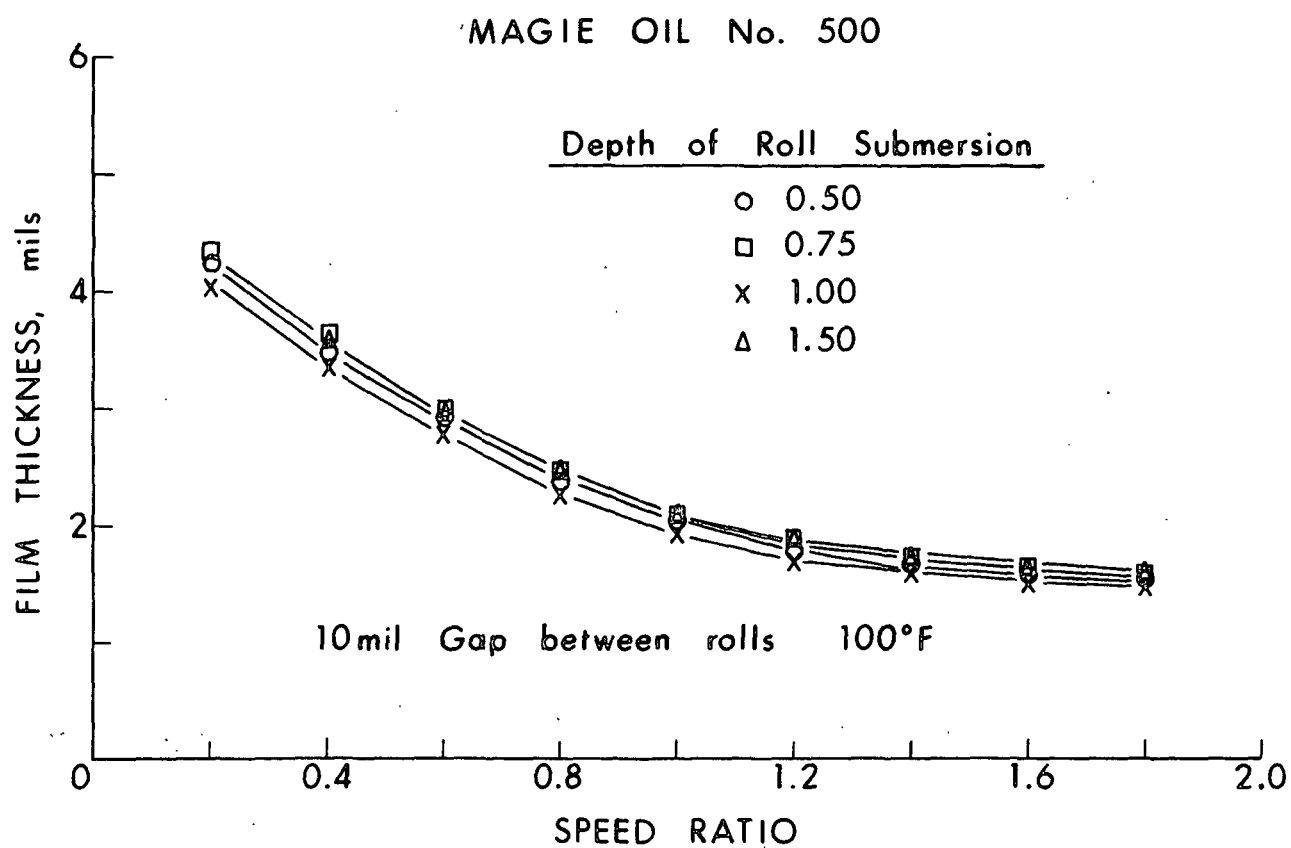
Figure 4.25. Depth of Submersion: Magie Oil #500

Polybutene #6

SPEED RATIO = 0.8
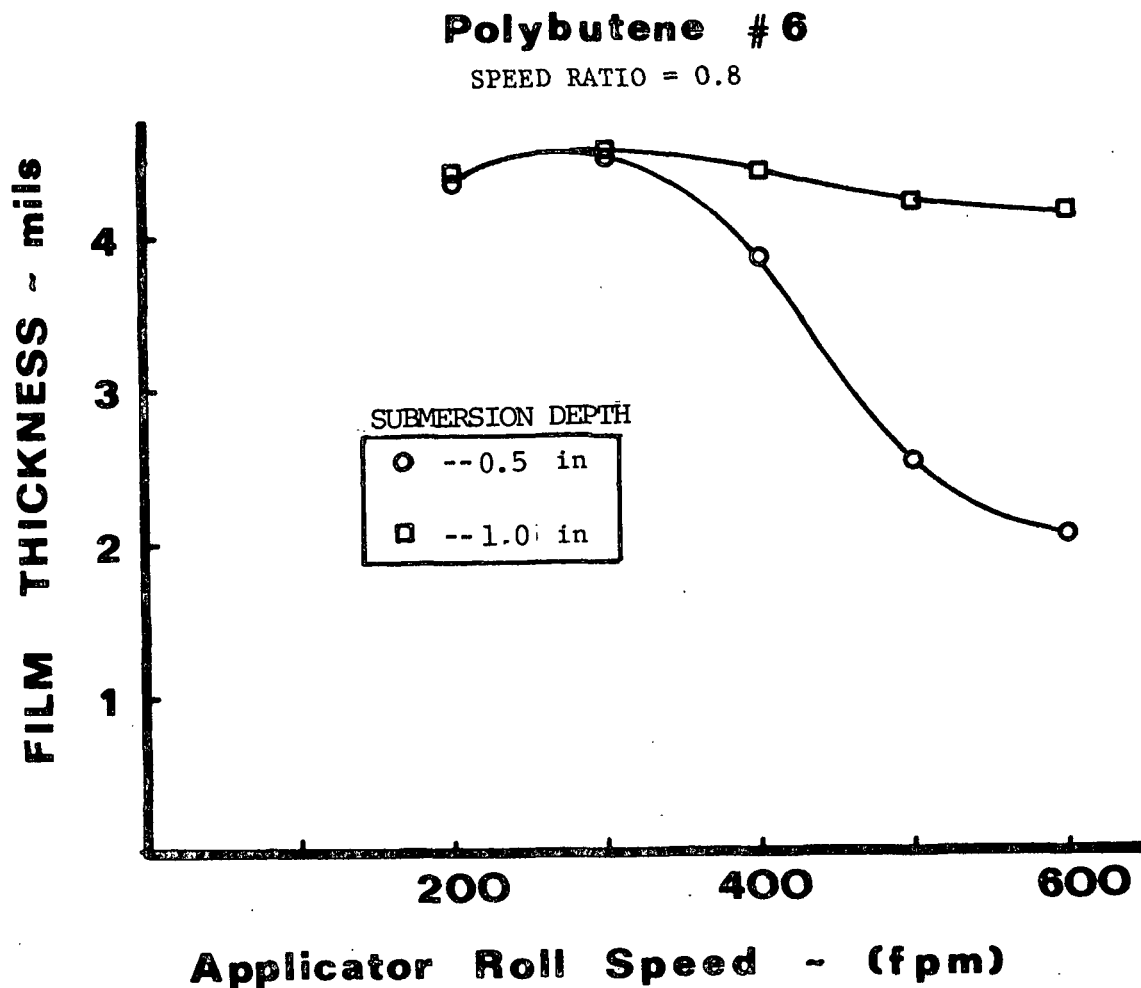
Figure 4.26. Depth of Submersion: Polybutene #6

Two experimental observations are essential to the discussion of some portions of the analytical model. They are:

1) The importance of the pressure distribution to the analytical model has been demonstrated in Section 2.0. Early in the experimental program it was realized that the pressure under the rolls has a significant influence on the adhesive film thickness. Therefore, a small flattened tube was placed into the nip area from below the rolls. The probe was attached to a static pressure manometer and produced the data shown in Fig. 4.27. The higher speeds

create much larger pressures in the nip. Since a simple

Bernoulli relationship indicates the pressure should increase

with the square of velocity, the results are expected. The

pressure drops rapidly with increasing M/A ratio because more

fluid is removed from the pick-up roll before being forced into

the nip. It was not possible to collect data closer than

3/8 of an inch from the nip because the probe was too large.

Since the separation point and the point of maximum pressure are

located much closer to the nip, an improved means of obtaining

pressure measurements is required and is part of the continuing

research effort.

STATIC PRESSURE

Machine Oil, $h_o = .015"$
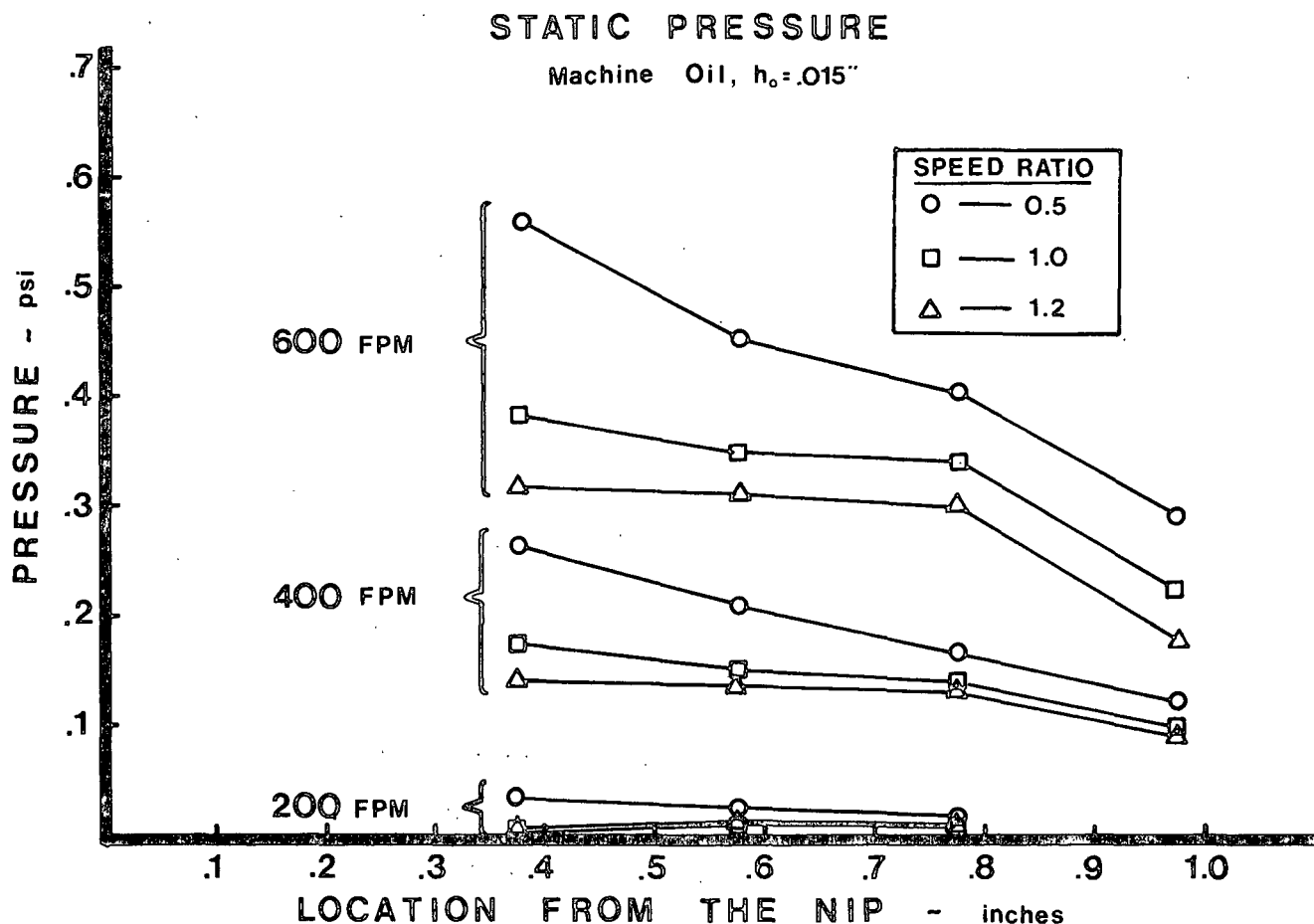
Figure 4.27. Static Pressure Measurements in the Nip

2) The point where the fluid separates from the metering roll (see
Fig. 4.28) moves either above or below the nip depending upon
the operating conditions and the fluid properties. At low M/A
ratios, the separation point is usually above the nip. As the
M/A ratio increases, the point of separation is pulled into the
nip. This tendency was confirmed by visual observations in
this project and also a photographic investigation by Nikkel (10).
In Nikkel's photographs, the thickness of the film is dependent
upon the point of separation. The film thickness decreases as
the separation point approaches the nip from above. After passing
through and separating inside the nip, the film thickness in-
creases again. The minimum film thickness seems to occur when
the film separates exactly at the nip.
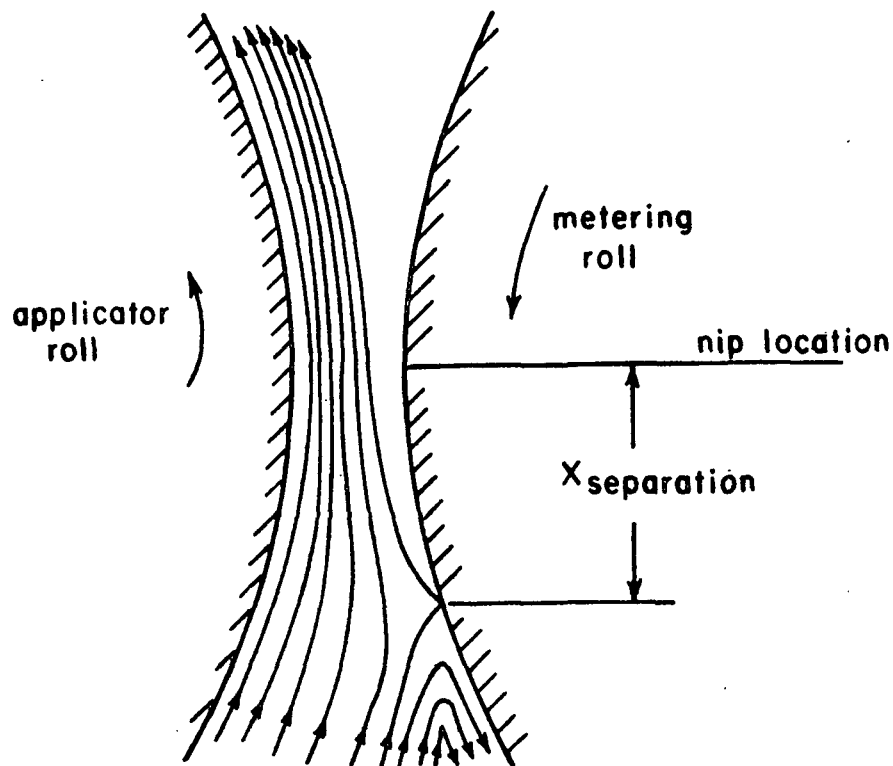
Figure 4.28. Fluid Separation from Metering Roll

The analyical results are presented by analyzing the relative importance of each term in Equation (4.1). The steady-state contribution is basically a linear relationship between the film thickness and speed ratio. In Fig. 4.29a, the three solid lines represent the steady-state contribution to a typical starch adhesive plot of film thickness _versus_ speed ratio. The inability of this term to model the complete speed ratio plot is clearly seen as the film thicknesses become negative at a speed ratio greater than 1.0. The differences in the levels of Curves A, B, and C must come from the quantity h_m, which is spacing between the rolls at the point of maximum pressure. Each curve represents a constant speed line with A being the largest value. If the fluid separates from the metering roll below the nip, the point of maximum pressure moves closer to the nip as the speeds are increased. For this case, the gap between the rolls h_m would become smaller and the levels of Curves A and C would be opposite of the experimental data.

Fortunately, the second observation which is the movement of the point of separation through the nip accounts for the proper tendencies in the steady-state term of the analytical model. At speed ratios less than unity, the fluid separates from the metering roll above the nip. A portion of the fluid forced through the nip forms a bubble of recirculation fluid as shown in Fig. 4.30. The size of the bubble is dependent upon the pressure below the nip which supports it. Since the pressures increase dramatically with speed, the size of the bubble and location of the separation point above the nip increase accordingly. This allows the film thickness to become slightly larger for increased speeds. The differences in the values of h_m for the cases when the fluid separates above or below the nip illustrates the importance of h_m in the analytical model and the need to accurately define the pressure distribution in the nip.
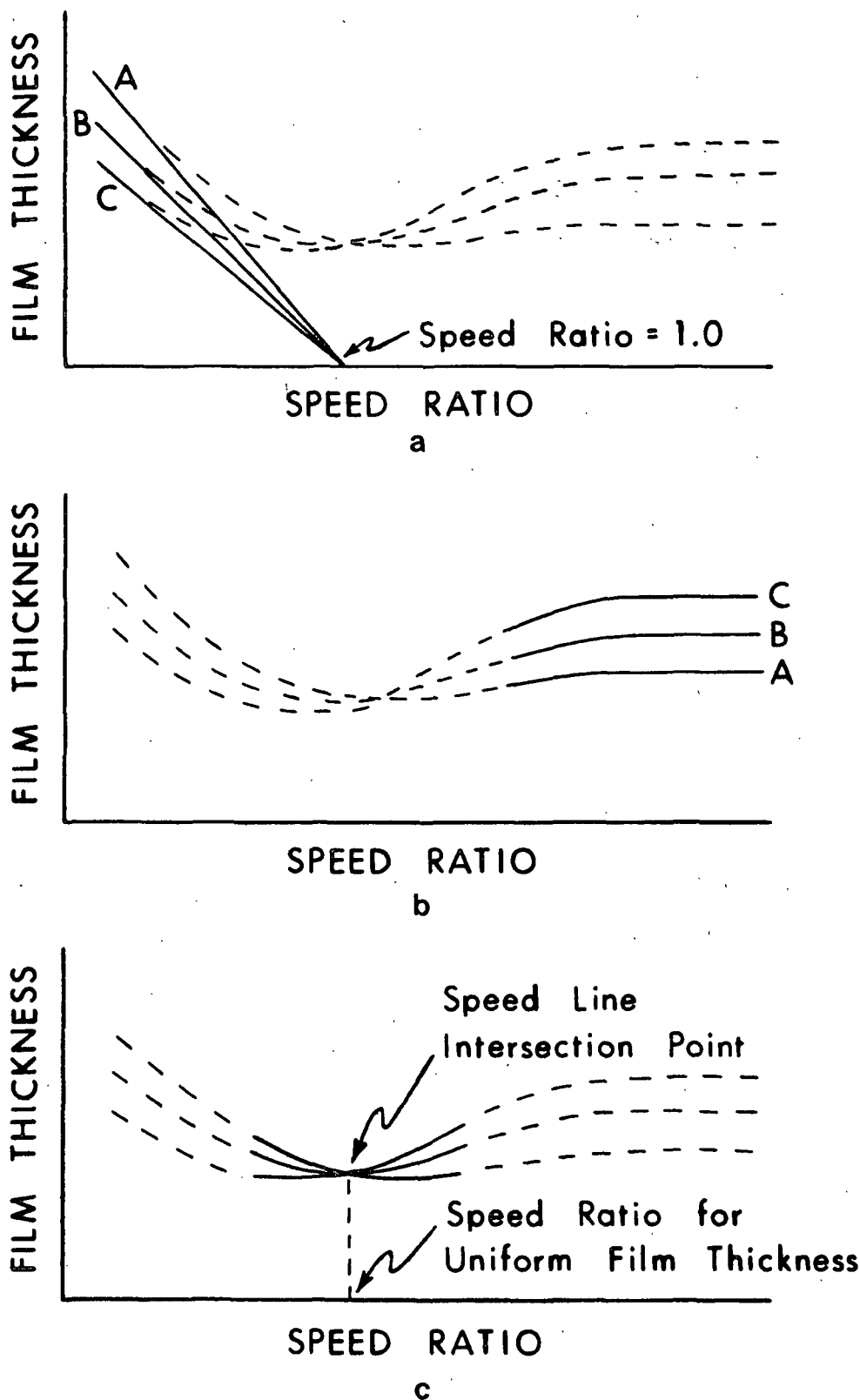
Figure 4.29. (a,b,c) Typical Speed Ratio Data

RECIRCULATING FLUID

APPLICATOR
ROLL

METERING
ROLL
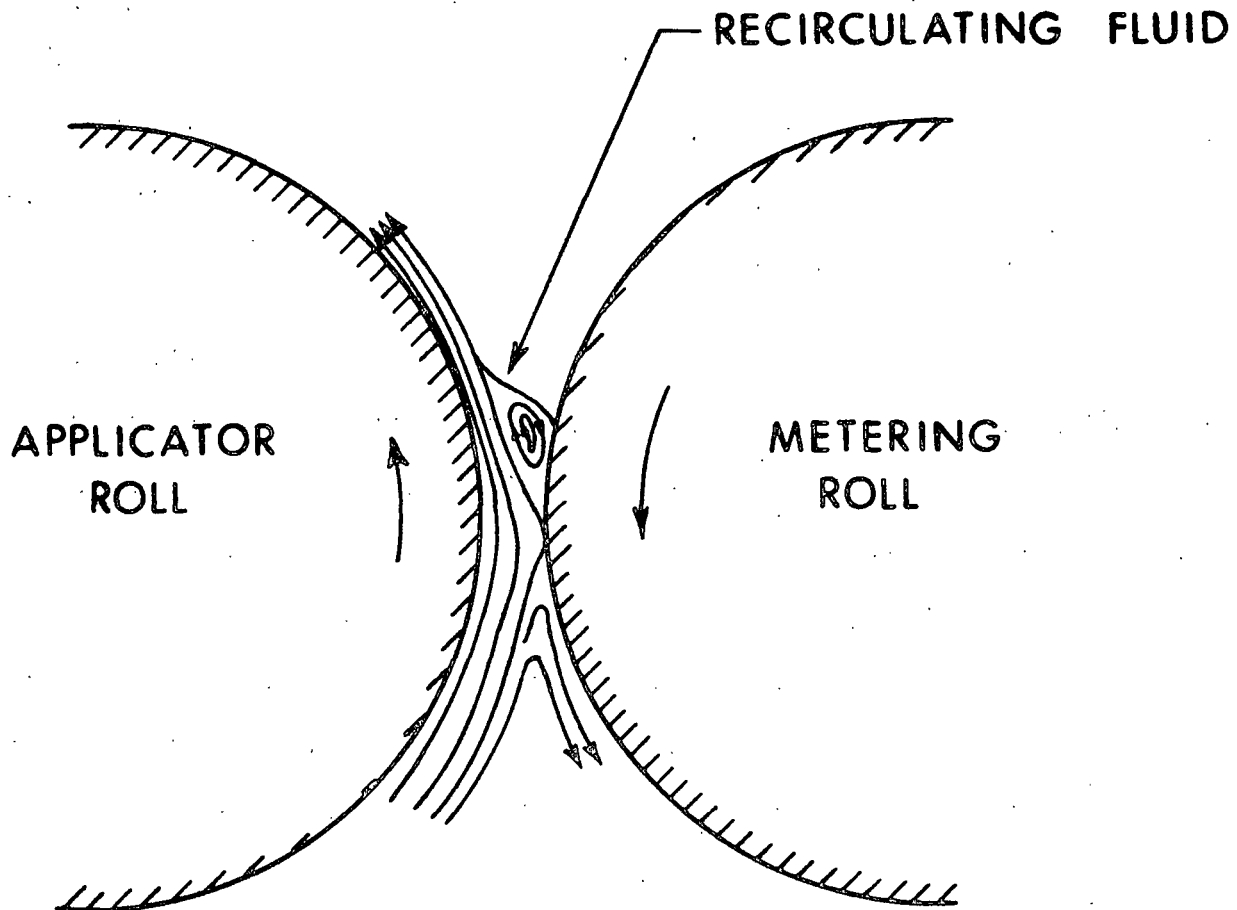
Figure 4.30. Recirculating Fluid Bubble

Additionally, the previous discussion implies that the film thickness

for low values of M/A ratio is controlled by the dynamics of the applicator system

rather than by the properties of the fluid. The second term of Equation (4.1) is

generally insignificant at the low speed ratios because the fluid is sheared for

a relatively long period of time. The spacing between rolls, h_m, is the only param-

eter in the first term of the equation that varies with machine speeds and can

create different levels of the speed lines. The value of h_m is dependent upon the

pressure below the nip. Since the pressure is a function of the roll speed squared

and fluid density, the film thickness is controlled primarily by the system param-

eters. This result is demonstrated in all the experimental data where the fluids,

all having approximately the same density but different viscosities, have nearly

equal film thicknesses at the low M/A ratios. When the viscosity of the adhesive

was modified by changing temperature as shown in Fig. 4.17, the changes in film

thickness occurred only at the higher M/A ratios. The curves were almost iden-

tical at the lower values of speed ratio.

The second term of Equation (4.1) accounts for developing flow effects

and becomes important when the speed ratios and speeds are large enough to reduce

the shearing time to where the velocity profile is fuller than the linear relation-

ship obtained for steady-state flow. The fuller profile creates a larger film on

the applicator roll. At high values of M/A ratio, the separation point moves

well within the nip where it becomes stationary because of the rapidly increase-

ing gap spacing. This stabilizes the exponential term and the value of h_m. The

result is a uniform film thickness at high speed ratios (see Fig. 4.29b). The

tendency is observed experimentally for all the fluids.

At high M/A ratios, the different levels of speed lines are associated

with the fluid separating and reaching a maximum pressure at various locations

within the nip. Higher speeds create larger pressures and force the points of

maximum pressure and separation closer to the nip. This phenomenon is confirmed

by the pressure data in Fig. 4.27. Moving the maximum pressure closer to the nip

reduces h_m and therefore reduces the film thickness. Since this occurs with in-

creasing speed, the tendencies of the experimental data at high speed ratios

are analytically predicted (see Fig. 4.29b).

At the high speed ratios where the developing flow term dominates the

film thickness calculations, the depth of the film is dependent upon both system

parameters and the fluid properties. This occurs because the exponential term

is dependent upon the time that the fluid is sheared and the fluid response to

that shearing action, i.e., viscosity. The effect of changing the fluid viscosity was clearly seen in Fig. 4.17. While the system parameters remain constant, the level of the film thickness increases with increasing viscosity.

The two terms in Equation (4.1) appear to represent the limiting cases for low and high values of speed ratio. The change from one to the other creates an intersection point similar to that seen in the experimental data (see Fig. 4.29c). The controlling mechanisms for the high and low values of M/A ratio are different. Before the intersection point of the speed lines, the film thickness is independent of the fluid properties. As the developing flow term begins to become significant, the speed lines intersect. Since the fluid properties affect the developing flow contribution and not the first term of the equation, they control the point where the speed lines intersect. The experimental data indicates that the fluid high shear viscosity has a significant influence on the second term of Equation (4.1) and therefore controls the intersection point. Again this is clearly seen in Fig. 4.17.

The analytical model also suggests that a change of gap spacing between the roll has only secondary effects on the intersection point. The gap change equally affects both terms of the equation and produces curves with the same shape and uniformly increased values of film thickness. This tendency is shown in the experimental data (see Fig. 4.19, 4.20, 4.21, and 4.22). The secondary effects are seen at high values of gap spacings (Fig. 4.21 and 4.22).

As a final illustration, it is assumed that the time constant in Equation (4.1) is inversely related to the fluid high shear viscosity and the effect of different levels of viscosity is shown in Fig. 4.31. The curves closely resemble the plots of experimental data. Increasing the viscosity causes the
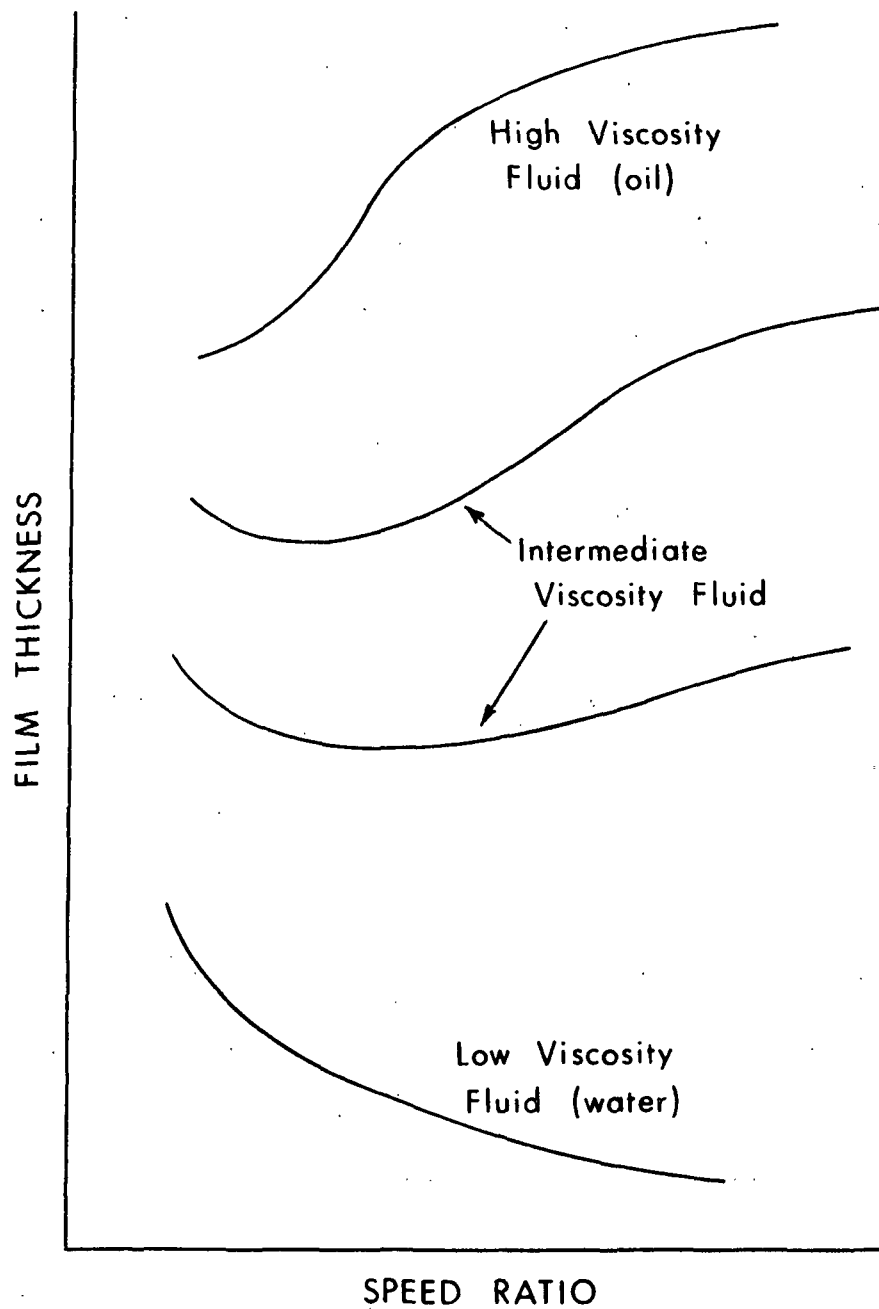
Figure 4.31. Analytical Predictions of Film Thickness Versus Speed Ratio

second term of the equation to dominate at a lower M/A ratio and the intersection point decreases accordingly. The actual values of the film thickness and the functional relationship of the time constant with fluid viscosity can be determined from the point of maximum pressure and the point where the fluid separates from the metering roll. These were not measured in this part of the project but will be obtained in the second portion of the study.

5.0 SUMMARY AND CONCLUSIONS

While describing the fundamental mechanics of the adhesive applicator system, two significant results were discovered. The first discovery was a M/A speed ratio for which the adhesive film thickness on the applicator roll is unchanged at different operating conditions. The importance of this phenomena in controlling the amount of adhesive placed on the flute tips is obvious. Additionally, a correlation between the desired M/A ratio and the high shear viscosity of the fluid was discovered. The speed ratio was found to be inversely related to the fluid viscosity. As a result of these findings, several implications of industrial importance can be drawn:

1) There is an optimum M/A speed ratio at which the glue machine should be set. Currently, industrial units operate at speed ratios that range from 0.33 to 1.0 and are specified by the manufacturer. The correct setting could be obtained by modifying the formulation of the starch adhesive (i.e., the high shear viscosity) to match the manufacturers setting or by mechanically adjusting the applicator speed ratio to match the starch adhesive.

2) For both methods of adjusting the desired speed ratio, the high shear viscosity of the fluid must be known. A Stein-Hall cup viscometer measures only the low shear viscosity. The high shear viscosity of the fluid can be substantially different from the low shear value. The industrial use of an expensive laboratory device such as the Hercules viscometer is prohibitive. However, a simple capillary tube viscometer in which the adhesive is forced under pressure through a small tube may be a practical alternative. The flow rate through the capillary tube for a given pressure differential is directly related to the high shear viscosity. The device is simple, rugged and therefore more suitable than the Hercules for industrial conditions.

3) If the speed ratio settings are variable and the high shear viscosity of the adhesive can be determined, then the control of the adhesive film thickness is predictable. Once the M/A ratio is set to obtain a constant film thickness, the actual thickness can be controlled by varying the gap spacing between the rolls. In Section 4.4, it was concluded that changes in the gap spacing had only minor effects on the intersection point while the magnitude of the film thickness changed uniformly with the gap spacing.

4) The predictability described in the previous paragraph allows other aspects of the applicator system to be studied. If the film thickness on the applicator roll can be controlled for various operating conditions, then the transfer of adhesive to the flute tips is open for analysis. The CID group is currently investigating starch consumption and its relation to the transfer of the adhesive to the flute tips. The proposed research objectives of this continuing project are also in this area.

The second important finding of the research effort contradicts traditional beliefs concerning the rheology of starch adhesives. The non-Newtonian behavior of the starch adhesive was traditionally used to explain the unpredictability of the adhesive film thickness. The experimental and analytical results presented here indicate that much of this variation is caused by the dynamics of the system and magnitude of the high shear viscosity. In fact, at the high shear rates experienced in the nip, the starch adhesives behave very much like the Newtonian fluids.

Additionally, the analytical model simulates the basic metering process of the system very well and it provides other valuable insights into the fluid dynamics of the glue machine. The principle addition that made it possible to model the nip flow was the inclusion of developing flow considerations to the analysis.

However, two parameters still need to be determined before the model can predict the film thicknesses for any particular fluid. The parameters are the point at which the fluid reaches its maximum pressure and the point where it separates from the metering roll. Both are probably related to fluid properties as well as the applicator system variables. One objective of the next phase of this program involves the determination of the fluid pressure distribution in the nip. The separation point and point of maximum pressure will be obtained from this distribution.

In conclusion, several other points of interest were found and while they are not as dramatic as those just mentioned, they do provide valuable information concerning the operation of the applicator system.
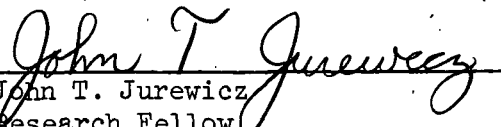
1) The effect of changing the gap between rolls should not be underestimated. Although a change from 10 to 12 mils seems like a minor adjustment, it is a variation of 20% and corresponds to a 20% change in the film thickness. This also illustrates the sensitivity of the two roll applicator system to misalignments and out-of-roundness of the rolls.

2) The results of Section 4.5 indicate that the depth of roll submersion can have significant effect on the film thickness, particularly when the fluid level is low. Generally, this is not a problem in industry but it can be easily neglected when modifications are made to an applicator system.

REFERENCES

1. Stevenson, J. F. President, SAS International, Inc., private communication, 1977.

2. Schlichting, H. Boundary Layer Theory. p. 108-114. New York, McGraw-Hill, 1968.

3. Hintermaier, J. C. and White, R. E. The splitting of a water film between rotating rolls. Tappi 48(11):617-25(Nov., 1965).

4. Turai, L. L. Analysis of the blade coating process. Tappi 54(8):1315-18 (Aug., 1971).

5. Flumerfelt, R. W., Pierick, M. W., Cooper, S. L., and Bird, B. B. Generalized plane Couette flow of a non-Newtonian fluid. I&EC Fundamentals 8(2):354-7 (May, 1969).

6. Jurewicz, J. T. A progress report on Project 2696-17 to FKGB, Feb., 1977.

7. Koning, J., Jr. Metering Characteristics of Starch Corrugating Adhesives. Unpublished report, Forest Products Laboratory, Forest Service, U.S. Dept. of Agriculture, 1975.

8. Brodkey, R. S. The Phenomena of Fluid Motions. p. 87-90. Reading, MA, Addison-Wesley, 1967.

9. Preparation, circulation, and storage of corrugating adhesives. Tappi-STAP Ser. (3):13-15(1965).

10. Nikkel, W. A. Westvaco Corp., private communication, 1977.

THE INSTITUTE OF PAPER CHEMISTRY

John T. Jurewicz
Research Fellow
Container Division

APPROVED BY

Terrence S. Fox
Director
Container Division

APPENDIX A

SOLUTION FOR THE VELOCITY PROFILE

The governing partial differential equation was given by Equation (2.2) as:

$$\frac{\partial u}{\partial t} = \nu \frac{\partial^2 u}{\partial y^2} \tag{A.1}$$

with boundary and initial conditions:

$$
\begin{aligned}
u &= u_a & y &= 0 \\
u &= -u_m & y &= h \\
u &= u_a & t &= 0
\end{aligned}
\tag{A.2}
$$

To simplify the analysis, the following variable changes are made

$$\bar{u} = \frac{u_a - u}{u_a + u_m} \tag{A.3}$$

$$\bar{y} = y/h \tag{A.4}$$

$$\bar{t} = \frac{t\nu}{h^2} \tag{A.5}$$

With these changes the governing equation and boundary conditions become

$$\frac{\partial \bar{u}}{\partial \bar{t}} = \frac{\partial^2 \bar{u}}{\partial \bar{y}^2} \tag{A.6}$$

and

$$
\begin{aligned}
\bar{u} &= 0 & \bar{y} &= 0 \\
\bar{u} &= 1 & \bar{y} &= 1 \\
\bar{u} &= 0 & \bar{t} &= 0
\end{aligned}
\tag{A.7}
$$

The problem is nonhomogeneous in the second boundary condition but can be converted to a homogeneous one by use of a partial solution. The common technique is to assume that the final solution consists of a steady state and transient term.

$$\bar{u}(\bar{y},\bar{t}) = \bar{U}(\bar{y}) + \bar{V}(\bar{y},\bar{t}) \tag{A.8}$$

The steady-state solution must satisfy

$$\frac{\partial^2}{\partial \bar{y}^2} \bar{U}(\bar{y}) = 0 \tag{A.9}$$

which can be easily integrated

$$\bar{U}(\bar{y}) = C_0 \bar{y} + C_1 \tag{A.10}$$

The boundary conditions are

$$\bar{U}(0) = 0$$
$$\bar{U}(1) = 1 \tag{A.11}$$

and the constants of integration become

$$C_0 = 1$$
$$C_1 = 0 \tag{A.12}$$

The steady-state solution is simply

$$\bar{U}(\bar{y}) = \bar{y} \tag{A.13}$$

The transient solution can be expressed as

$$\bar{V}(\bar{y},\bar{t}) = \bar{u}(\bar{y},\bar{t}) - \bar{U}(\bar{y}) \tag{A.14}$$

Fourdrinier Kraft Board Group
of The American Paper Institute
Project 2696-17 .

Page 73
Report One

Substituting Equation (A.14) into Equation (A.6) yields

$$\frac{\partial \bar{V}(\bar{y},\bar{t})}{\partial \bar{t}} = \frac{\partial^2 \bar{V}(\bar{y},\bar{t})}{\partial \bar{y}^2} \tag{A.15}$$

The boundary and initial conditions for the transient solution are:

$$\bar{V}(0,\bar{t}) = 0$$

$$\bar{V}(1,\bar{t}) = 0 \tag{A.16}$$

$$\bar{V}(\bar{y},0) = -\bar{y}$$

The problem now has homogeneous boundary conditions and can be solved using

separation of variables.

Let the solution $\underline{\bar{V}}(\bar{y},\bar{t})$ be expressed as a product of separate functions

of $\underline{\bar{y}}$ and $\underline{\bar{t}}$, i.e.,

$$\bar{V}(\bar{y},\bar{t}) = Y(\bar{y})T(\bar{t}) \tag{A.17}$$

Since the substitution of Equation (A.17) into Equation (A.15) allows the equa-

tion to be separated so that one side is a function only of $\underline{\bar{y}}$ while the other is

only a function of $\underline{\bar{t}}$, both sides can be set equal to an arbitrary constant, λ^2.

$$\frac{\partial^2 Y(\bar{y})}{\partial \bar{y}^2} \bigg/ Y(\bar{y}) = \frac{\partial T(\bar{t})}{\partial \bar{t}} \bigg/ T(\bar{t}) = -\lambda^2 \tag{A.18}$$

The partial differential equation is separated into two ordinary differential

equations.

$$\frac{\partial^2 Y(\bar{y})}{\partial \bar{y}^2} + \lambda^2 Y(\bar{y}) = 0 \tag{A.19}$$

$$\frac{\partial T(\bar{t})}{\partial \bar{t}} + \lambda^2 T(\bar{t}) = 0 \tag{A.20}$$

The solutions for the equations are respectively

$$Y(\bar{y}) = A \sin \lambda \bar{y} + B \cos \lambda \bar{y} \qquad (A.21)$$

and

$$T(\bar{t}) = e^{-\lambda^2 \bar{t}} \qquad (A.22)$$

The combined solution for $\bar{V}(\bar{y},\bar{t})$ is

$$\bar{V}(\bar{y},\bar{t}) = \bar{Y}(\bar{y})T(\bar{t}) = e^{-\lambda^2 \bar{t}} (A \sin \lambda \bar{y} + B \cos \lambda \bar{y}) \qquad (A.23)$$

The first of boundary Conditions (A.16) is

$$\bar{V}(0,\bar{t}) = 0 = e^{-\lambda^2 \bar{t}} (+A \sin \lambda 0 + B \cos \lambda 0) \qquad (A.24)$$

or

$$Be^{-\lambda^2 \bar{t}} = 0 \qquad (A.25)$$

Since $\bar{t}$ is arbitrary, B must be zero.

The next boundary condition is

$$\bar{V}(1,\bar{t}) = Ae^{-\lambda^2 \bar{t}} \sin \lambda = 0 \qquad (A.26)$$

Since $\bar{t}$ is again arbitrary and $A = 0$ is a trivial solution, the boundary condition must be satisfied by

$$\sin \lambda = 0 \qquad (A.27)$$

The zeros of the $\sin \lambda$ are determined from

$$\lambda_n = n\pi \qquad n = 0, 1, 2 \ldots \qquad (A.28)$$

and the solution can be written as

$$\bar{V}(\bar{y},\bar{t}) = \sum_{n=0}^{\infty} A_n \sin n \pi \bar{y} \, e^{-n^2 \pi^2 t} \qquad (A.29)$$

For $\underline{n} = 0$, the first term of the series is zero and can be dropped.

$$\bar{V}(\bar{y},\bar{t}) = \sum_{n=1}^{\infty} A_n \sin n \pi \bar{y} \, e^{-n^2\pi^2 t} \tag{A.30}$$

The initial condition and orthogonality are used to determine the constants $A_{\underline{n}}$

$$\bar{V}(\bar{y},0) = -\bar{y} = \sum_{n=1}^{\infty} A_n \sin n \pi \bar{y} \tag{A.31}$$

$$-\bar{y} \sin m \pi \bar{y} = \sum_{n=1}^{\infty} A_n \sin n \pi \bar{y} \sin m \pi \bar{y} \tag{A.32}$$

$$- \int_0^1 \bar{y} \sin m \pi \bar{y} d\bar{y} = \sum_{n=1}^{\infty} A_n \int_0^1 \sin n \pi \bar{y} \sin m \pi \bar{y} d\bar{y} \tag{A.33}$$

$$\left[- \frac{1}{(m\pi)^2} \sin m \pi \bar{y} + \frac{\bar{y}}{m\pi} \cos m \pi \bar{y} \right] \Big|_0^1 = 1/2 \, A_m \tag{A.34}$$

$$A_m = \frac{2 \cos m\pi}{m\pi} \tag{A.35}$$

The transient solution is

$$\bar{V}(\bar{y},\bar{t}) = \frac{2}{\pi} \sum_{n=1}^{\infty} \frac{\cos n \pi \sin n \pi \bar{y}}{n} e^{-n^2\pi^2\bar{t}} \tag{A.36}$$

and the complete solution can be written

$$\bar{u}(\bar{y},\bar{t}) = \bar{y} + \frac{2}{\pi} \sum_{n=1}^{\infty} \frac{\cos n \pi \sin n \pi \bar{y}}{n} e^{-n^2\pi^2\bar{t}} \tag{A.37}$$

Transforming the variables according to Equations (A.3), (A.4), and (A.5) yields

$$u(y,t) = u_a - (u_a + u_m) y/h - \frac{2(u_a + u_m)}{\pi} \sum_{n=1}^{\infty} \frac{\cos n \pi \sin n \pi \bar{y}/h}{n}$$

$$e^{\frac{-n^2\pi^2}{h^2} \nu t} \tag{A.38}$$

or

$$u(y,t) = u_a - (u_a + u_m) y/h - \frac{2}{\pi} (u_a + u_m) \sum_{n=1}^{\infty} \frac{(-1)^n \sin n \pi y/h}{n}$$

$$e^{-(n\pi/h)^2} \nu t \qquad\qquad\qquad (A.39)$$

APPENDIX B

STARCH ADHESIVE FORMULATION

NO-CARRIER ADHESIVE
(20% Solids)

All Pearl Starch

1 Tank Mix

Add water	10.22 liters	10.22 liters
Heat to 135°		
Add starch	2.20 lb	2.20 lb
Add sodium borate (10 mol)		13.6 g
Add sodium hydroxide solution (50%)		157.2 g/0.157 ml
Mix 20 minutes		
Add water		15.52 liters
Add sodium borate (10 mol)		86.2 g
Add starch		12.8 lb
Add sodium borate (20 mol)		68 g
Mix 20 minutes		

Viscosity 30-40 seconds @ 100°F
Gel Point 145°F

STEIN-HALL ADHESIVE
(17.6% Solids)

Primary

1. Add water	5.806 liters	18.54%
2. Add starch	1.93 lb	13.68%
3. Add caustic/water[a]	160.4 g/1.052	2.5%/3.36%

Heat to 135–140°F and caustic solution to increase temperature to 180°F; hold 15 minutes

4. Add water	3.157 liters	10.08%

Secondary

1. Add water	18.934 liters	60.46%
2. Add bentonite[a]	99.42 g	1.55%
3. Add sodium borate[a]	87.87 g	1.37%
4. Add starch	12.21 lb	86.32%
5. Add water — after dropping Primary	1.790 liters	7.56%

---

[a] Caustic, bentonite, and sodium borate based on the weight of dry starch.

STEIN-HALL ADHESIVE
(20% Solids)

Top Mixer

Primary

Add water	5.520 liters
Add starch	2.4 lb
Increase temperature to 100°F-120°F	
Add sodium hydroxide solution	199 g/1.0 liters
Increase temperature to 180°F and hold 15 minutes	
Add water	3.0 liters

Bottom Mixer

Secondary

Add water	18.0 liters
Add bentonite	123.5 g
Add sodium borate (10 mol)	108.9 g
Add starch	15.15 lb
Add primary slowly — about 30 minutes	
Add water	2.25 liters
Mix 30 minutes	

STEIN-HALL ADHESIVE
(26.0% Solids)

Primary

1. Add water	5.246 liters		18.54%
2. Add starch	2.85 lb		13.68%
3. Add caustic/water	235.9 g/0.950 ml		2.5%/3.36%

Heat to 135-140°F; add caustic solutions; increase temperature
to 180°F; hold for 15 minutes

4. Add water	2.852 liters	10.08%

Secondary

1. Add water	17.108 liters		60.46%
2. Add bentonite	146.2	g	1.55%
3. Add sodium borate	129.3	g	1.37%
4. Add starch	17.95	lb	86.32%
5. Add water after dropping primary	2.139 liters		7.56%

Caustic, bentonite, sodium borate based on weight of dry starch.